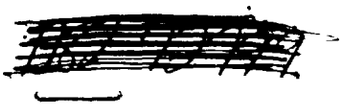

NASA CR-165567
PWA-5594-152

NASA

ENERGY EFFICIENT ENGINE
COMPONENT DEVELOPMENT AND INTEGRATION PROGRAM

HIGH-PRESSURE TURBINE SUPERSONIC CASCADE TECHNOLOGY REPORT

by

Frederick C. Kopper, et al

UNITED TECHNOLOGIES CORPORATION
Pratt & Whitney Aircraft
Commercial Products Division

(NASA-CR-165567) ENERGY EFFICIENT ENGINE HIGH-PRESSURE TURBINE SUPERSONIC CASCADE TECHNOLOGY REPORT (United Technologies Corp.) 155 p EC A08/MF A01 CSCL 21E

N84-27739

G3/07 19784

Unclas

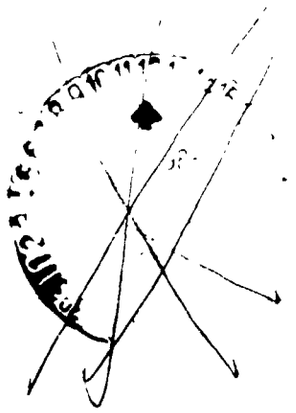

...pared for

NATIONAL AERONAUTICS AND SPACE ADMINISTRATION
Lewis Research Center
Cleveland, Ohio 44135

Contract NAS3-20646

1 Report No	2 Government Accession No	3 Recipient's Catalog No
NASA-CR-165567		

4 Title and Subtitle	5 Report Date
Energy Efficient Engine High-Pressure Turbine Supersonic Cascade Technology Report	Nov 1981
	6 Performing Organization Code
7 Author(s)	8 Performing Organization Report No
Mr. Frederick C. Kopper, Mr. Robert Milano, Mr. Roger L. Davis, Dr. Robert P. Dring, Mr. Richard C. Stoeffler	PWA-5594-152
	10 Work Unit No
9. Performing Organization Name and Address	
United Technologies Corporation Pratt & Whitney Aircraft Group - CPD East Hartford, Connecticut 06108	11 Contract or Grant No NAS3-20646
	13 Type of Report and Period Covered
12 Sponsoring Agency Name and Address	Technology Report
National Aeronautics and Space Administration Lewis Research Center 21000 Brookpark Road, Cleveland, Ohio 44135	14 Sponsoring Agency Code

15 Supplementary Notes

Project Manager: C.C. Ciepluch, NASA Lewis Research Center
Cleveland, Ohio 44135

16 Abstract

The performance of two vane endwall geometries and three blade sections for the high-pressure turbine was evaluated in terms of the efficiency requirements of the Energy Efficient Engine high-pressure turbine component. The vane endwall designs featured a straight wall and S-wall configuration. The blade designs included a "base" blade, "straightback" blade, and "overcambered" blade. Test results indicated that the S-wall vane configuration and the "base" blade configuration offered the most promising performance characteristics for the Energy Efficient Engine high-pressure turbine component.

17 Key Words (Suggested by Author(s))

S-Wall	Straightback
Straight Wall	Cooled
Base	Uncooled
Overcambered	Cascade

19 Security Classif (of this report)	20 Security Classif (of this page)	21 No of Pages	22 Price*
Unclassified	Unclassified	140	

FOREWORD

The Energy Efficient Engine Component Development and Integration Program is being conducted under parallel National Aeronautics and Space Administration contracts to the Pratt & Whitney Aircraft Group and General Electric Company. The overall project is under the direction of Mr. Carl C. Ciepluch. Mr. John W. Schaefer is the NASA Assistant Project Manager for the Pratt & Whitney Aircraft effort under Contract NAS3-20646, and Mr. Michael Vanco is the NASA project engineer responsible for the portion of the project described in this report. Mr. William B. Gardner is manager of the Energy Efficient Engine Program at Pratt & Whitney Aircraft Group. Mr. Frederick Kopper provided technical direction for this supporting technology program. Mr. Robert Milano conducted the vane cascade testing and analysis. The blade cascade testing and analysis was conducted by Mr. Roger Davis of Pratt & Whitney Aircraft, Dr. Robert Dring and Mr. Richard Stoeffler of the United Technologies Research Center.

TABLE OF CONTENTS

TABLE OF CONTENTS (Cont'd)

LIST OF ILLUSTRATIONS

LIST OF ILLUSTRATIONS (Cont'd.)

LIST OF ILLUSTRATIONS (Cont'd.)

LIST OF ILLUSTRATIONS (Cont'd.)

LIST OF ILLUSTRATIONS (Cont'd.)

LIST OF ILLUSTRATIONS (Cont'd.)

LIST OF ILLUSTRATIONS (Cont'd.)

LIST OF ILLUSTRATIONS (Cont'd.)

LIST OF ILLUSTRATIONS (Cont'd.)

LIST OF ILLUSTRATIONS (Cont'd.)

1.0 SUMMARY

The single stage high-pressure turbine for the Energy Efficient Engine employs air-cooled blades and vanes and advanced aerodynamic concepts such as contoured vane endwalls to achieve its goal efficiency and life. The turbine was designed to have a high ratio of wheel speed to specific work (velocity ratio), a low ratio of through-flow to wheel tangential velocity (C_x/U) and high AN^2 (product of annulus area and wheel speed squared). In addition, design studies indicated that turbine efficiency could be further improved by increasing the turbine reaction level from a balanced Mach number design to a design with a subsonic vane and a supersonic blade, with careful attention paid to blade airfoil curvature aft of the throat. Cooling is achieved by a combination of internal conductive and external film cooling techniques.

Testing of straight endwall and contoured endwall (S-wall) vane cascades indicated that the S-wall cascade had 17 percent less full-passage, mass-averaged pressure loss than the straight wall cascade. In the mid-span two-dimensional flow region of the cascade, vane exit air angle was generally insensitive to changes in endwall configuration as well as variations in exit Mach number and coolant flow rates. However, mid-span total pressure loss almost doubled when design-point coolant flow was ejected from all discharge ports. The largest contributor was suction surface coolant flow injection, which had a penalty about 5 times higher than that due to either pressure surface or trailing edge coolant flow. Variations in exit Mach number confirmed that the component vane design was free of transonic drag rise in the range of intended operating conditions.

Testing of blade cascades representing the high-pressure turbine component airfoil baseline design and two alternate distributions of airfoil curvature verified the acceptability of the component design. In addition, base airfoil pressure loss was relatively insensitive to variations in inlet gas angle over a range of 25 degrees, indicating that the component blade design has good incidence range. The addition of trailing edge coolant flow ejection caused a slight increase in base blade pressure loss at subsonic exit Mach numbers, but reduced total pressure loss at supersonic exit Mach numbers relative to the base blade without coolant flow ejection. This was attributable to the fact that flow ejection reduced the trailing edge shock strength such that decreases in shock losses predominated over corresponding increases in wake mixing losses. Measured exit air angles were within +1.0 to -2.0 degrees of the design exit air angle of 17 degrees at the design point exit Mach number. Trailing edge flow ejection had little effect on exit air angle.

Predicted airfoil pressure distributions were in good agreement with measured distributions for both the cooled and uncooled vane and blade cascades at subsonic exit Mach numbers. At supersonic exit Mach numbers, agreement for the blade cascades was fair due to data scatter in the airfoil flow recompression region. This was attributable to non-periodic shocks in the blade passage.

2.0 INTRODUCTION

The objective of the NASA Energy Efficient Engine Development and Integration program is to develop, evaluate, and demonstrate the technology for achieving lower installed fuel consumption and lower operating costs in future commercial turbofan engines. NASA has set minimum goals of 12 percent reduction in thrust specific fuel consumption (TSFC), 5 percent reduction in direct operating cost (DOC), and 50 percent reduction in performance degradation for the Energy Efficient Engine (flight engine) relative to the JT9D-7A reference engine. In addition, environmental goals on emissions (meet the proposed Environmental Protection Agency 1981 regulation) and noise (meet Federal Aviation Regulations 36-1978 standards) have been established.

The Pratt & Whitney Aircraft Energy Efficient Engine high-pressure turbine is a single-stage design. A single-stage design has certain advantages when compared to its multi-stage counterpart. Single stage turbines require no interstage seals, require fewer cooled airfoils, and contain fewer leakage paths. The inherent design simplicity of the single stage reduces engine intitial cost, maintenance material cost, and overall engine weight.

The purpose of the Energy Efficient Engine High-Pressure Turbine Supersonic Cascade Test Program was to (1) verify the benefits of vane endwall contouring in the high-pressure turbine component, (2) determine the performance penalties or benefits associated with the injection of coolant flow into the flow field surrounding the vane and blade airfoils, and (3) verify that the distribution of curvature selected for the component blade airfoil geometry achieves design performance objectives. An additional objective was to employ measured data to assess the accuracy of analytical methods and to gain a better understanding of the flow field within the cascade, particularly as it is affected by vane endwall contouring and shock-boundary layer interactions on the blade. The program was conducted to ensure timely interaction with the high-pressure turbine component effort, as shown in Figure 1.

To satisfy the objectives, two vane cascades and three blade cascades were designed and tested. The vane cascades comprised an S-wall cascade, which incorporated the same endwall shape envisioned for the component vane outer diameter platform, and a straight-wall cascade, which served as a baseline configuration for comparison. The blade cascades comprised three different airfoil geometries: (1) base, (2) overcambered, and (3) straightback. The base airfoil represented the component design; the overcambered airfoil featured more camber toward the trailing edge than the base design, and the straightback design featured a flatter suction surface downstream of the throat than the base design.

This report presents the program test procedures and results associated with the testing of these cascades. It is divided into two major sections; Section 3.0, which discusses the vane cascade program and Section 4.0, which discusses the blade cascade program. Section 5.0 contains the overall program conclusions.

ORIGINAL PAGE IS
OF POOR QUALITY

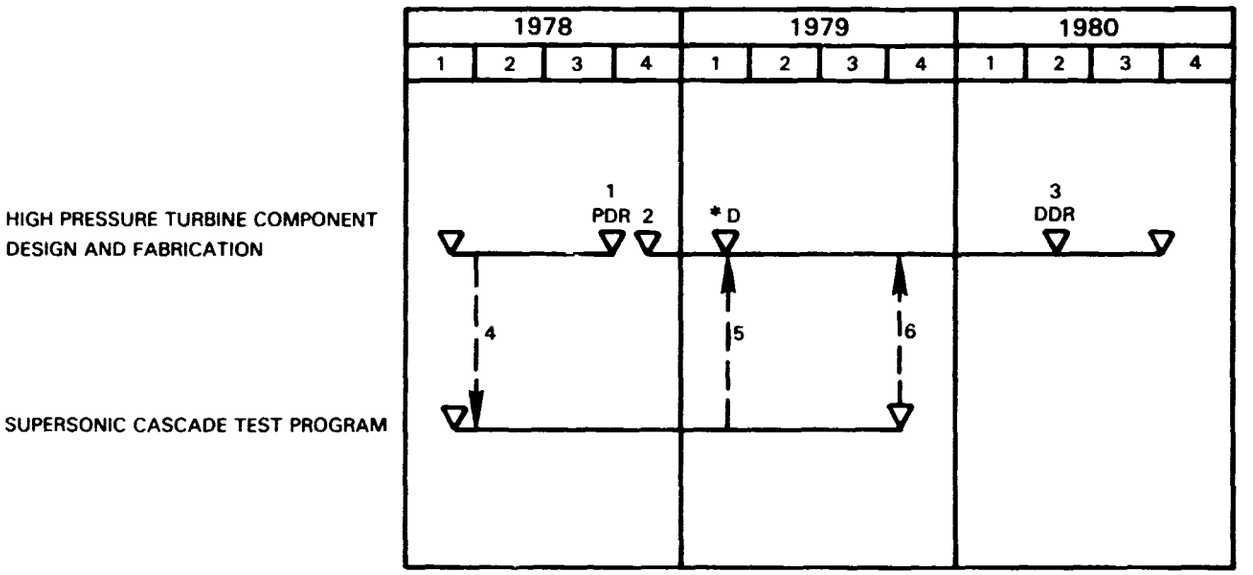

*D – CRITICAL DECISION POINT FOR SELECTION OF VANE & BLADE AERODYNAMICS
1 – COMPONENT PRELIMINARY DESIGN COMPLETED
2 – COMPONENT DETAILED DESIGNED INITIATED
3 – COMPONENT DETAILED DESIGN COMPLETED
4 – AIRFOIL SELECTION CRITERIA PROVIDED TO TEST PROGRAM FROM COMPONENT PRELIMINARY DESIGN EFFORTS
5 – BENEFITS OF S-WALL CONFIRMED, BASE BLADE AIRFOIL SHAPE CONFIRMED AS PROVIDING BEST PERFORMANCE
6 – VANE AND BLADE LOSS CHARACTERISTICS WITH COOLING FLOW VERIFIED

Figure 1 Supersonic Cascade Program Logic Diagram

ORIGINAL PAGE IS
OF POOR QUALITY

3.0 VANE CASCADE PROGRAM

3.1 Analysis and Design

Published literature along with Pratt & Whitney Aircraft cascade and engine test results have shown that turbine inlet vane losses can be reduced by contouring the outer diameter platform in the manner illustrated in Figure 2. This contouring reduces the vane inlet Mach number and reduces the diffusion on the suction side of the vane near the trailing edge; both of which can improve turbine performance through a reduction in secondary losses.(Deich et. al [1] and Ewen et. al [2]). Both report achieving increases in efficiency in rotating rigs attributed to endwall profiling.

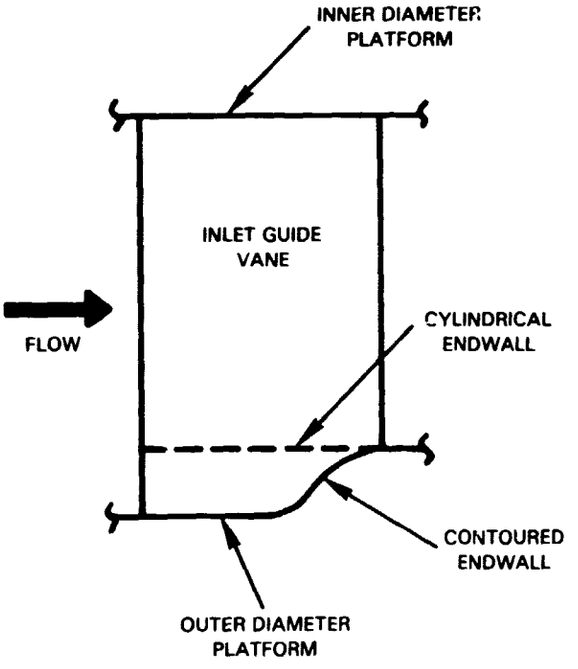

Figure 2 Schematic of Turbine Inlet Vane Endwall Contour

Previous research in the area of endwall profiling was conducted by Morris and Hoare [3], who investigated a linear cascade fitted with several different endwall geometries. This testing was conducted at an exit Mach number in the incompressible range and at a Reynolds number about an order of magnitude below that of typical commercial engine service conditions. Also, exit air angle data were not obtained so that mass averaged losses could not be properly determined at the measurement plane.

Since the Energy Efficient Engine high-pressure turbine component inlet guide vane is a high turning design employing a contoured endwall, as well as internal conductive and external film cooling, it was desirable to (1) verify the expected performance benefit associated with the contoured endwall and (2) determine the performance penalty associated with the injection of coolant flow into the flow field surrounding the airfoil.

ORIGINAL PAGE IS
OF POOR QUALITY

An additional objective was to employ measured data to assess the accuracy of analytical methods and to gain a physical understanding of the effect of endwall profiling on the vane cascade intra-passage flow field. These methods range from secondary loss correlations to the numerical modeling of the three-dimensional inviscid flow field.

To satisfy this objective, two vane cascades were designed: (1) an S-wall cascade, which incorporated the same endwall shape envisioned for the high-pressure turbine component vane outer diameter platform and (2) a straight wall cascade, which served as a baseline configuration for comparison. Flowpaths for these cascades are compared in Figure 3. To conduct the cooling flow tests, the airflow in the straight wall cascade was designed to incorporate internal flow passages (see Figure 7(b)).

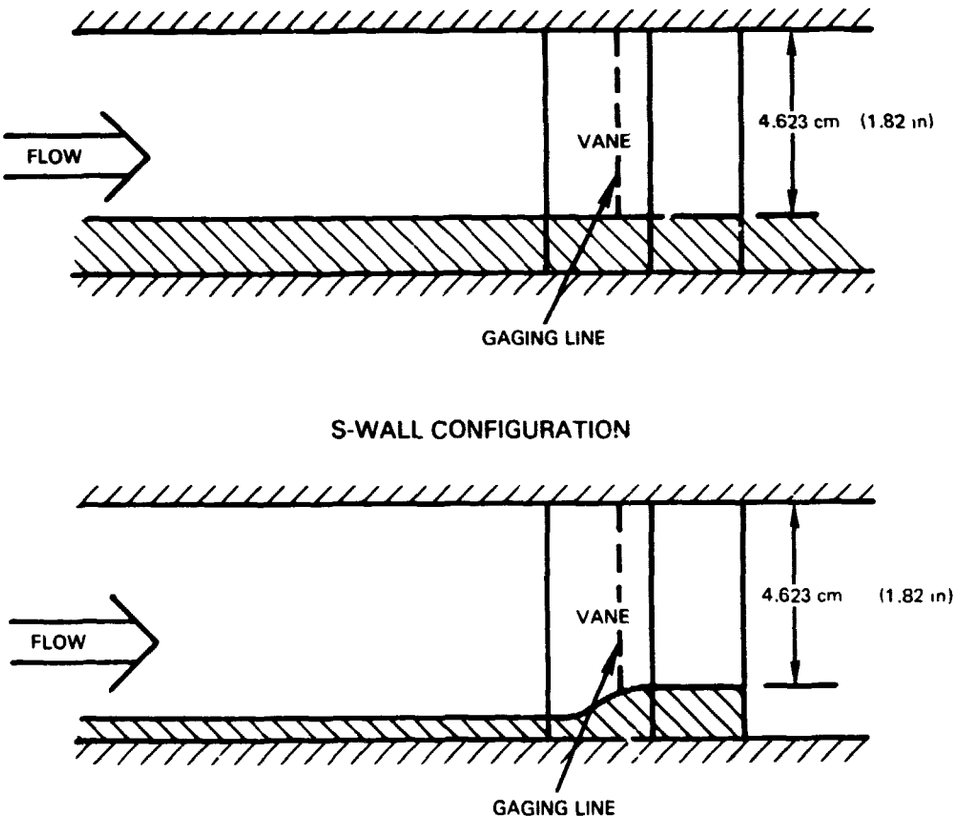

Figure 3 Straight Wall and S-Wall Cascade Configurations

ORIGINAL PAGE IS
OF POOR QUALITY

The aspect ratio of each configuration, based on axial chord, equaled the 1.4 aspect ratio of the corresponding vanes for the high-pressure turbine component. The tip section airfoil geometry from a 43 percent reaction design was selected because the effects of the flow characteristics at the vane airfoil outer diameter platform intersection were of primary interest. The 43 percent reaction level was chosen for the cascades because component design studies had shown this high reaction to provide slightly better performance than a lower reaction design. Both cascades used this same untwisted spanwise section geometry, as shown in Figure 4. Refer to Appendix A for a listing of the airfoil coordinates used for the S-wall cascade (Table A-1) and the straight wall cascade (Table A-2).

43 PERCENT REACTION TIP SECTION

	S-WALL		STRAIGHT WALL	
AXIAL CHORD ~ CM (IN)	3.340	(1.315)	3.465	(1.364)
PITCH ~ CM (IN)	8.466	(3.333)	8.466	(3.333)
THROAT ~ CM (IN)	1.425	(0.561)	1.516	(0.597)
LEADING EDGE RADIUS ~ CM (IN)	0.523	(0.206)	0.523	(0.206)
TRAILING EDGE RADIUS ~ CM (IN)	0.053	(0.021)	0.053	(0.021)
INLET METAL ANGLE (DEG)		90.00°		89.33°
INLET WEDGE ANGLE (DEG)		90.00°		90.00°
EXIT METAL ANGLE (DEG)		10.43°		11.10°
EXIT WEDGE ANGLE (DEG)		4.00°		4.00°
UNCOVERED TURNING* (DEG)		12.00°		11.73°
ACTUAL CHORD ~ CM (IN)	9.012	(3.548)	9.012	(3.548)

*NOTE:
THE STRAIGHT WALL VANE IS ROTATED OPEN 0.67°

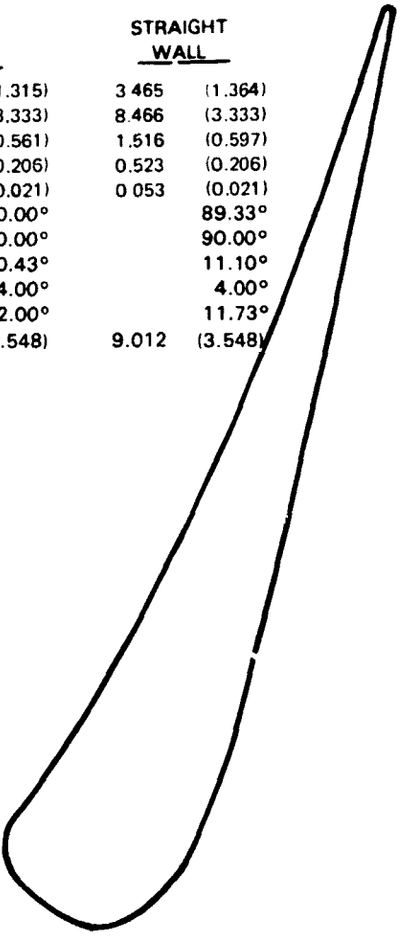

Figure 4 Vane Cascade Geometry

ORIGINAL PAGE IS
OF POOR QUALITY

Meanline analysis was performed to optimize the turbine configuration. Primary considerations during the meanline analysis were inlet and exit Mach triangles and gas turning angles. A streamline analysis was subsequently employed to generate radial profiles. This analysis utilized both twoand three-dimensional analytical procedures to produce suitable airfoil pressure distributions. The analysis also determined the radial distribution of aerodynamic properties. Boundary layer calculations were then used to verify the loss characteristics of the airfoils. Through this approach, criteria were established for the design of both cascades.

The vane airfoil sections were designed so that the flow was accelerated past the gage point (throat) with low, smooth backend diffusion. The uncovered turning and exit wedge angle were optimized to minimize the two-dimensional loss. An iterative procedure using a computer interactive airfoil design system was used to design the external contours of the airfoils and to establish the desired airfoil static pressure distribution.

The predicted pressure distribution for each cascade at 50-percent span and the pressure distribution at the vane tip section of the high-pressure turbine component (for reference) are presented in Figure 5. The vanes of the straight wall cascade were rotated open to provide the cascade with an exit air angle equal to the S-wall cascade. This approach permitted a one-to-one comparison of the exit flow conditions. Each cascade was limited to three airfoils to ensure proper fit in the cascade tunnel. Flow uniformity from airfoil passage to passage (periodicity) was achieved with these three airfoils by contouring the sidewalls to match the applicable flow streamline as established by potential flow computations. In addition, the sidewalls were adjustable to permit minor periodicity adjustments once the cascade was installed in the tunnel (see Figure 6).

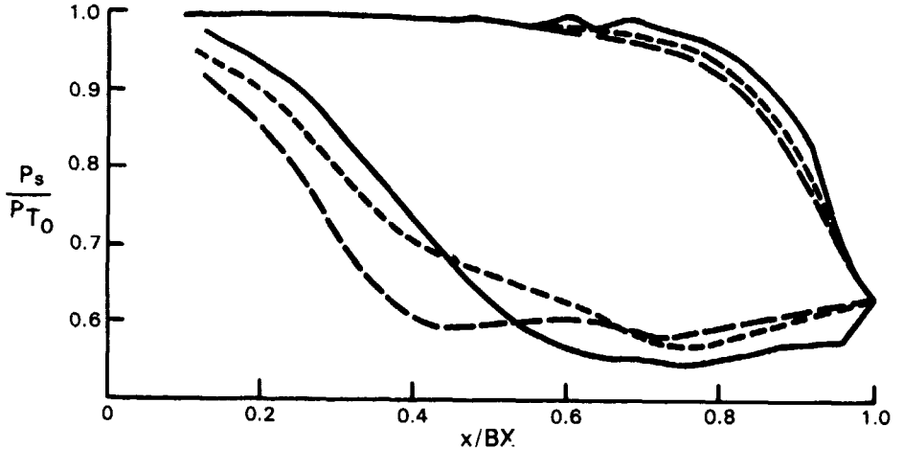

CASCADE AERODYNAMICS

	MACH NO. IN	MACH NO. OUT	AIR ANGLE IN	AIR ANGLE OUT	MAX MACH NO.
ENGINE (HPT COMPONENT)	.070	.84	90.00°	10.43°	.98
S-WALL CASCADE	.082	.84	90.00°	10.43°	.95
STRAIGHT WALL CASCADE	.100	.84	90.00°	10.43°	.92

Figure 5 Comparison of Pressure Distributions

ORIGINAL PAGE IS
OF POOR QUALITY

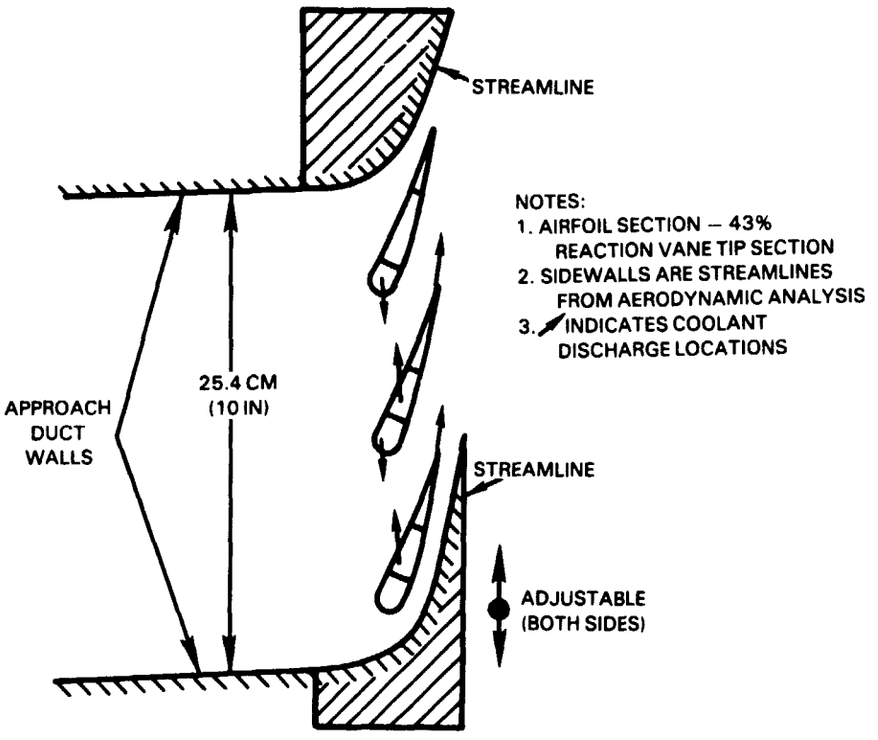

Figure 6 Cascade Configuration

To understand how cooling air affects performance, the flow rate for each cooling site must be accurately known. When one plenum feeds several cooling sites, it is not always possible to control the cooling flow split to within desired limits. Therefore, in this cascade design each cooling site was metered by a separate plenum. Two changes to the internal cooling flow passage scheme envisioned for the high-pressure turbine component vane, shown in Figure 7(a) were necessary to execute this approach: (1) the showerhead cooling holes were eliminated, and (2) the pressure side film cooling was "combined" at one injection site instead of being separately metered (see Figure 7 (b)). The reason for the first change is that it was mechanically impossible to properly meter both the showerhead and the suction side cooling film. Since showerhead losses are considered unimportant relative to suction side losses, showerhead holes were eliminated. The pressure side film cooling was combined because its rear set of film holes were too near the trailing edge to permit each site to be independently metered. Details of the cooling geometry are presented in Table 1.

ORIGINAL PAGE IS
OF POOR QUALITY

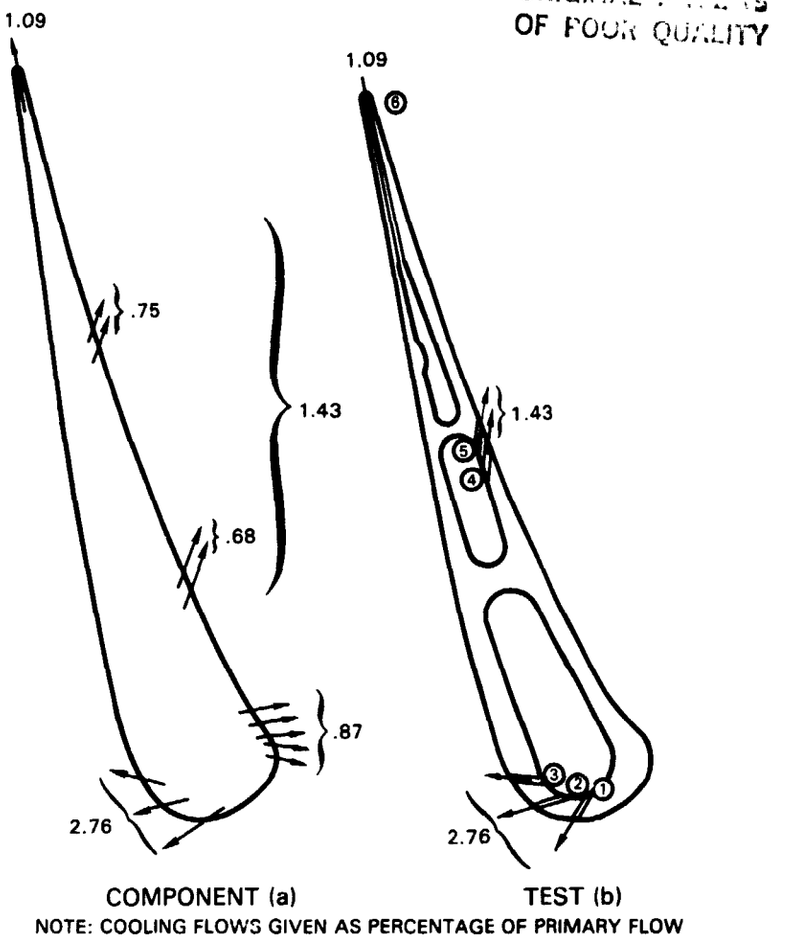

Figure 7 High-Pressure Turbine Blade Cooling Model

TABLE 1

VANE COOLING GEOMETRY

Row	Location	X/BX	No. Holes	Hole Dia. cm (in.)
1	SS	0.028	36	0.06 (0.025)
2	SS	0.042	36	0.06 (0.025)
3	SS	0.052	36	0.06 (0.025)
4	PS	0.52	25	0.08 (0.032)
5	PS	0.60	25	0.08 (0.032)
6	TE	1.00	40	0.05 (0.021)

SS - suction surface
PS - pressure surface
TE - trailing edge

ORIGINAL PAGE
BLACK AND WHITE PHOTOGRAPH

3.2 Fabrication and Assembly

The cascade models were prepared for test by standard fabrication and assembly techniques. The models were fabricated from stainless steel, and were provided with instrumentation to allow achieving test objectives.

Each vane cascade consisted of three constant section untwisted airfoils, which were welded to the endwalls. The complete assembly was in turn mounted in the test section. The passages for the coolant flows were generated by standard machining techniques. Electro-discharge machining was used for some of the smaller passages. The fully-instrumented straight wall vane cascade pack is shown in Figure 8.

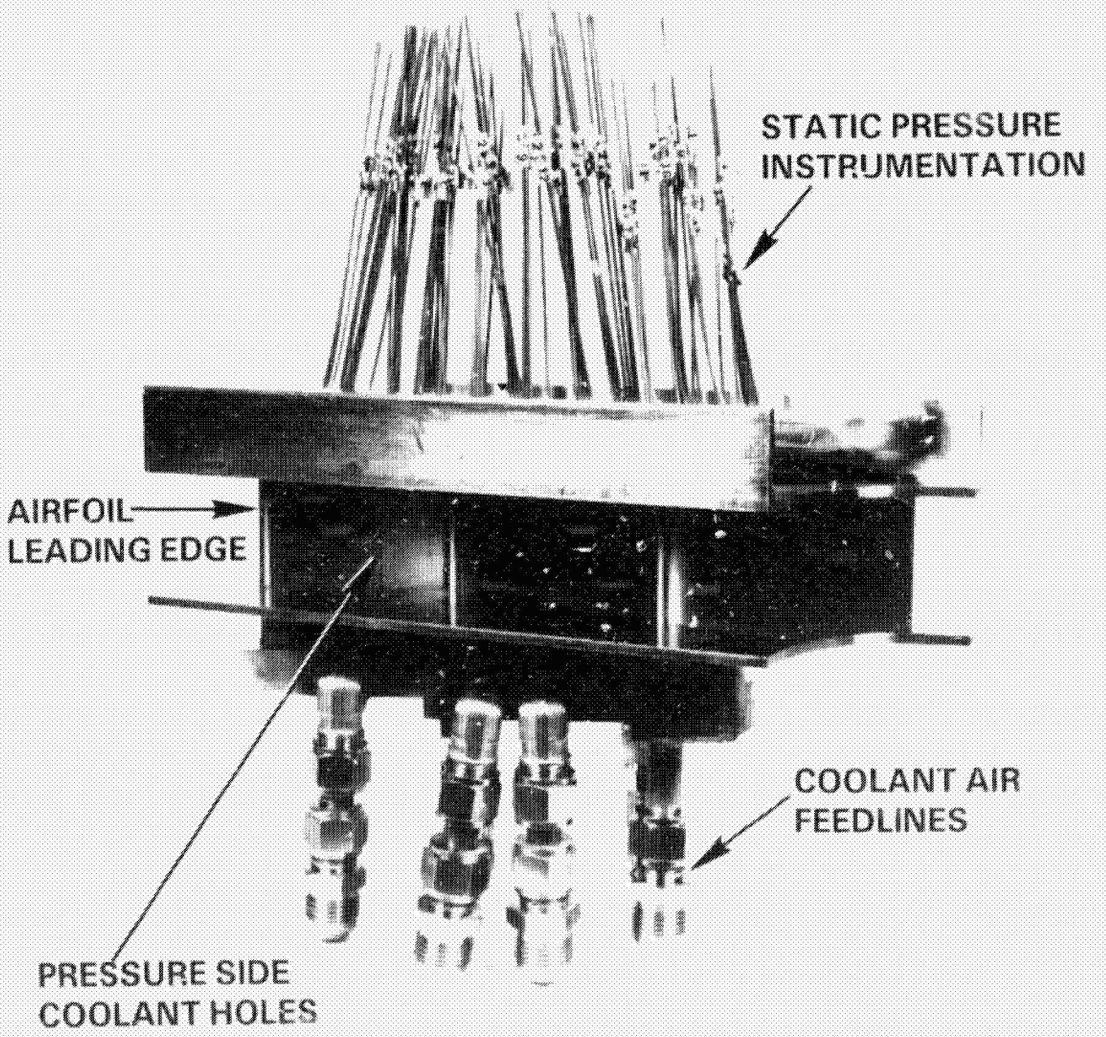

Figure 8 High-Pressure Turbine Assembled Straight Wall Vane Cascade Before Installation in Test Tunnel

3.3 Testing

3.3.1 General Description

The vane cascade test program examined two important aspects of the vane component design: (1) endwall configuration and (2) cooling flow arrangement. In the endwall evaluation, the straight wall and the S-wall cascades were tested to compare the relative performance of these endwall configurations. The cooling flow tests were conducted to assess the total pressure loss penalty associated with cooling air introduction (separate and combined) at the pressure and suction surfaces and at the trailing edge of the vane airfoils.

3.3.2 Test Facility and Instrumentation

3.3.2.1 Test Facility

The Pratt & Whitney Aircraft Plane Cascade Wind Tunnel (Test Stand X-32) is a steady flow tunnel consisting of a large plenum, test section, and discharge cell. Figure 9 presents a schematic representation of this facility. The primary airflow enters the plenum chamber and is discharged against the plenum endwall. The flow subsequently passes through a honeycomb flow straightener and fine mesh screens, which remove swirl and make the flow uniform before it enters a rectangular bellmouth to the cascade approach duct. After passing through the cascade, the air discharges to the test cell, which is maintained at atmospheric pressure. Cascade incidence air angles are set by rotating the cascade assembly relative to the direction of the airflow in the approach duct.

A square bar grid was placed in the duct downstream of the bellmouth entrance in order to increase the turbulence in the flow, thus minimizing any potential flow separation within the cascade. For this configuration, the predicted free stream turbulence level (u'/u) was 2.7 percent at the entrance to the cascade 17 inches downstream of the grid. Hot wire measurements were taken at this location, without a span reducing sideplate and at a Mach number of 0.1, corresponding to that encountered in the cascade testing. The measured value of 2.6 percent u'/u was in excellent agreement with the prediction. Installation of span reducing sideplates employed in the testing produced an area contraction ratio of approximately 1.5 downstream of the grid, causing a reduction of free stream turbulence into the cascade. This contraction was calculated to reduce the turbulence level from 2.6 to 1.8 percent.

3.3.2.2 Instrumentation

The vane cascade was equipped with endwall static pressure taps to obtain data on endwall cross-passage pressure gradients (see Figure 10). Because the straight wall cascades were symmetrical about the 50 percent span location, only one of the endwalls required static pressure taps. The asymmetrical S-wall cascade, however, required taps on both endwalls. The center airfoil of the straight wall cascade was provided with pressure taps as shown in Figure 11. The airfoils on each side were provided with pressure taps on the side bordering a full passage and at the trailing edge. The center airfoil of the S-wall cascade was equipped with static taps as shown in Figure 12. As with the straight wall cascade, airfoils on either side had static taps on the side bordering a full vane passage.

ORIGINAL PAGE IS
OF POOR QUALITY

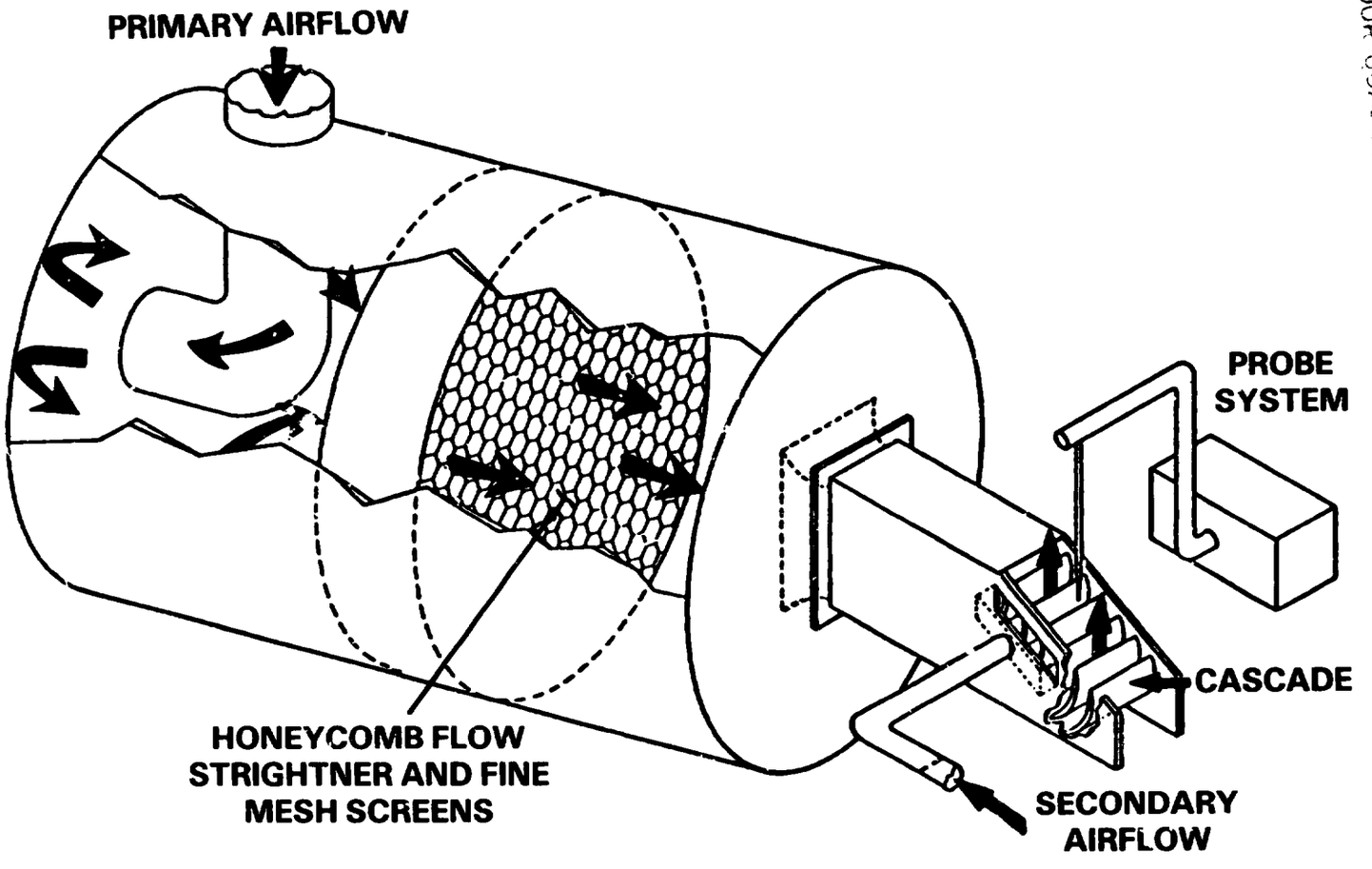

Figure 9 High-Pressure Turbine Vane Cascade Test Facility

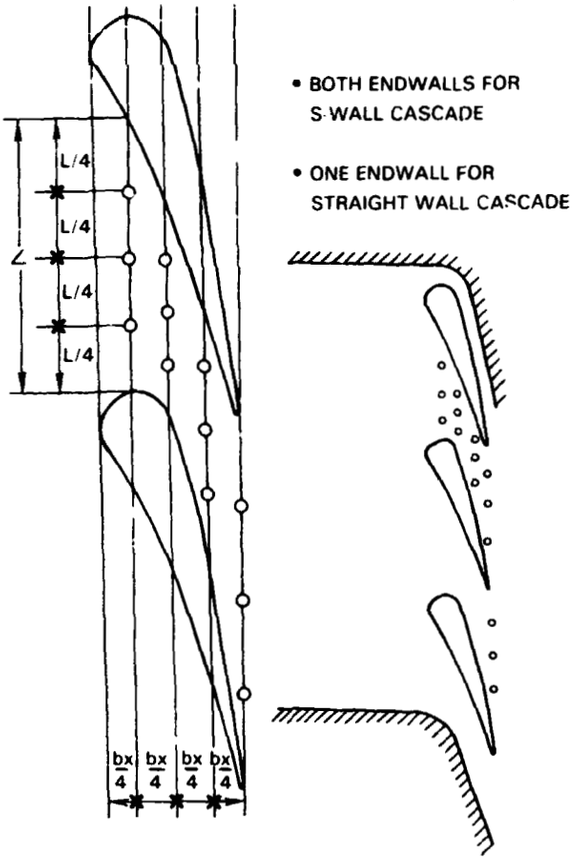

Figure 10 High-Pressure Turbine Vane Cascade Endwall Static Pressure Tap Locations

The instrumentation employed for vane cascade testing is presented in Table 2.

Both the cone probe and the cobra probe were run in a free jet calibration facility to develop calibration curves for total pressure, static pressure, yaw angle, and pitch angle (5-port combination probe only). This calibration was conducted at approximately the same unit Reynolds number as the cascade exit flow and over the range of Mach numbers and angles required for the testing.

TABLE 2

VANE TEST PROGRAM INSTRUMENTATION

Location	Measurement	Type	Quantity
Tunnel Plenum	Total Temperature	Thermocouple	1
	Total Pressure	Kiel Probe	1
Approach Duct	Static Pressure	Static Taps	3
Discharge Cell	Barometric Pressure	Barometer	1
Coolant Supply (each injection site)	Flow Rate	Rotameter	1
	Total Pressure	Pitot Probe	1
	Total Temperature	Thermocouple	1
Survey Plane Downstream of Cascade	Total Pressure	Cone Probe (1)	1
	Static Pressure	Cobra Probe (2)	1
	Yaw Angle		
	Pitch Angle		
Vane Surfaces (Straight Endwall Cascade)	Static Pressure	Static Taps	25
Vane Endwalls (Straight Endwall Cascade)	Static Pressure	Static Taps	15
Vane Surfaces (S-Wall Cascade)	Static Pressure	Static Taps	56
Vane Endwalls (S-Wall Cascade)	Static Pressure	Static Taps	30

(1) The cone probe is a 5-port combination probe used to obtain measurements of total pressure, static pressure, and pitch and yaw angles over most of the traverse plane. This probe has a stem diameter of 3.97 mm (0.156 in.) and a conical tip with a 70-degree included angle.

(2) The cobra probe consists of three capillary tubes brazed in parallel. It was used to measure flow conditions close to the endwalls (i.e., within the boundary layer).

ORIGINAL PAGE IS
OF POOR QUALITY

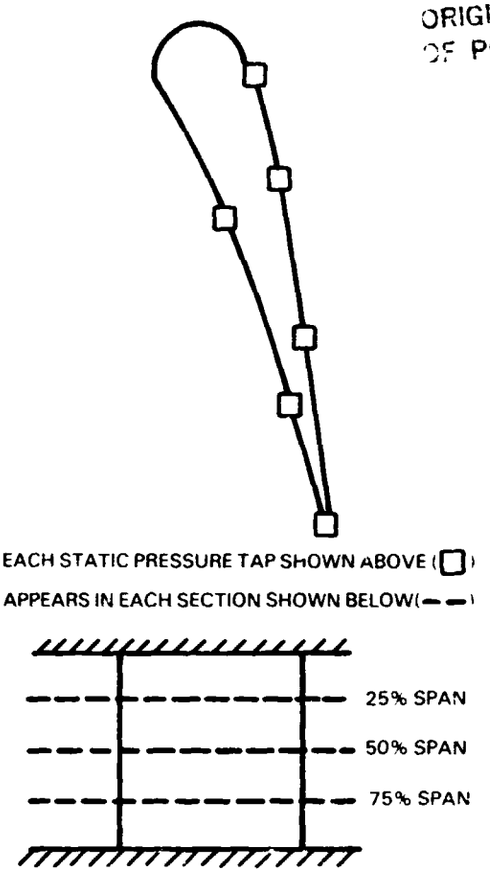

Figure 11 High-Pressure Turbine Straight Wall Vane Cascade Static Pressure Tap Locations

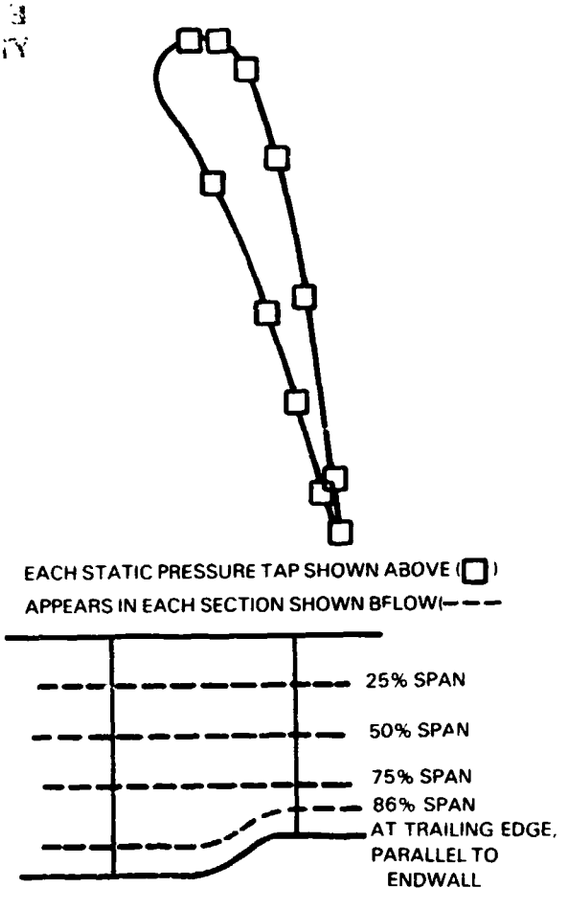

Figure 12 High-Pressure Turbine S-Wall Vane Cascade Static Pressure Tap Locations

3.3.3 Test Procedures

3.3.3.1 Establishing Test Conditions

Test conditions were established to provide nominal exit Mach numbers equal to the design point exit Mach numbers of 0.84 and 0.92 for the component vane tip and mean sections, respectively. These Mach numbers were obtained by setting exit static-to-inlet pressure ratios of 0.63 (Mn 0.84) and 0.58 (Mn 0.92). The main stream total temperature was a nominal 65°C (150°F). Since the flow exited to atmospheric pressure, the total pressure approaching the cascade was in the range of 20,685 to 89,635 pa (9 to 13 psig). The expansion ratios of 0.63 and 0.58 were calculated to yield Reynolds numbers of 6.0×10^5, and 7.0×10^5, based on exit flow conditions and on airfoil axial chord. Design point coolant flow rates are summarized in Table 3 (see also Figure 7-b).

TABLE 3

DESIGN POINT COOLANT FLOW RATES

Location	Coolant Flow Rate (percent mainstream flow)
Suction Surface	2.76
Pressure Surface	1.43
Trailing Edge	1.09

Endwall boundary layer characteristics entering the cascade were determined by measurements taken at a location in the approach duct 2.54 cm (1 in.) in front of the leading edge plane of the cascade. These data were necessary to fully characterize the conditions at the inlet to the cascade. Data were obtained for the range of Mach numbers and Reynolds numbers to be encountered during testing. A cobra probe was used to obtain these data. Integral boundary layer parameters were determined for the measured velocity profiles and were found to be in reasonable agreement with those calculated using a well-accepted formulation for the development of a zero pressure gradient fully turbulent boundary layer originating at the grid. Interpolation between the measured data was subsequently used to obtain the inlet displacement and momentum thicknesses for the two cascades at their respective test point conditions. These are given in Table 4. For the endwall comparison, full passage exit plane surveys and surface static pressure data were obtained for each cascade at a nominal exit isentropic Mach number of 0.85. Table 5 presents the measured test conditions for each cascade. These conditions are representative of altitude cruise conditions for the high-pressure turbine component design.

TABLE 4

INLET BOUNDARY LAYER PARAMETERS

	Straight Wall Cascade	S-Wall Cascade
Displacement Thickness	0.117 cm (0.046 in.)	0.124 cm (0.049 in.)
Momentum Thickness	0.089 cm (0.035 in.)	0.092 cm (0.036 in.)
Momentum Thickness Reynolds No.	2900	2500
Displacement Thickness/Chord	0.0130	0.0138

TABLE 5

TEST CONDITIONS

	Straight Wall Cascade	S-wall Cascade
Isentropic Exit Mach No.	0.849	0.845
Upstream Air Angle (α_1)	90 degrees	90 degrees
Upstream Mach No.	0.109	0.091
Reynolds No. $(Re)_{BX}$	6.41×10^5	7.00×10^5
Upstream Total Pressure	160,653pa(23.29PSIA)	162,032pa(23.53PSIA)
Total Temperature	624^oR (347^oK)	574^oR (319^oK)

3.3.3.2 Shakedown Testing

Shakedown testing consisted of pressure leak checks and calibration of all instrumentation before performance testing was initiated. A preliminary data point was run to verify performance of the instrumentation and data acquisition systems. The performance test program was initiated after it was ascertained that all instrumentation and systems were operating properly.

3.3.3.3 Performance Testing

The vane cascade test program was structured to permit separate performance evaluations of (1) endwall configurations (S-wall and straight wall cascades) and (2) cooling flow effects (i.e., performance effects of the three areas of cooling flow injection: trailing edge, suction surface, and pressure surface). The tests conducted to evaluate performance focused on total pressure loss, airfoil pressure distribution, and exit angle.

Wake traverse data were used to assess cascade performance in terms of total pressure loss. These traverses were made 1.02 cm (0.4 in.) downstream of the trailing edge. The 5-port combination probe was used to obtain measurements of total pressure, static pressure, and pitch and yaw angles over most of the traverse plane. This probe was traversed in the pitchwise direction at a constant span height taking measurements at 0.15 cm (0.060 in.) increments. Yaw angles (angles in plane parallel to endwalls) were obtained by nulling the probe aerodynamically to within one degree and then employing calibration curves. The probe drive axis of rotation passed through the tip of the probe. Pitch angles were obtained for the 5-port combination probe through the calibration curves. Each full passage exit survey nominally consisted of 35 pitchwise traverses covering the full span of the cascade.

For the coolant injection tests, air was metered to the vane plenums. Coolant total pressure, total temperature, and flow rate were measured.

3.3.4 Performance Test Plan

The test plan for the vane cascade tests is shown in Table 6. This plan was formulated to meet the following test objectives:

- o Establish the performance in terms of total pressure loss and exit angle for the S-wall configuration relative to the straight wall cascade, and
- o Establish the total pressure loss penalty associated with coolant injection at different locations in the vane (separate and combined injection).

3.3.5 Data Reduction and Analysis

The data acquisition sequence for the vanes is presented in Table 7.

The data analysis methods for the vanes are:

1. Comparison of the static pressure distribution between the S-wall and straight wall configurations.
2. Comparison of measured airfoil static pressures with analytical predictions.
3. Comparison of the full passage performance, in terms of total pressure loss and exit air angle, between the S-wall and straight wall con- figurations.
4. Comparison of total pressure losses with analytical predictions (with and without coolant ejection).
5. Determination of the performance sensitivity to cooling flow rate variations.
6. Determination of the performance sensitivity to exit Mach number variations.

3.3.6 Experimental Uncertainty

Experimental uncertainties for the results obtained are estimated to be ± 0.02 P/P_T for surface static data; ± 0.4 degree for gap average mass weighed exit air angle (α_2) and ± 0.02 for the gap average exit Mach number. Mass averaged total pressure loss results are estimated to be accurate within +5 percent to -8 percent $\Delta P_T/P_T$ inside the profile loss region and +10 percent to -14 percent $\Delta P_T/P_T$ inside the secondary loss region.

3.4 Results

The analysis of the vane cascade data was divided into two areas (1) uncooled cascade tests and (2) cooling flow discharge tests. The results of this analysis are discussed in the following sections.

TABLE 6

VANE CASCADE TEST PLAN

Test	Endwall Shape	Exit Mach No.	Expansion[1] Ratio	Cooling	Data Scan
1	Straight	0.84	0.63	No coolant ejection	Full passage exit plane survey
2	Straight	0.88	0.66	No coolant ejection	Mid-span exit plane survey
		0.92	0.58		
		0.96	0.55		
3	Straight	0.84	0.63	Trailing edge, pressure side and suction side ejection at design point coolant flow rate	Full passage exit plane survey
4	Straight	0.84	0.63	Trailing edge ejection at design point coolant flow rate	Mid-span exit plane survey
5	Straight	0.84	0.63	Pressure side ejection at 70, 100, and 130 percent of design point coolant flow rate	Mid-span exit plane survey
6	Straight	0.84	0.63	Suction side ejection at 70, 100, and 130 percent of design point coolant flow rate	Mid-span exit plane survey
7	Straight	0.92	0.58	Suction side ejection at 70, 100, and 130 percent of design point coolant flow rate	Mid-span exit plane traverse
8	S-wall	0.84	0.63	No coolant ejection	Full passage exit plane survey

(1) Ratio of Exit Static to Inlet Total Pressure.

TABLE 7

DATA ACQUISITION SEQUENCE (VANES)

Sequence	Data Obtained
1. Apply known pressures to transducers	Transducer calibration
2. Set cascade expansion ratio	None
3. Set coolant flow rates	Primary flow inlet total pressure Primary flow temperature Cell static pressure Airfoil static pressures Endwall static pressures Coolant flow rates Coolant total pressures
4. Program probe controller and start data acquisition sequence	Flow field exit traverse for local total pressure, static pressure, pitch angle, and yaw angle
5. Check cascade expansion ratio and coolant flow rates; to be repeated periodically during data acquisition sequence	Check for drift of test conditions; test ended if significant drift occurs
6. After test is completed, repeat (1)	Check of transducer calibration; repeat test if calibration has drifted.

3.4.1 Flow Visualization

Before the start of performance testing, surface flow visualizations were conducted for both cascades to assess the behavior of the limiting streamlines and to establish whether there were any flow separation problems. These flow visualizations were made by applying a mixture of lampblack and oil to the airfoil and endwall surfaces and subsequently operating the cascade tunnel at test point conditions for approximately one minute. Figure 13 presents the flow visualization achieved for the straight wall cascade viewed from upstream. Figure 14 shows the S-wall cascade viewed from downstream. Both cascades exhibited the same qualitative features found in previous testing of a large scale cascade of turbine airfoils.

ORIGINAL PAGE IS
OF POOR QUALITY

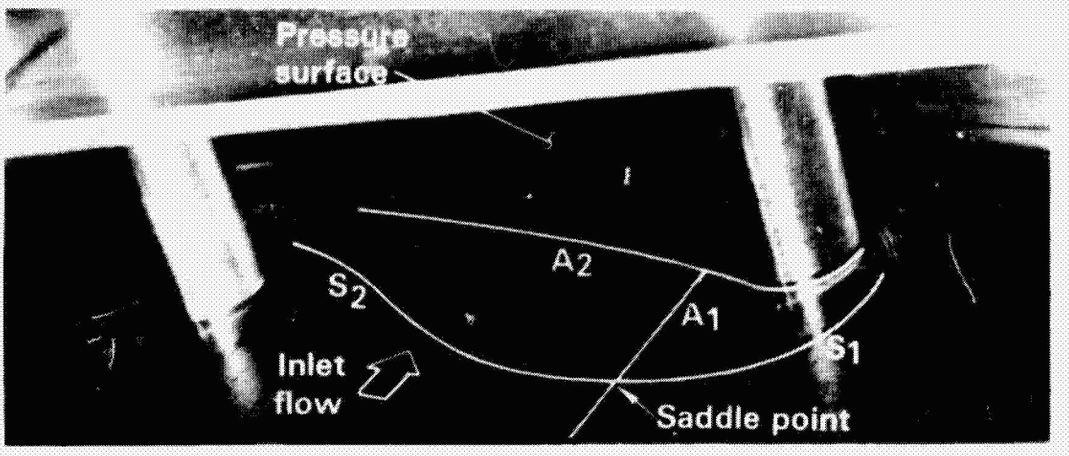

Figure 13 Straight Wall Cascade Flow Visualization Viewed from Upstream

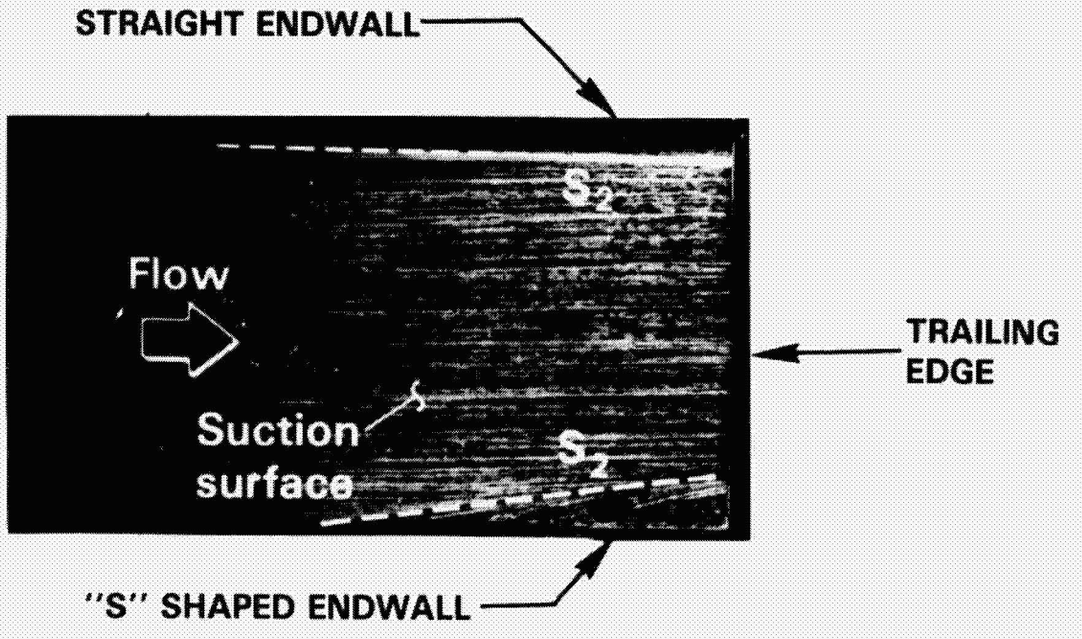

NOTE: LINES S_2 ARE PASSAGE VORTEX SEPARATION LINES

Figure 14 S-Wall Cascade Flow Visualization Viewed from Downstream

ORIGINAL PAGE
BLACK AND WHITE PHOTOGRAPH

ORIGINAL PAGE IS
OF POOR QUALITY

The features of a three-dimensional separation at the cascade inlet are shown in Figure 13. Here, the inlet boundary layer is seen to separate along lines S_1 and S_2 to form a "horseshoe" shaped vortex containing the low momentum boundary layer fluid (see Figure 15). The leg corresponding to S_1 gets wrapped around the suction surface of the airfoil to form what has been called the "counter vortex," while the leg corresponding to S_2 moves toward the suction surface of the adjacent airfoil to form the passage vortex. The new boundary layer formed within the region bounded by separation line S_2 and attachment lines A_1 and A_2 is swept toward the suction surface of the adjacent airfoil by the cross channel pressure gradient. This low momentum fluid subsequently contributes to the growth of the passage vortex, making it the dominant feature of cascade secondary flow. Toward the rear of the airfoil, separation line S_2 moves onto the suction surface of the adjacent airfoil as can be seen in Figure 14 of the cascade exit plane.

From the flow visualizations of the rear of the suction surface, the straight wall cascade features were found to be symmetric about midspan; those of the S-wall cascade were slightly asymmetric (see Figure 14), which is to be expected. In particular, the passage vortex separation line alongside of the straight wall was found to be closer to the endwall than the opposing S-wall side (approximately 5.08 mm (0.20 in.) at the trailing edge of the straight wall side compared to 6.35 mm (0.25 in.) for the S-wall side). This distance was found to be approximately 6.35 mm (0.25 in.) for both sides of the straight wall cascade.

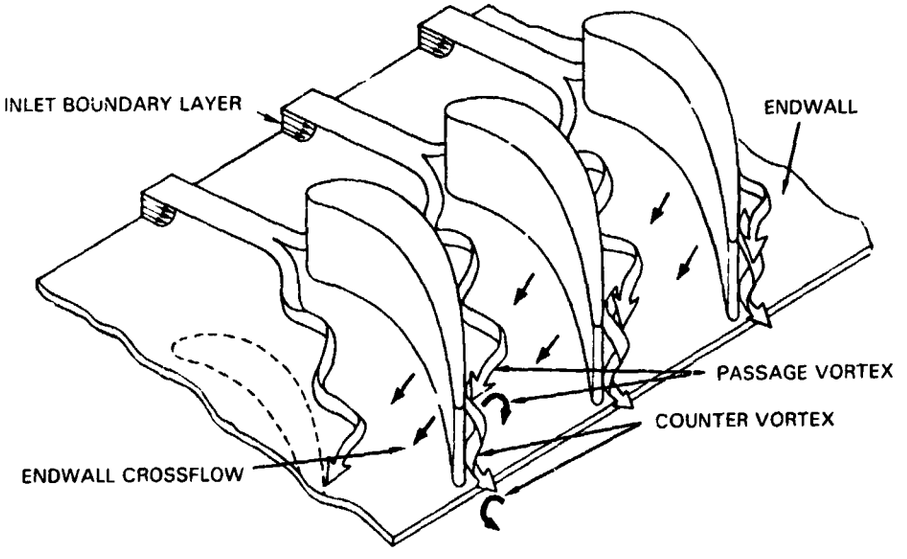

Figure 15 Cascade Secondary Flow Schematic

3.4.2 Periodicity Evaluation

To achieve a good cascade performance evaluation, it is important that the flow characteristics within adjacent vane passages (see Figure 16) be as nearly identical as possible. That is to say good periodicity must be achieved. To assess the passage flow characteristics, static pressure data were obtained on adjacent airfoils in each cascade. Airfoil-to-airfoil comparison of these data were used to established periodicity within the cascade before any performance testing was conducted. As can be seen by the pressure distribution data in Figures 17 and 18 (which are representative of the other spanwise measurements taken), both the straight wall and the S-wall cascades showed excellent agreement between the passage readings corresponding to the adjacent flow passages, indicating that excellent periodicity was attained.

3.4.3 Pressure Distribution Analysis

Static pressure data were also obtained for each cascade at the cross-channel locations identified in Figure 10 and spanwise locations identified in Figures 11 and 12. (See Section 3.3.2.2, Instrumentation). These data verified the prediction techniques used to calculate the flow within the cascade.

Cross-channel static pressure measurements obtained at one endwall of the straight wall cascade are shown in Figure 19 along with the predicted results from a two-dimensional compressible potential flow calculation.

The asymmetric geometry of the S-wall cascade produces a three-dimensional flow field. Consequently, the two-dimensional prediction method employed for the S-wall cascade was replaced with a three-dimensional inviscid flow field calculation method. This method was used to predict the cross-channel and spanwise pressure distributions in the S-wall cascade. Cross-channel data were taken on both the straight wall and S-wall, and spanwise data were recorded at the spanwise locations shown in Figure 12. Results are presented in Figures 20 through 23.

The three-dimensional effects of the S-wall are most noticeable by comparing the cross-channel data in Figures 19 and 20. The effect of the S-wall on the straight endwall is to decrease the maximum Mach number on the suction surface and shift its location from approximately 50 percent chord to 70 percent chord. These factors contribute to a reduction in the endwall cross-channel pressure gradient with a subsequent reduction in secondary loss. (See section 3.4.4.1.2 for a more detailed discussion.) Overall, there is good agreement between the test data and the predictions.

3.4.4 Uncooled Cascade Results

Uncooled cascade test data were analyzed with regard to making a comparison between the straight wall design and the S-wall design. In addition, the performance of the straight wall cascade was assessed in terms of exit Mach number variations.

ORIGINAL PAGE IS
OF POOR QUALITY

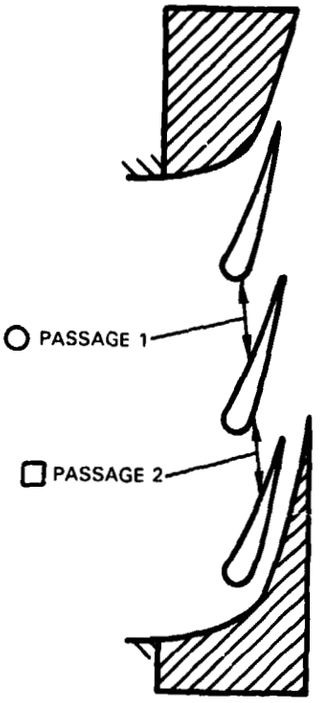

Figure 16 Cascade Flow Passages

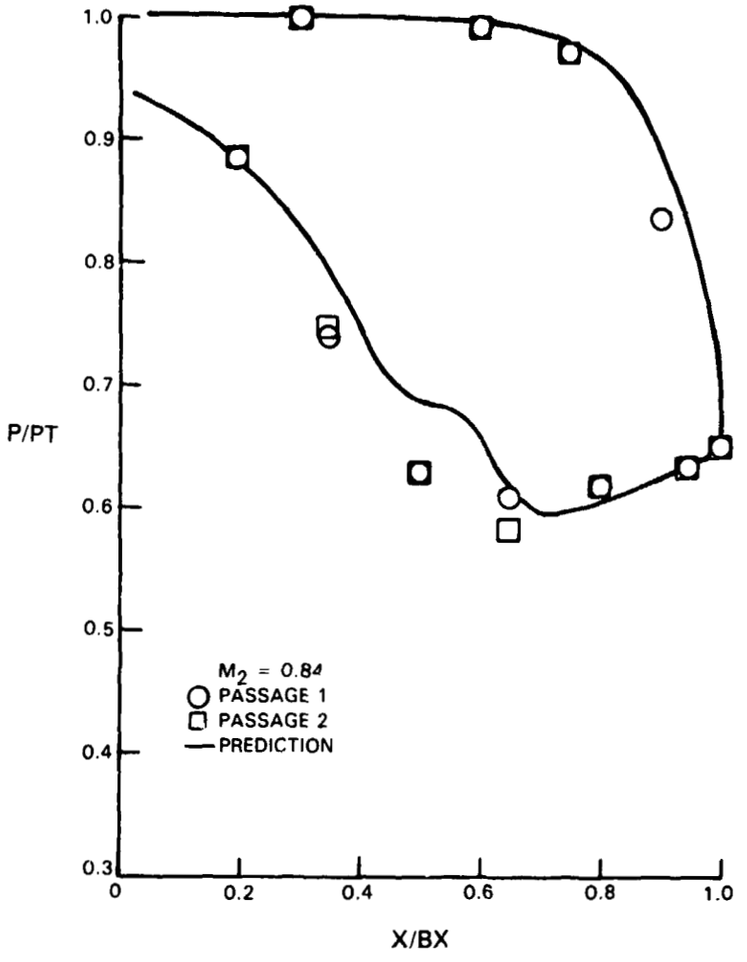

Figure 17 S-Wall Cascade Mid-Span Pressure Distribution Periodicity Evaluation

ORIGINAL PAGE IS
OF POOR QUALITY

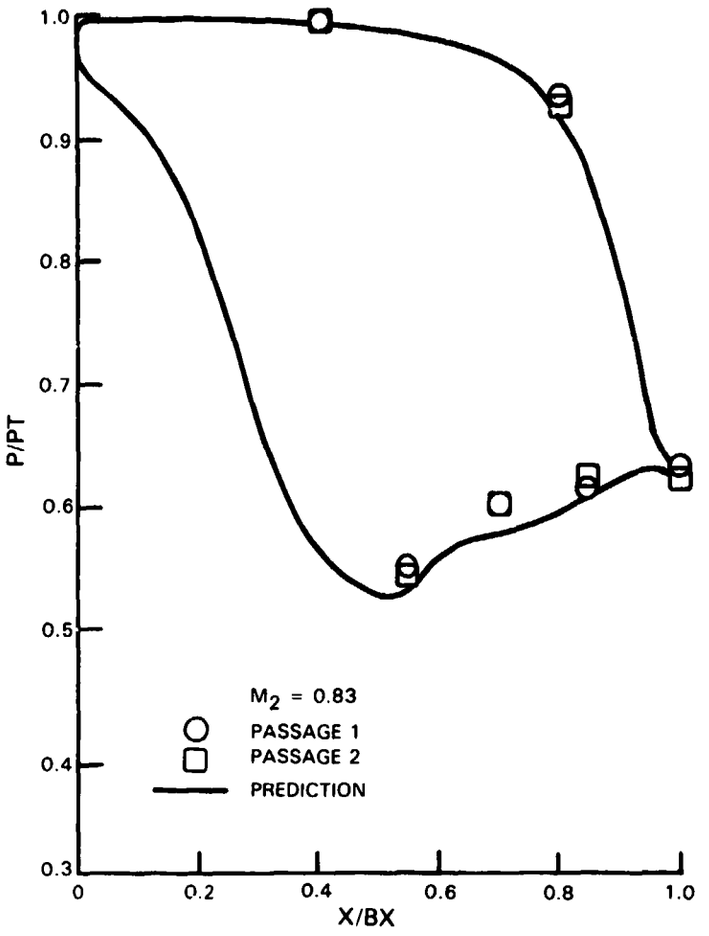

Figure 18 Straight Wall Mid-Span Pressure Distribution Periodicity Evaluation

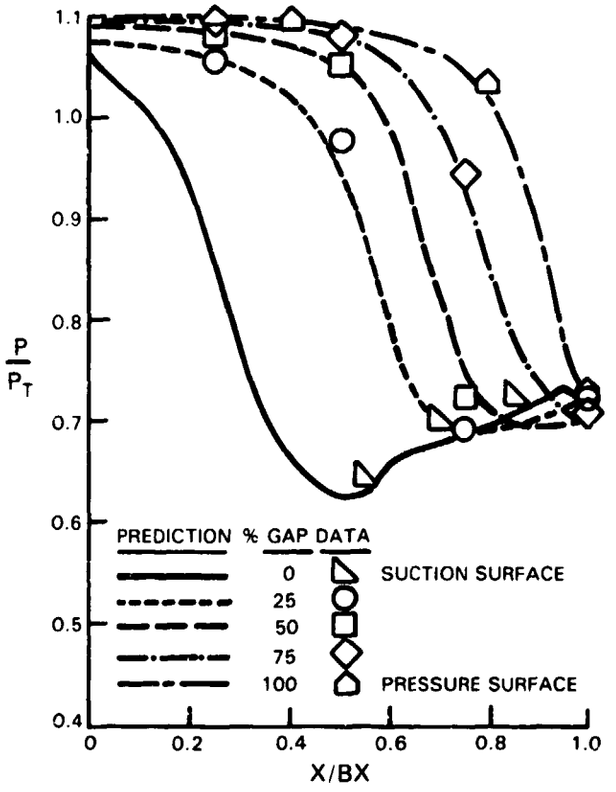

Figure 19 Straight-Wall Cascade - Comparison of Cross-Channel Data With Two-Dimensional Potential Flow Computation

ORIGINAL PAGE IS
OF POOR QUALITY

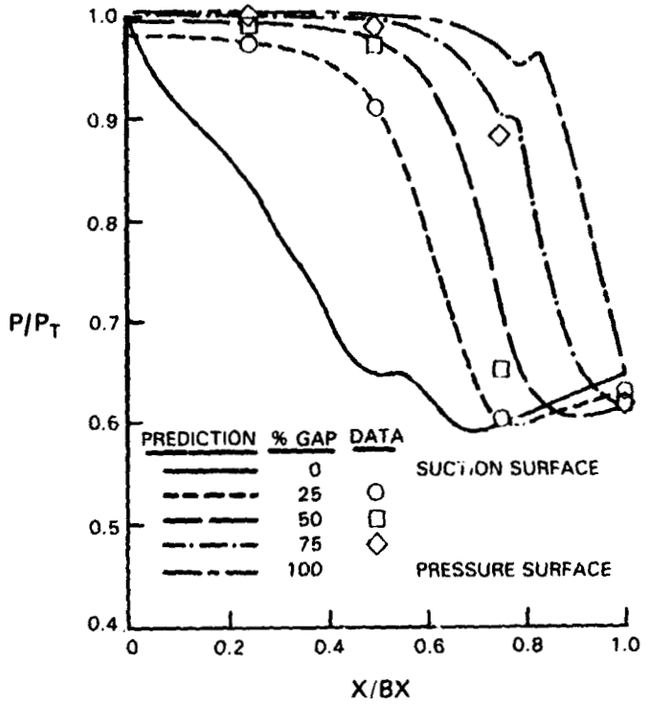

Figure 20 S-Wall Cascade - Comparison of Cross-Channel Data with Three-Dimensional Inviscid Flow Field Computation at Straight Wall End of Cascade

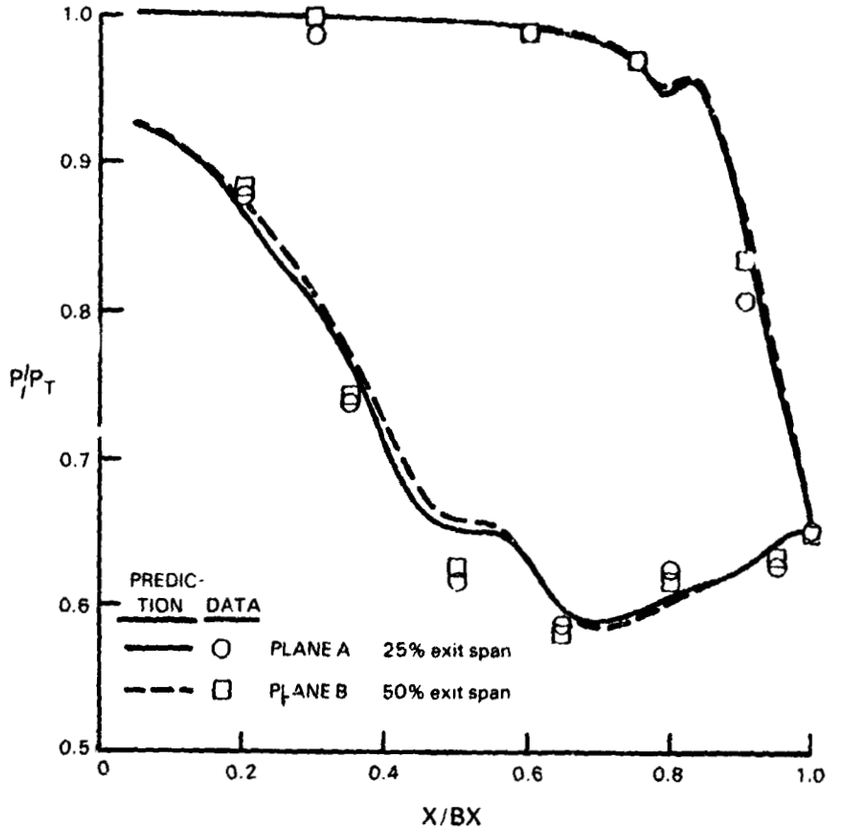

Figure 21 S-Wall Cascade - Comparison of Spanwise Data at Planes A and B with Three-Dimensional Inviscid Flow Field Computation

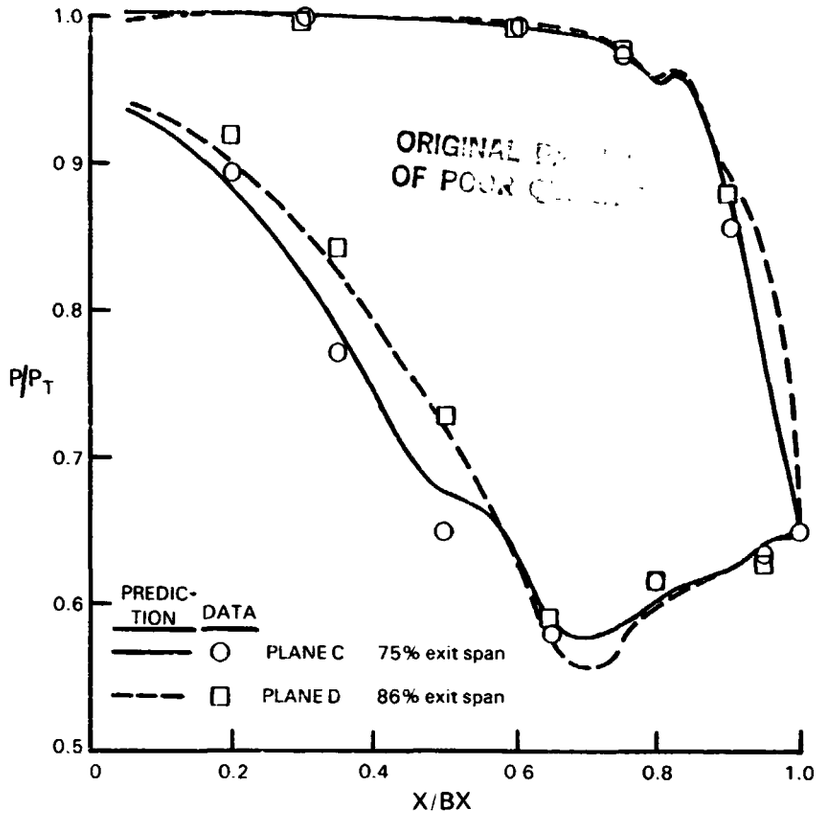

Figure 22 S-Wall Cascade - Comparison of Spanwise Data at Planes C and D with Three-Dimensional Inviscid Flow Field Computation

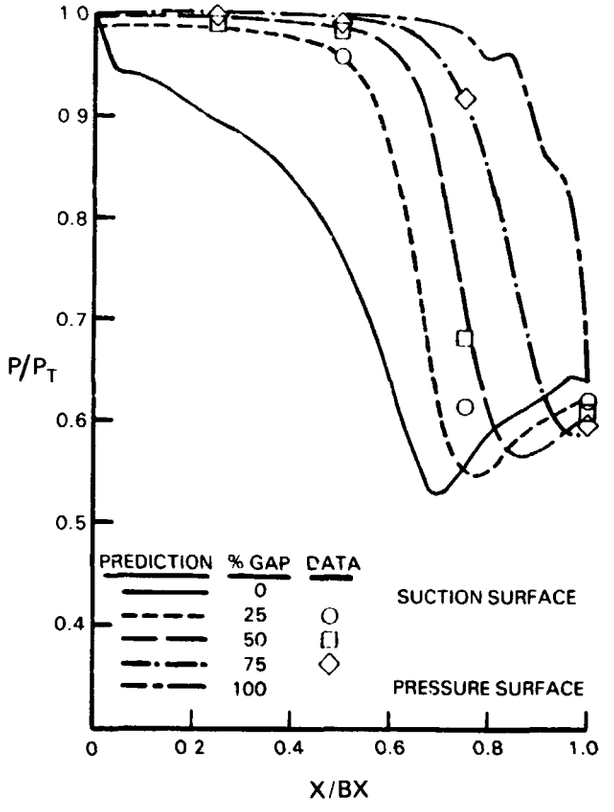

Figure 23 S-Wall Cascade - Comparison of Cross-Channel Data with Three-Dimensional Inviscid Flow Field Computation at S-Wall End of Cascade

3.4.4.1 Comparison of S-wall and Straight Wall Vane Cascade Results

3.4.4.1.1 Cascade Performance at Mach 0.84

Cascade performance, judged in terms of total pressure loss and exit air angles, was determined from wake traverse data. Contour plots of total pressure loss in the exit plane were then produced from these data. Figure 24 shows the loss contours for the straight wall cascade over one pitch. The airfoil wake is characterized by near parallel contours running spanwise within the profile loss region of span. Nearer the endwalls, the regular pattern is disrupted by the secondary flows. The passage vortex appears in the contour plots as the circular region of high-pressure loss near the endwalls. Closer to the endwalls, the boundary layers that developed within the passage produced a sharp increase in total pressure loss.

The pressure loss contour plot for the S-wall cascade (see Figure 25) exhibits features similar to those of the straight wall cascade. The only difference is that the high loss region (passage vortex) on the straight wall side is smaller and lies somewhat closer to the endwall than the high loss region on the S-wall side. This is consistent with the suction surface separation lines observed in the flow visualizations conducted.

Comparison of the spanwise distributions of mass-averaged total pressure loss for both cascades (see Figures 26 and 27) shows that the most notable feature of the S-wall cascade is the apparent lack of the total pressure loss peak, caused by the vortex on the straight wall side. The vortex on this side was closer to the endwall, and pitchwise integration of loss data merged this loss region into that of the endwall boundary layer.

Yaw angle data were mass-averaged in the pitchwise direction in the same manner as the pressure loss data. The yaw angle distribution for the straight wall cascade (Figure 28) shows good symmetry about midspan. The passage vortices near the endwalls result in a region of first underturning and then overturning, proceeding from midspan across the vortices toward the endwalls. Closer to the endwalls, the flow again exhibits decreased turning. This is attributed to the suction surface leg of the leading edge counter vortex (see Figure 15). The prediction of the cascade exit air angle is presented in Figure 28 and is seen to yield a slightly smaller average exit air angle than measured.

The spanwise distribution of yaw angle for the S-wall cascade (Figure 29) shows the same overall turning as the straight wall cascade. The flow on the S-wall side, however, exhibits appreciably more overturning. This trend is well predicted, in an average sense, by the three-dimensional flow field calculation shown, which suggests that the inviscid contribution to the behavior of the endwall flow is appreciable.

3.4.4.1.2 Loss Assessment

Total cascade loss can be treated as the sum of the profile (two-dimensional) loss associated with the geometric shape of the airfoil section and the secondary loss resulting from endwall boundary layer effects. Understanding these loss elements is crucial to the assessment of a particular design.

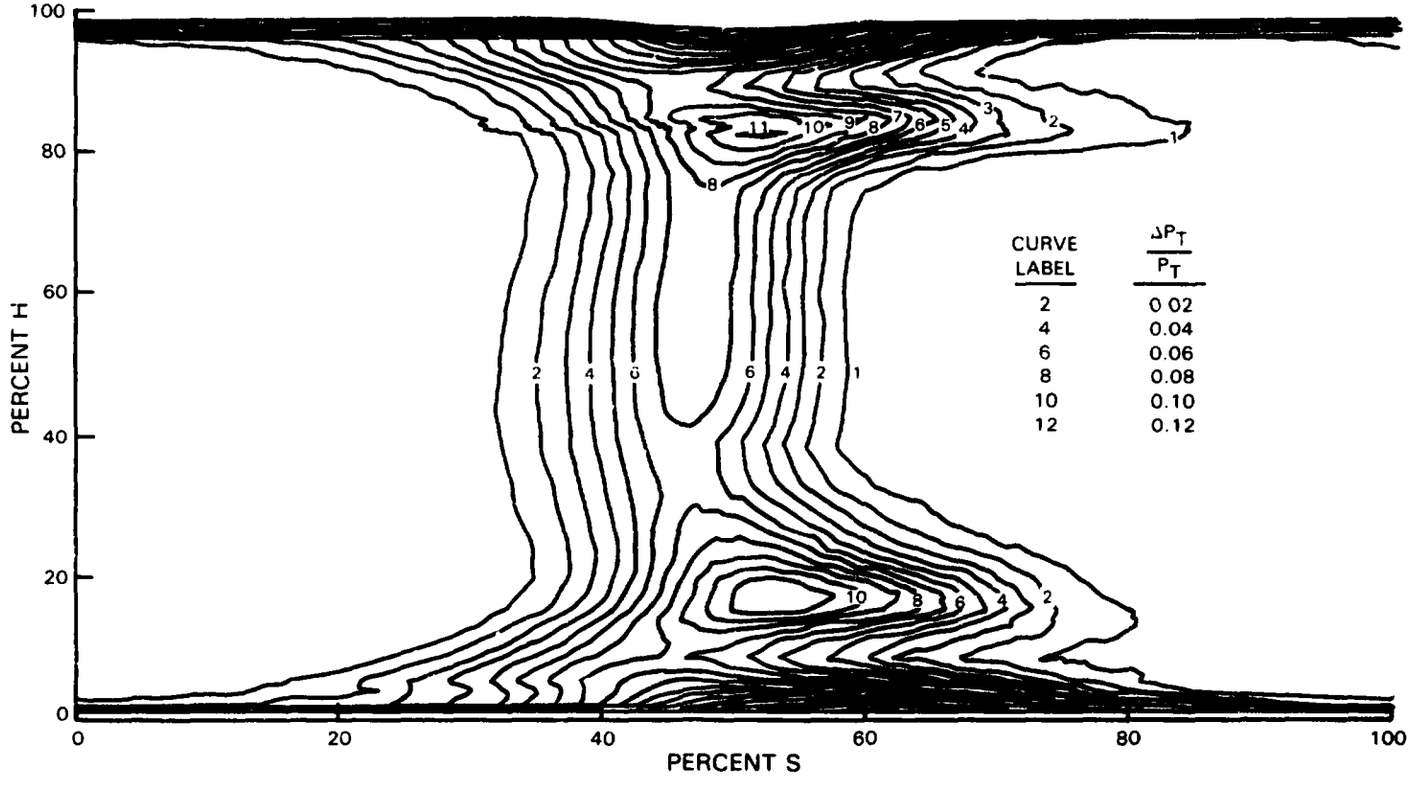

Figure 24 Straight Wall Cascade Pressure Loss Contours

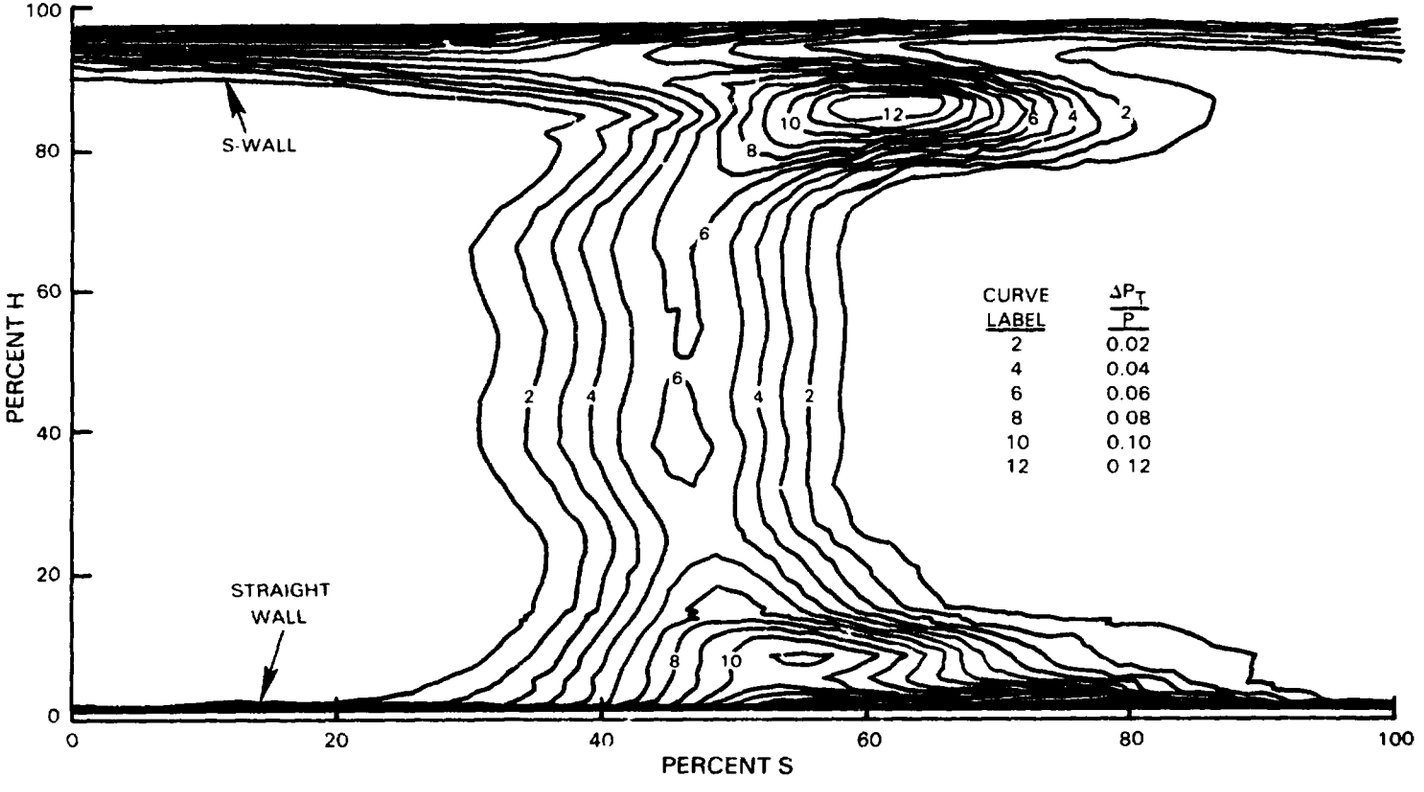

Figure 25 S-Wall Cascade Pressure Loss Contours

ORIGINAL PAGE IS
OF POOR QUALITY

ORIGINAL PAGE IS
OF POOR QUALITY

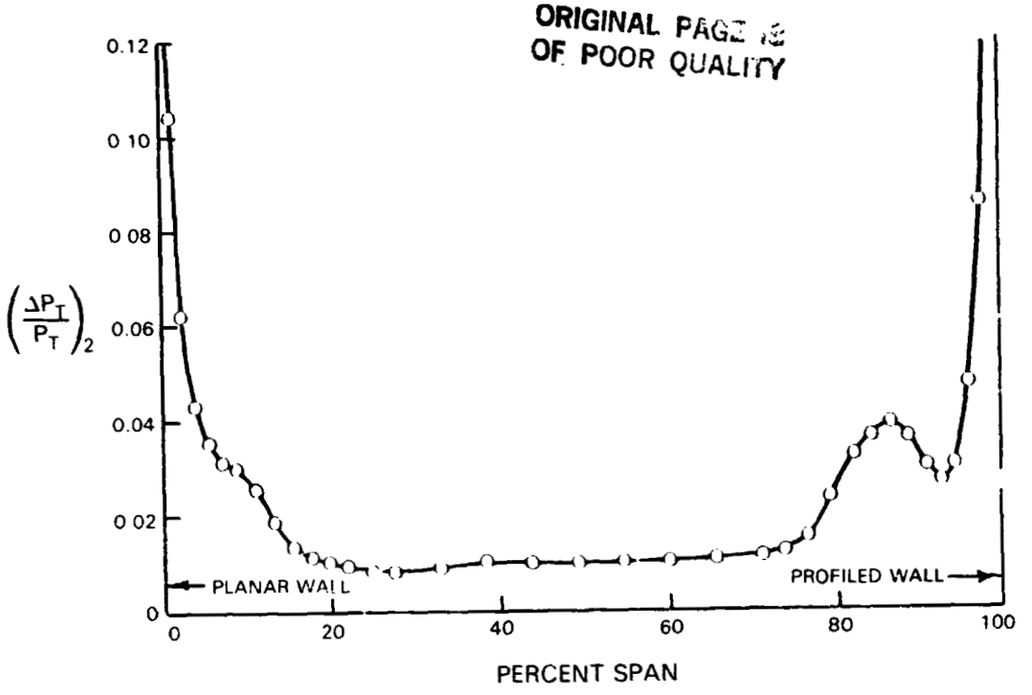

Figure 26 Spanwise Distribution of Total Pressure Loss for S-Wall Cascade

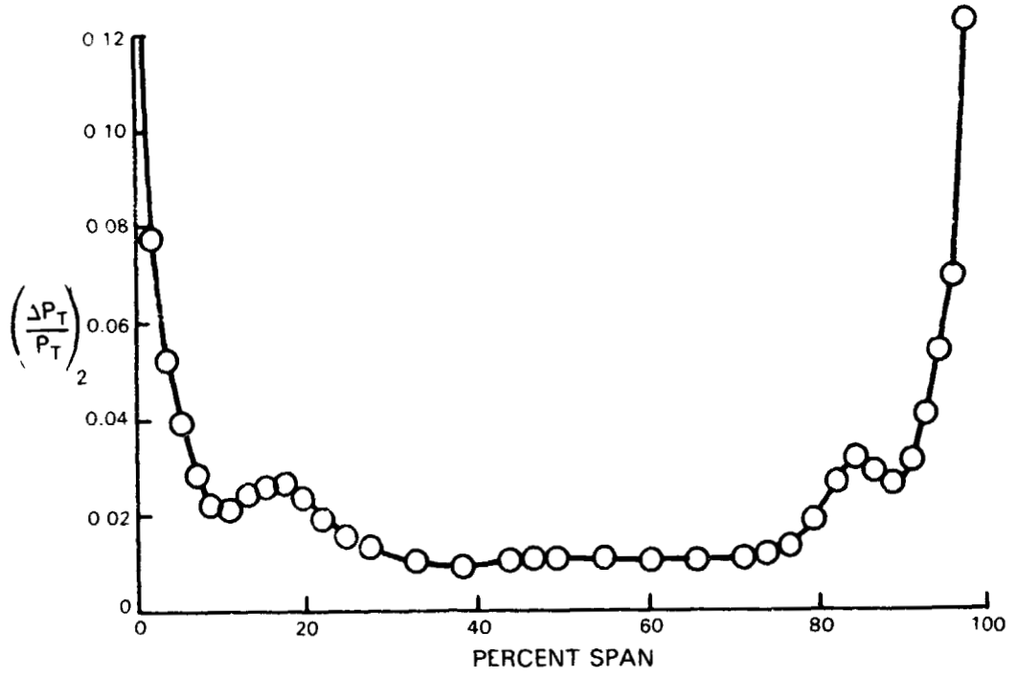

Figure 27 Spanwise Distribution of Total Pressure Loss for Straight Wall Cascade

ORIGINAL PAGE IS
OF POOR QUALITY

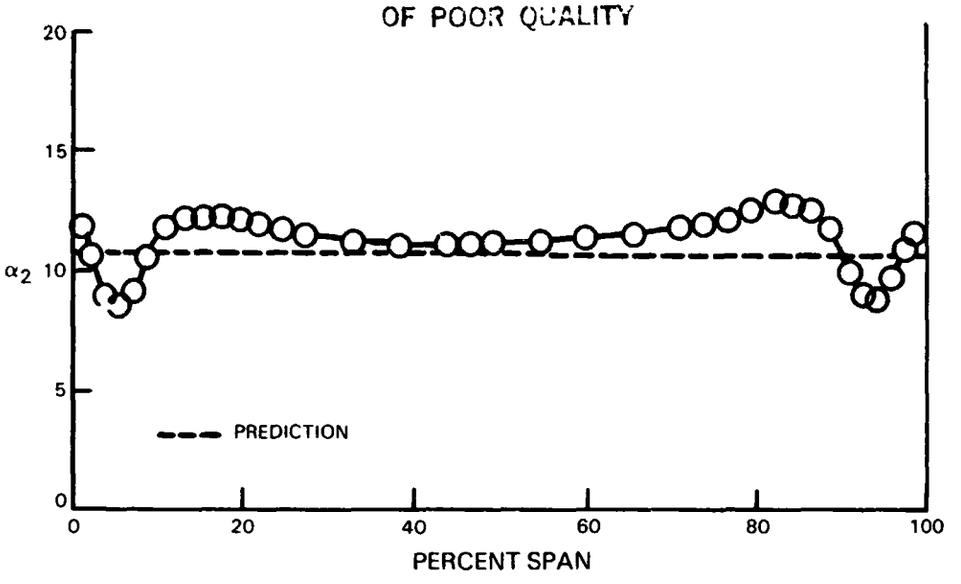

Figure 28 Spanwise Distribution of Exit Yaw Angle for the Straight Wall Cascade

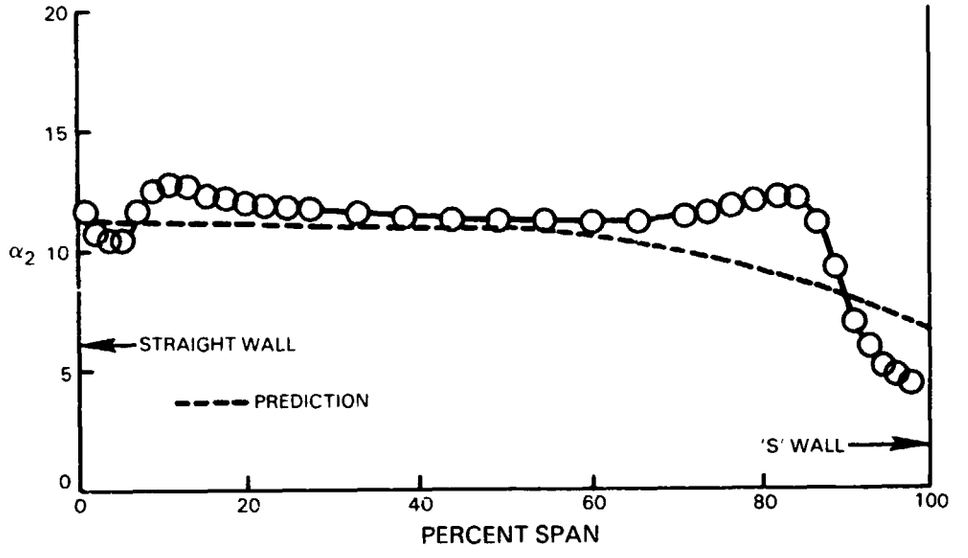

Figure 29 Spanwise Distribution of Exit Yaw Angle for the S-Wall Cascade

Profile Loss Analysis

Because of the strong overall acceleration experienced by the flow in the cascades under investigation, it would be expected that even at the relatively low aspect ratio of 0.5, the midspan region would be reasonably two-dimensional in nature, and therefore amenable to two-dimensional analytical methods.

The results from the pressure distribution calculations were used to execute two-dimensional boundary layer computations for both the pressure and suction surfaces. For the S-wall cascade, the pressure distribution remains nearly constant over 75 percent of the span on the S-wall side, justifying the approach. A wake mixing calculation was subsequently used to "mix out"* the boundary layers and to account for the finite thickness of the airfoil trailing edge.

Boundary layer calculations for both cascades predicted that transition occurs on the suction surface slightly downstream of the start of the adverse pressure gradient. The pressure surface in both instances was predicted to remain laminar to the trailing edge. The predicted total pressure loss for both cascades using this procedure was within 12 percent of the values obtained by mixing out the respective wake traverse data. Table 8 summarizes these results.

TABLE 8
MIDSPAN REGION PRESSURE LOSS COMPARISON

	Predicted Pressure Loss ($\Delta P/P$)	Measured Pressure Loss ($\Delta P/P$)
Straight Wall Cascade	0.0134	0.0120
S-Wall Cascade	0.0124	0.0118

Secondary Loss Analysis

The wake traverse plane was chosen at a distance downstream of the cascade where the flow is sufficiently mixed out to permit a good assessment of the secondary losses to be made. In addition, the test results were analyzed on both an area-averaged and a mass-averaged basis. Secondary loss results were obtained by subtracting the profile loss from the full passage loss. Profile loss was evaluated by using the appropriate massor area-averaged loss over 20 percent of the span about midspan. The resulting values for secondary loss thus include contributions from the inlet boundary layer, endwall boundary layer, and the interaction between the endwall and airfoil boundary layers.

"*Mix Out" Refers to the analytical mixing of the measured two-dimensional wake traverse data to a homogeneous state through the application of the equations for conservation of mass and momentum. It is a technique commonly used to calculate total cascade loss.

Table 9 presents the results for both the S-wall and the straight wall cascades in terms of mass and area-averaged values. These results are presented for each half span, as well as over the full passage, in order to bring out the effect of profiling one endwall. In general, the results indicate that the secondary loss comprises over half of the total loss. The area-averaged loss does not account for the reduced mass flow in regions of higher total pressure loss. Consequently, the area-averaged losses are somewhat higher than the mass-averaged values.

TABLE 9
Secondary Loss Measurements

A) Planar Wall Cascade

	Mass Averaged			Area Averaged		
% Span	0-50	50-100	0-100	0-50	50-100	0-100
Total $\Delta PT/PT$	.022	.025	.023	.027	.032	.030
Profile $\Delta PT/PT$	.011	.011	.011	.012	.012	.012
Secondary $\Delta PT/PT$	.012	.014	.013	.016	.020	.018

B) Profiled Wall Cascade

% Span	0-50	50-100*	0-100	0-50	50-100*	0-100
Total $\Delta PT/PT$	.018	.021	.019	.021	.030	.026
Profile $\Delta PT/PT$	.010	.010	.010	.012	.012	.012
Secondary $\Delta PT/PT$	.007	.011	.009	.010	.019	.014

* Profiled wall side

Comparison of the mass-averaged data for the two cascades shows that the S-wall cascade has 17 percent less full passage loss than the straight wall cascade. Since the measured "profile" losses were approximately equal for both cascades, this improvement was in the secondary losses (approximately 30 percent reduction). Comparison of the data for each half span indicates that approximately 65 percent of this secondary loss improvement occurred on the straight wall half of the S-wall cascade. Area averaging of the data also shows a substantial reduction in secondary loss for the straight wall side of the S-wall cascade. Area averaging of the secondary losses for the S-wall half, however, shows negligible change from the results of the straight wall cascade tests. The reason for this result is that the increased turning near the S-wall causes a reduction in the mass flow through this region which is not accounted for by area-averaging.

An understanding of secondary flows and the availability of reliable prediction methods is crucial for the design of low aspect ratio configurations. The flow in the endwall region, however, is extremely complicated, as evidenced by previous flow visualizations. Consequently, the prediction of cascade secondary loss is mostly limited to empirical correlations of experimental data.

ORIGINAL PAGE IS
OF POOR QUALITY

Morris and Hoare[3] obtained secondary loss data for a straight wall cascade featuring inlet guide vanes with 65 degrees of turning. Their data, along with the data of Came[4] for the same configuration, are presented in Figure 30 in terms of the resulting correlation. While the Morris and Hoare results are reported to be mass-averaged, without local angles and velocities being obtained, the data would actually reflect more of an area averaging. For this reason, the current area-averaged straight wall cascade data have been included in Figure 30 and are in good agreement with predictions.

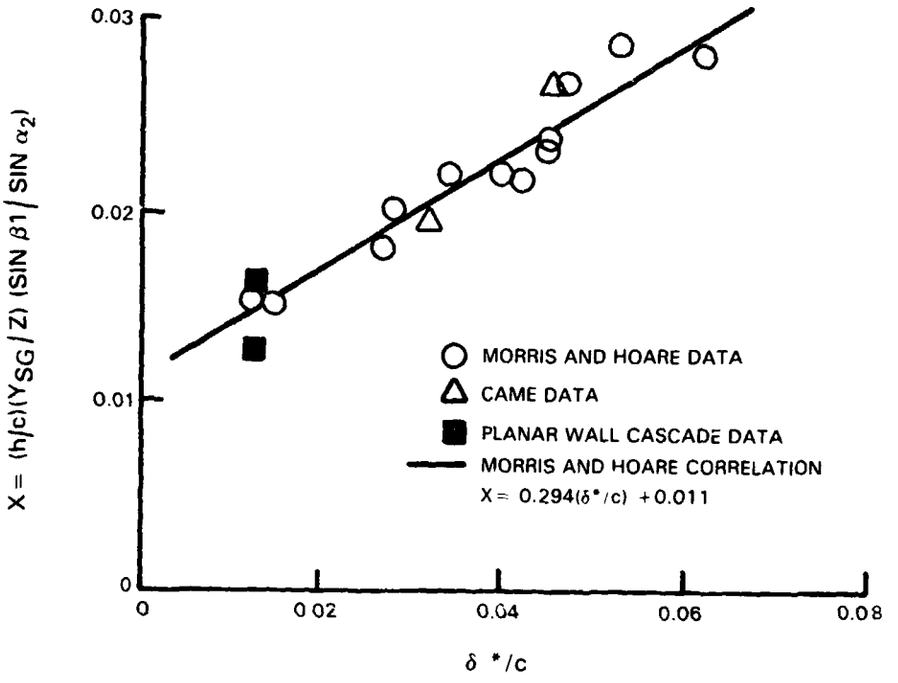

Figure 30 Comparison of Straight Wall Cascade Data with the Correlation of Morris and Hoare

The secondary loss results obtained for the S-wall cascade are presented in Figure 31, along with the data of Morris and Hoare for their "Profile A" configuration, which is similar to the current profile contour. Again, area-averaged losses have been reported for reasons previously discussed. Also shown in Figure 31 are the correlations developed for this particular endwall geometry. As indicated, the current data fall within the scatter band of the Morris and Hoare data.

An explanation of these experimental results can best be made in terms of the endwall pressure distribution (loading). In comparing the loading of the straight wall of the S-wall cascade (see Figure 20) with the loading on endwalls of the straight wall cascade (see Figure 19), it can be seen that (1) the S-wall cascade endwall is not as heavily loaded, (i.e., the average pressure surface to suction surface pressure differential is reduced) and (2) the center of pressure is located farther aft. These features contribute to a reduction in the cross-passage pressure gradient which, in turn, reduces the endwall cross-passage boundary layer flow (see Figure 15). It is this low momentum boundary layer fluid which contributes to the growth of the passage vortex and a corresponding increase in secondary losses. Although a detailed evaluation of the endwall boundary layer characteristics was not within the scope of this program effort, reduced cross-passage boundary layer flow is felt to be the primary contributor to the reduced secondary losses noted.

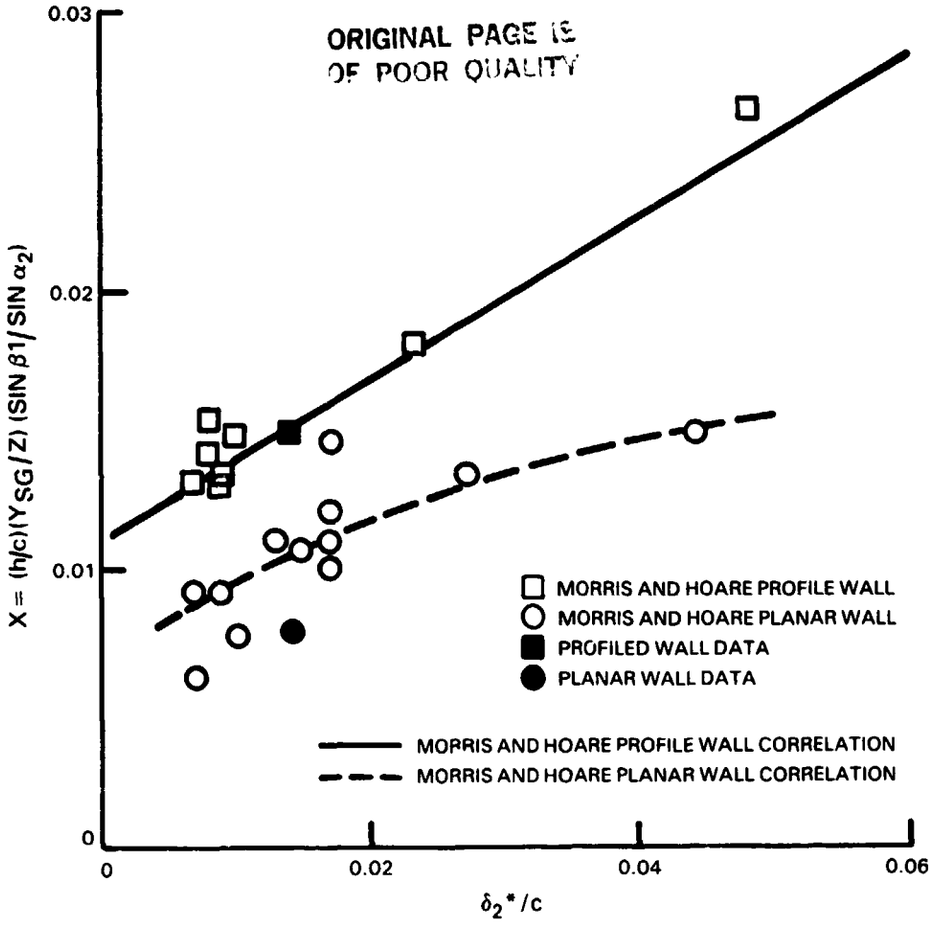

Figure 31 Comparison of S-Wall Cascade Data with the 'Profile A' Correlation of Morris and Hoare

A comparison between the loadings of the profiled endwall of the S-wall cascade (see Figure 23) and the straight wall cascade (see Figure 19) also shows the profiled endwall is not as heavily loaded and its center of pressure is further aft; again suggesting improved performance, which is consistent with the data. However, the secondary loss reduction at the S-wall is only about one-half that achieved at the straight wall; even with the reduced loading. Two possible reasons for this are (1) the maximum Mach numbers for the two endwalls are approximately equal and (2) the S-wall has a slightly larger wetted surface.

3.4.4.2 Effects of Exit Mach Number Variation on Straight Wall Cascade Performance

The straight wall vane cascade was designed using the high-pressure turbine component vane tip section airfoil geometry and incorporated no twist in the spanwise direction. In the component vane design, a slight amount of twist is incorporated and this changes the flow passage characteristics between adjacent airfoils such that exit Mach number increases from tip to root (i.e., 0.84 and 0.92 for the component vane tip and root sections, respectively). It

ORIGINAL PAGE IS
OF POOR QUALITY

was desirable to examine this spanwise Mach number variation in order to determine if transonic drag rise (evidenced by a sharp increase in pressure loss) might occur near the root section. Since the airfoil geometry of the root, mean, and tip sections is nearly identical, changing cascade exit Mach number provided the desired simulation.

The results of these tests are shown in the predicted and measured pressure loss data of Figure 32 and in the predicted and measured pressure distributions shown in Figures 33 through 36. These results indicate good agreement between predicted and measured data. More importantly, they indicate that there was no abrupt pressure rise, even though the exit Mach number approached sonic conditions. Flow in the root area of the component vane, therefore, can be expected to be free of transonic drag rise, confirming the aerodynamic acceptability of the vane design.

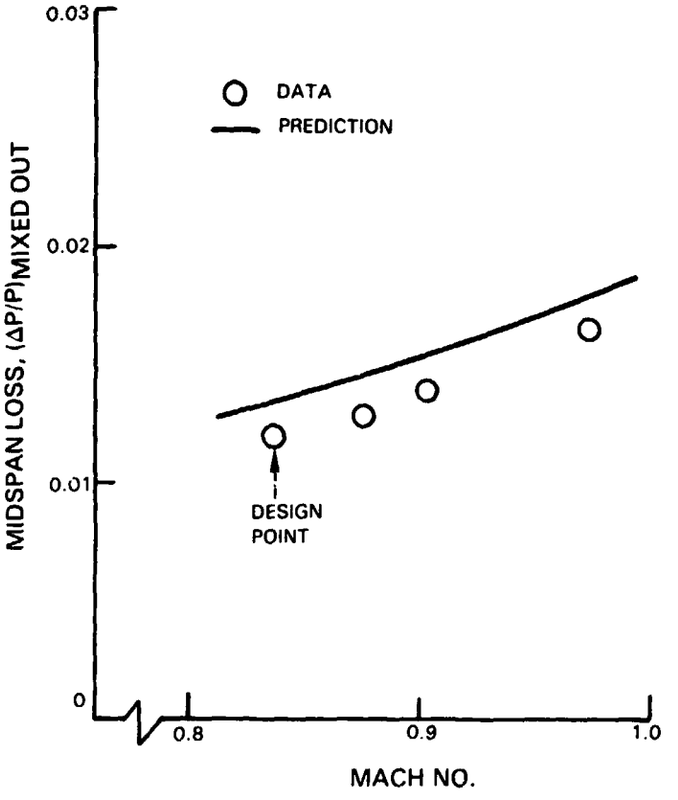

Figure 32 Straight Wall Cascade Midspan Pressure Loss vs. Mach Number

Exit air angle variation with Mach number is compared to analytical predictions in Figure 37. Failure in the test equipment precluded measurements at other than the tip section design point Mach number, however, data taken at a higher Mach number in the suction surface injection tests indicated, as predicted, that exit air angle is relatively insensitive to exit Mach number variation (see Figure 55). Good agreement is shown between prediction and test data at the design point Mach number.

ORIGINAL PAGE IS
OF POOR QUALITY

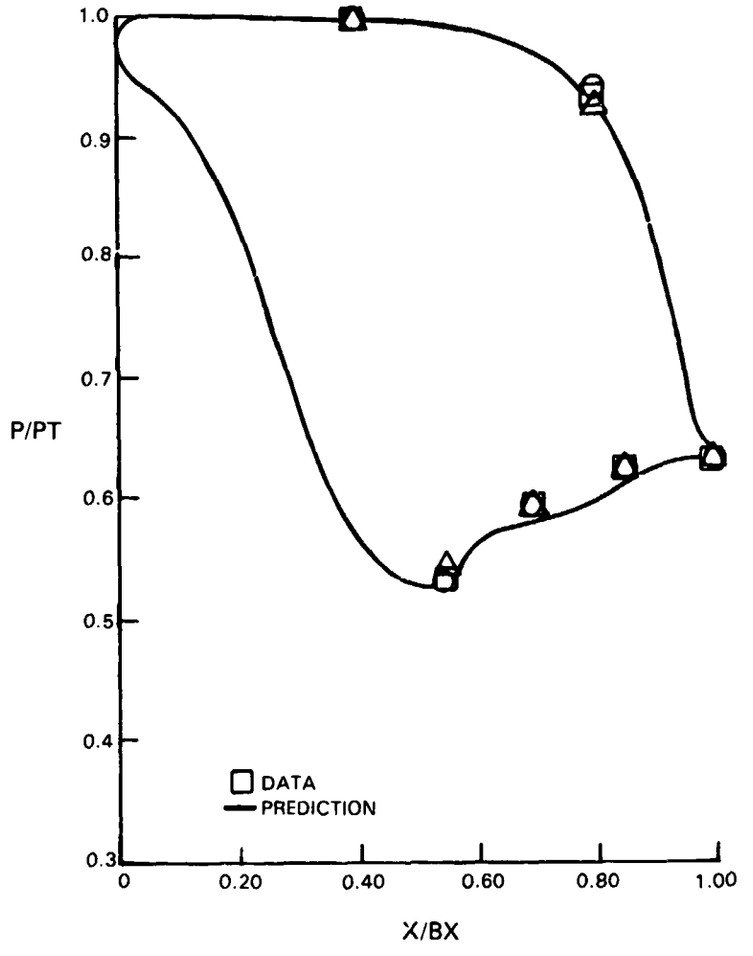

Figure 33 Straight Wall Cascade Predicted and Measured Pressure Distributions - Mach Number = 0.837

3.4.5 Cooled Cascade Results for Straight Wall Cascade

Using the straight wall cascade, secondary air flow was discharged from the vane trailing edge and from the pressure and suction sides of the airfoil to establish the effects of these flows on cascade pressure loss and exit air angle. The performance sensitivity to cooling flow variations was assessed at each location individually. In one test, exit Mach number was varied to assess the cooled cascade configuration for possible drag rise at near sonic Mach numbers. In another test, all cooling air discharge sites were provided with metered flow simultaneously to establish whether any interaction effects existed. Slight differences in exit Mach number, Reynolds number, and design point coolant flows result from the inability to exactly duplicate test conditions for each test series. The impact of these slight differences on test results is considered to be negligible. Actual test conditions are summarized in Table 10.

ORIGINAL PAGE IS
OF POOR QUALITY

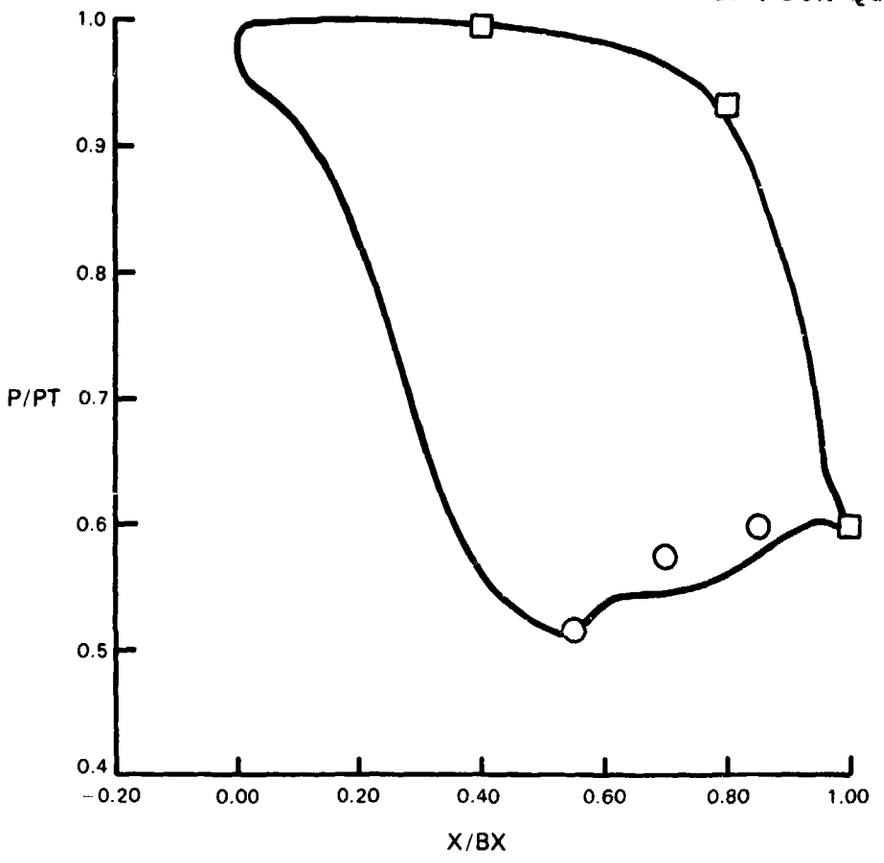

Figure 34 Straight Wall Cascade Predicted and Measured Pressure Distributions - Mach Number = 0.877

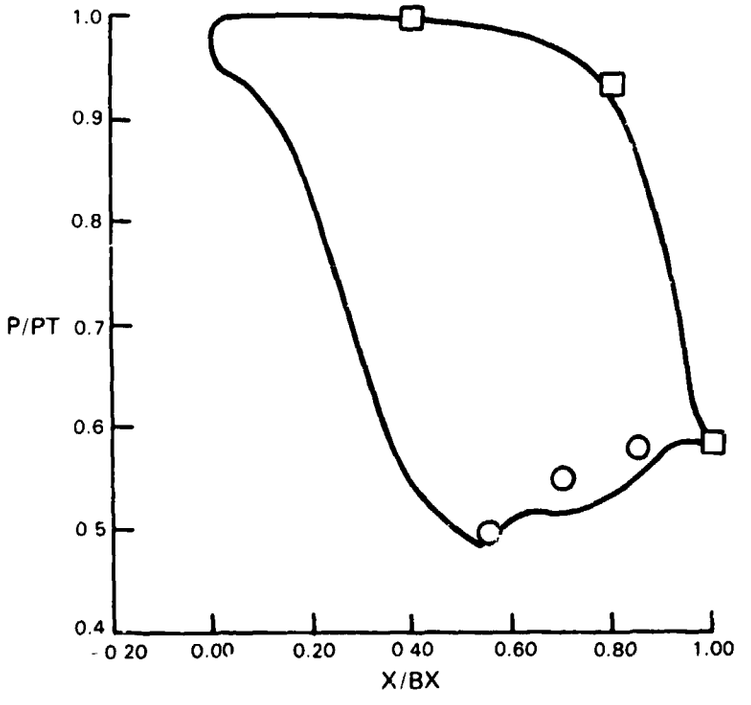

Figure 35 Straight Wall Cascade Predicted and Measured Pressure Distributions - Mach Number = 0.906

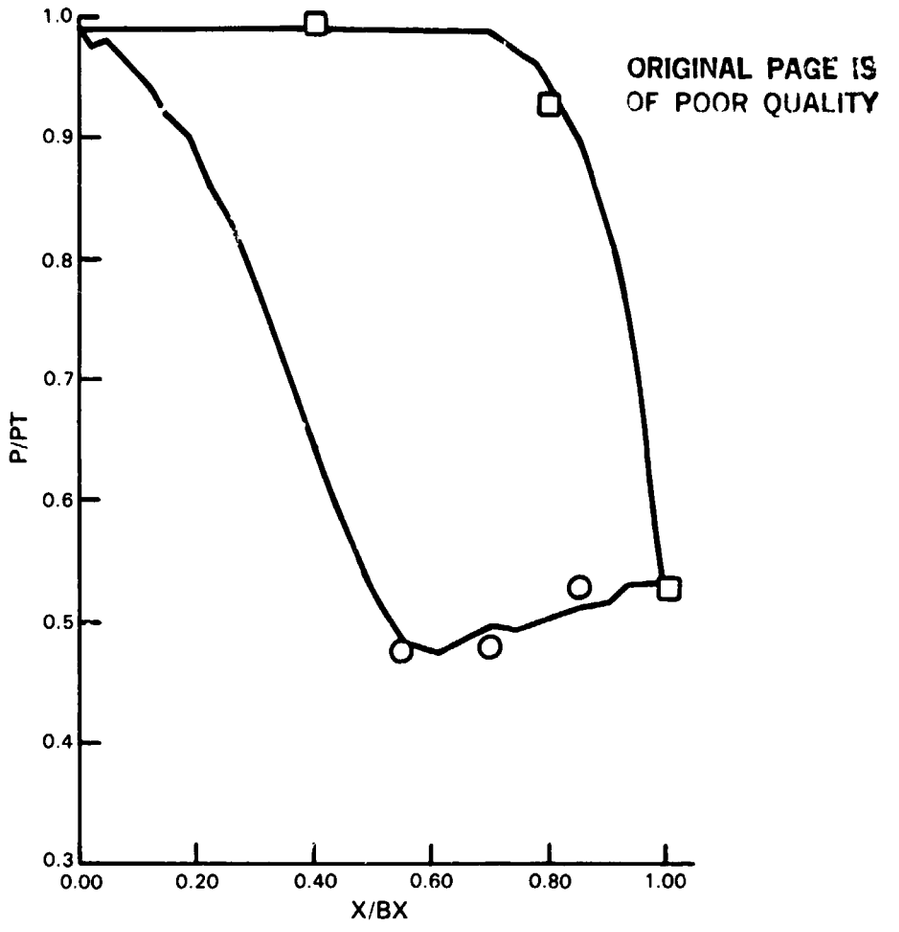

Figure 36 Straight Wall Cascade Predicted and Measured Pressure Distributions - Mach Number = 0.974

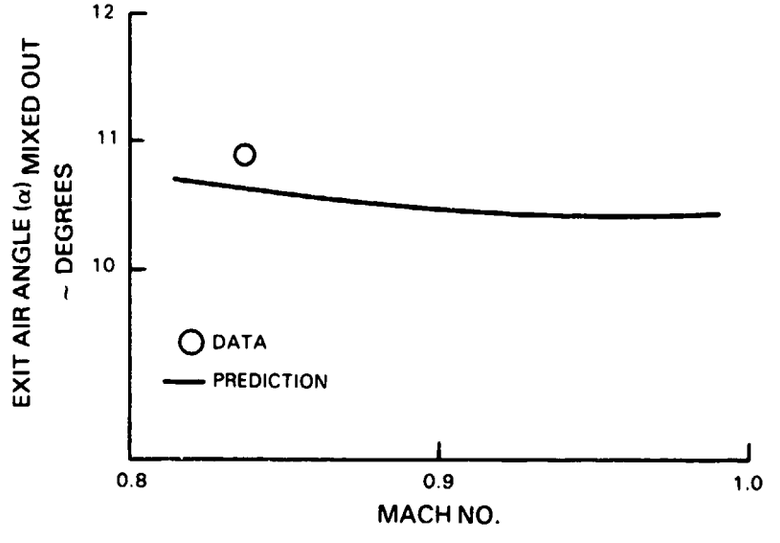

Figure 37 Straight-Wall Cascade Midspan Exit Air Angle vs. Mach Number

TABLE 10
COOLANT FLOW TEST CONDITIONS

	Exit Mach No.	Reynolds Number	W_c/W_p (%)	To_c/To_p
All Film Cooling Sites Flowing (Design Point)	0.82	6.7×10^5		
Trailing Edge			0.96	0.984
Pressure Surface			1.27	0.984
Suction Surface			2.49	0.984
Trailing Edge Injection Only	0.83	7.0×10^5	0.91	0.985
Pressure Surface Injection Only	0.83	6.7×10^5	0.87	0.987
	0.83	6.7×10^5	1.23	0.987
	0.83	6.7×10^5	1.50	0.987
Suction Surface Injection Only (Baseline)	0.83	6.8×10^5	1.71	0.987
	0.83	6.8×10^5	2.38	0.987
	0.83	6.8×10^5	3.18	0.987
Suction Surface Injection only (Increased Exit Mach No.)	0.90	7.7×10^5	1.43	1.056
	0.90	7.7×10^5	2.16	0.986
	0.90	7.7×10^5	2.86	0.978

W_c/W_p = Ratio of coolant flow to cascade passage inlet flow

To_c/To_p = Ratio of coolant flow total temperature to cascade passage inlet flow total temperature.

To preclude endwall effects on the individual trailing edge, pressure side, and suction side flow injection tests, cascade performance measurements were obtained only between 25 and 75 percent span. In this region, the exit flow characteristics were shown to be nearly two-dimensional in nature, thus making the measurements amenable to comparison with two-dimensional prediction methods. For the test point having all the injection sites flowing at design point rates, a full span survey was obtained.

3.4.5.1 Effects of Simultaneous Design Point Coolant Flow Injection at Trailing Edge and on Pressure and Suction Surfaces of Airfoil

Cooling air was simultaneously metered to the airfoil trailing edge, pressure and suction surface sites at design point flow rates. Static pressure data were subsequently obtained at 25, 50, and 75 percent span locations and compared to the predicted two-dimensional pressure distribution. The results are shown in Figure 38. This figure shows that the measured vane loading does not vary significantly in the spanwise direction and that the data are well predicted.

ORIGINAL PAGE IS
OF POOR QUALITY

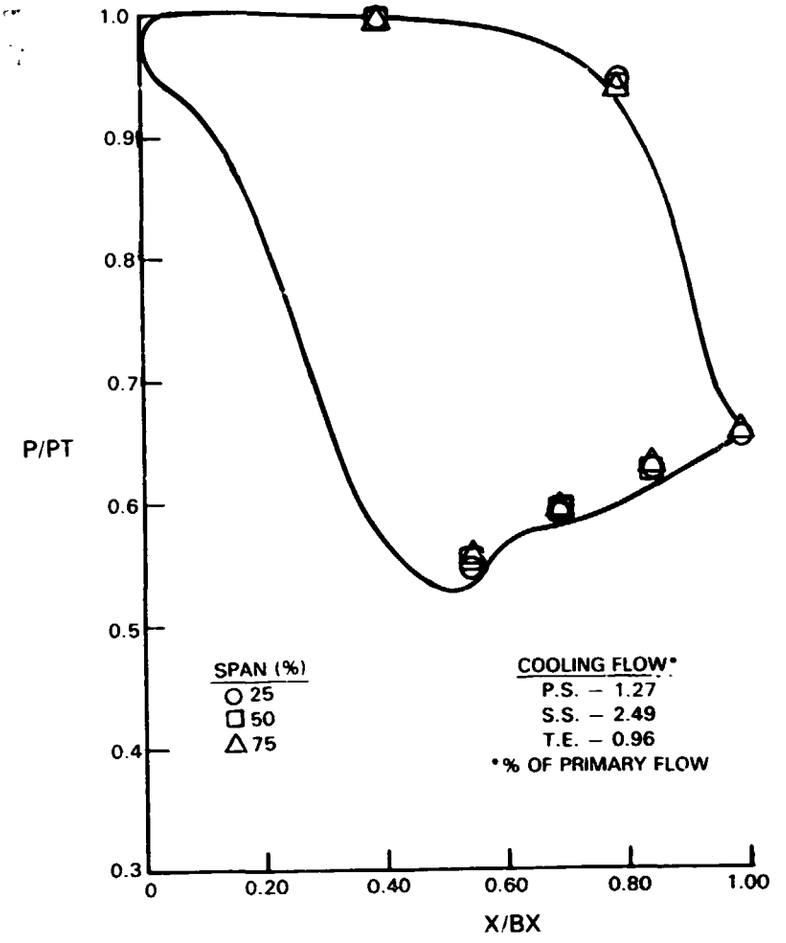

Figure 38 Pressure Distribution vs Chord at Three Span Locations

Full passage total pressure loss and air angle measurements were obtained at the same location (1.02 cm (0.4 in.) axially downstream of trailing edge plane) as for the uncooled cascade. These results are compared with the uncooled cascade results in Figures 39 and 40, and show that the exit air angle was relatively insensitive to coolant flow injection; however, total pressure loss almost doubled in the two-dimensional flow region of the span.

The measured exit flow conditions in the midspan region (25-75 percent span) were subsequently mixed-out analytically to a homogeneous state. This approach permitted a comparison to be made with analytical predictions. Table 11 compares the mixed-out losses with predictions for the uncooled and cooled cascades. This table shows that (1) pressure loss increased 75 percent as a result of coolant mixing, and (2) the predicted cooled pressure loss is higher than the measured value, indicating that the prediction method is conservative. The following sections of this report address the impact on performance associated with flow injection from the individual sites.

ORIGINAL PAGE IS
OF POOR QUALITY

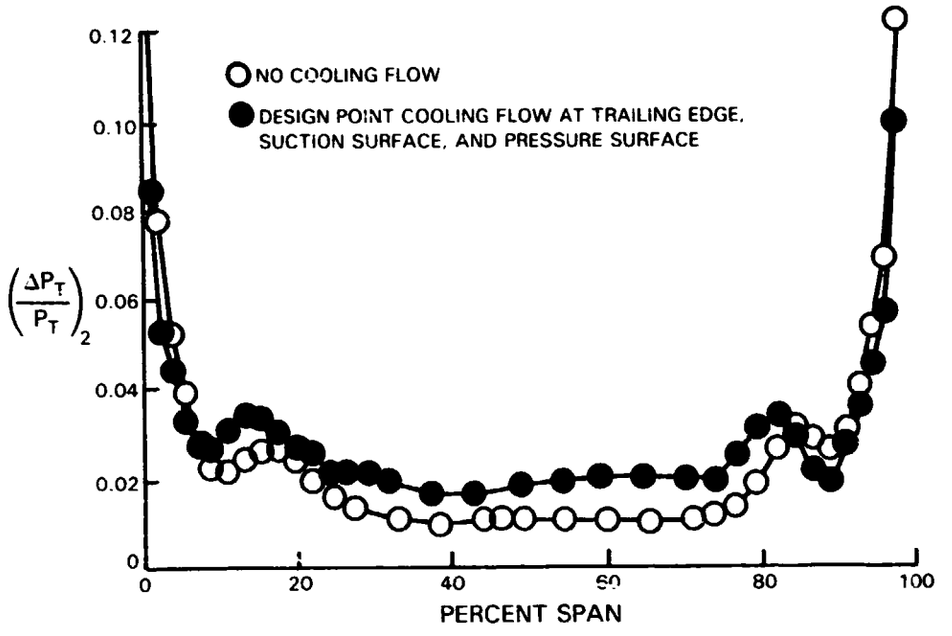

Figure 39 Spanwise Distribution of Total Pressure Loss for the Straight Wall Cascade

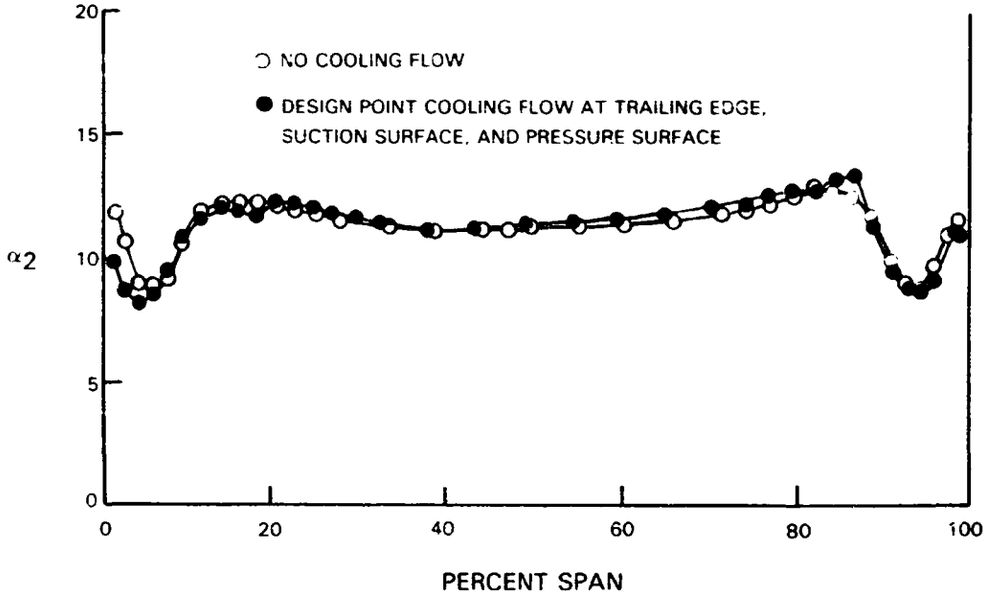

Figure 40 Spanwise Distribution of Exit Yaw Angle for the Straight Wall Cascade

TABLE 11
COMBINED INJECTION PRESSURE LOSS COMPARISON
(Design Point Coolant Flow Rates)

	Predicted Pressure Loss ($\Delta P/P$)	Measured Pressure Loss ($\Delta P/P$)
Cooled Cascade	0.0312	0.0210
Uncooled Cascade	0.0134	0.0120
Cooling Penalty	0.0178	0.0090

3.4.5.2 Trailing Edge Coolant Flow Rate Effects

To determine the effects of the rate of coolant flow injection at the trailing edge, flow was metered to the trailing edge slots at the design point coolant flow rate. Pressure loss and gap-averaged exit air angle measurements were obtained and compared to those for the uncooled cascade. Test results indicated that (1) pressure loss was increased and (2) exit air angle was insensitive to coolant flow injection (see Figures 41 and 42).

In executing a prediction to compare with the measured cascade performance, the total pressure of the coolant flow at the trailing edge exit plane must be known. For a short coolant flow passage between the plenum and trailing edge exit, it could be assumed that coolant flow total pressure at the trailing edge is equal to plenum pressure. However, the trailing edge coolant flow passage in the high-pressure turbine component vane design is long enough so that a significant pressure drop occurs. A methodology was therefore established to account for this.

Since plenum and trailing edge exit static pressures and passage flow area were easily determined, the only necessary ingredient remaining to calculate trailing edge exit plane total pressure was coolant flow rate through the passage. This was established experimentally by metering the flow to the plenum while holding trailing edge static pressure constant and recording plenum pressure at each flow rate. The resultant "calibration" curve is shown in Figure 43. The predicted theoretical flow rate shown in the figure was determined by assuming pipe flow in the passage, along with the known passage flow area, and plenum and trailing edge exit static pressures. The results indicate excellent agreement between predicted and measured values of trailing edge coolant flow over the range of test program plenum pressures.

"Mixed-out" pressure losses were subsequently calculated and compared both to predictions and to the uncooled cascade loss. These comparisons showed that the measured cooling penalty is small and is well predicted (see Table 12). Because of these results, it was considered unnecessary to test at other than design point cooling flow rates.

ORIGINAL PAGE IS
OF POOR QUALITY

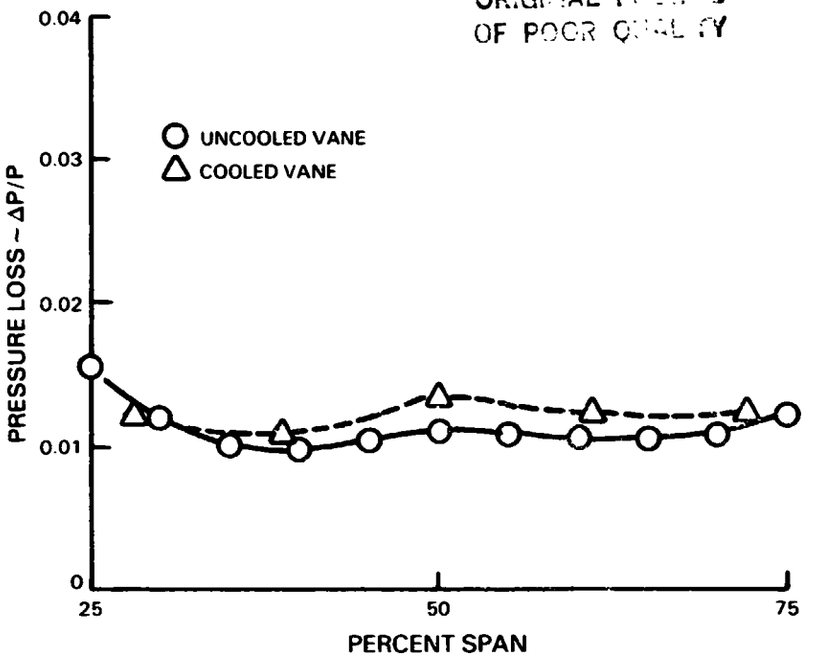

Figure 41 Pressure Loss Effects Due to Trailing Edge Injection at Design Point Coolant Flow

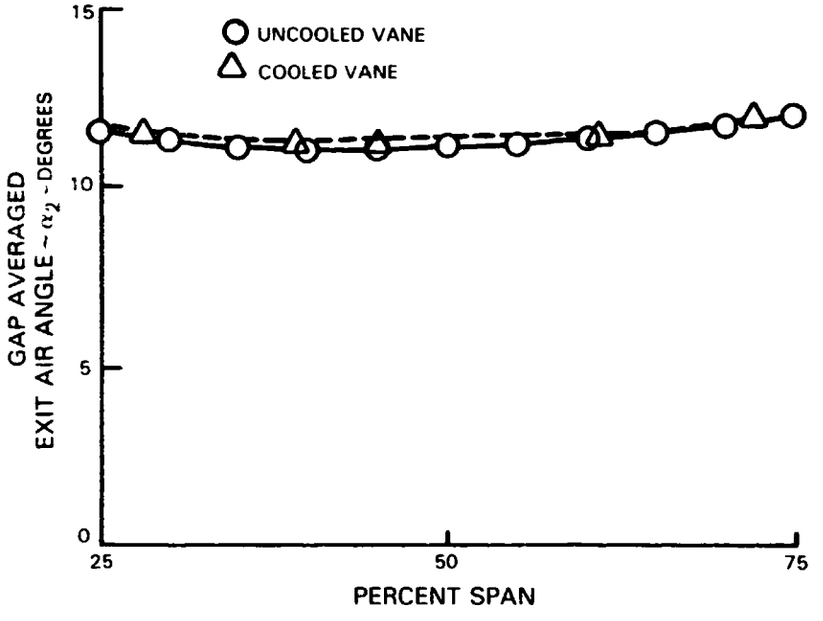

Figure 42 Exit Air Angle Effects Due to Trailing Edge Injection at Design Point Coolant Flow

ORIGINAL PAGE IS
OF POOR QUALITY

TABLE 12
TRAILING EDGE DISCHARGE PRESSURE LOSS COMPARISON
(Approximate Design Point)

	Predicted Pressure Loss ($\Delta P/P$)	Measured Pressure Loss ($\Delta P/P$)
Cooled Cascade	0.0143	0.0134
Uncooled Cascade	0.0134	0.0120
Cooling Penalty	0.0009	0.0014

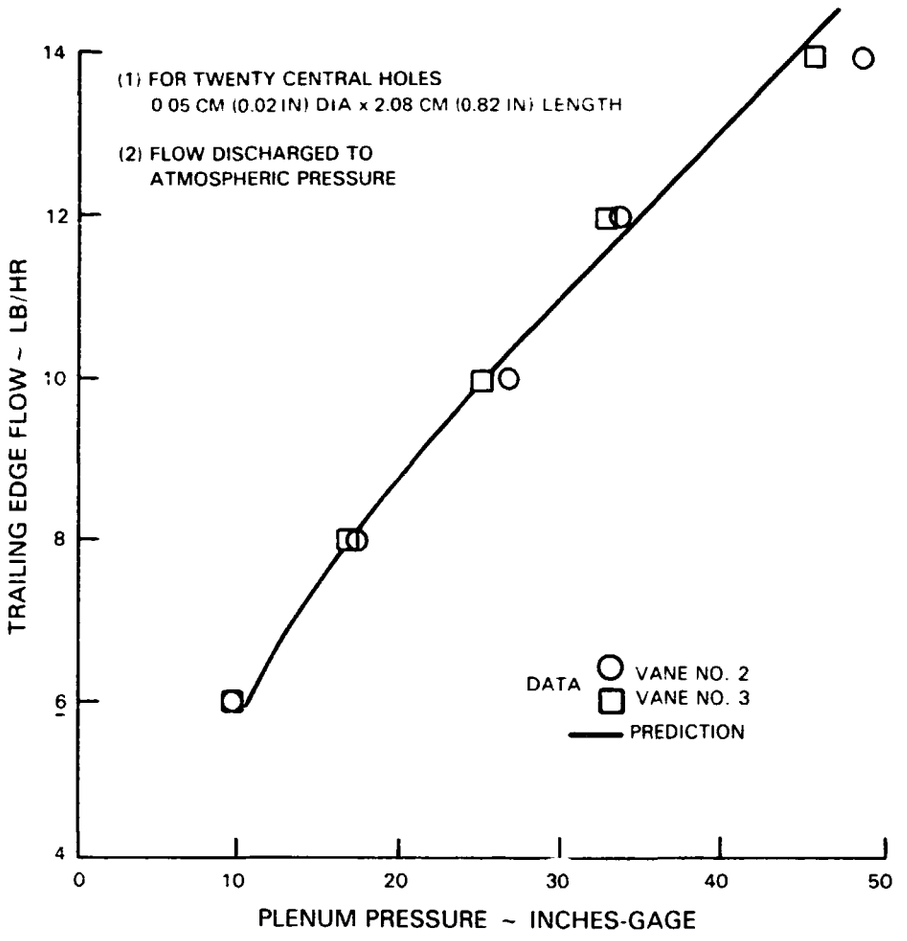

Figure 43 Vane Cascade Trailing Edge Flow Calibration

3.4.5.3 Pressure Side Coolant Flow Rate Effects

To assess the effects of pressure side coolant flow discharge, flow was metered from the middle plenum through two rows of holes located at the beginning of the strong favorable pressure gradient on the pressure surface of the airfoil (see Figure 7(b), locations ④ and ⑤). Pressure loss and gap-averaged exit air angle measurements were obtained at three cooling flow rates and are compared to those for the uncooled cascade in Figures 44 and 45, respectively. The slight skew of the spanwise pressure loss distributions with coolant flow when compared to the uncooled distribution is believed to be attributable to a variation in cooling hole flow coefficients.

"Mixed out" pressure losses were subsequently calculated with the spanwise average values being presented as a function of coolant flow rate in Figure 46 along with a prediction of the data. These pressure losses at the design point flow rate are compared with predictions and with the uncooled cascade losses in Table 13. Figure 47 presents the spanwise average exit air angle as a function of coolant flow rate along with a prediction.

These results indicate that the pressure loss penalty for pressure surface coolant discharge is small, the level being reasonably well predicted. Exit air angle results indicate that the angle is insensitive to coolant flow rate variations and is well predicted.

TABLE 13
PRESSURE SURFACE DISCHARGE PRESSURE LOSS COMPARISON
(Approx. Design Point)

	Predicted Pressure Loss ($\bar{\omega}$P/P)	"Mixed Out" Pressure Loss ($\bar{\omega}$P/P)
Cooled Cascade	0.0144	0.0139
Uncooled Cascade	0.0134	0.0120
Cooling Penalty	0.0010	0.0019

3.4.5.4 Suction Side Coolant Flow Rate Effects

To assess the effects of suction side coolant flow discharge, flow was metered from the forward plenum through three rows of holes located in the accelerating flow region of the airfoil suction surface (see Figure 7(b), locations ①, ② and ③). Pressure loss and gapaveraged exit air angle measurements were obtained at three cooling flow rates at a 0.84 exit Mach number. These results are compared to those for the uncooled cascade in Figures 48 and 49.

ORIGINAL PAGE IS
OF POOR QUALITY

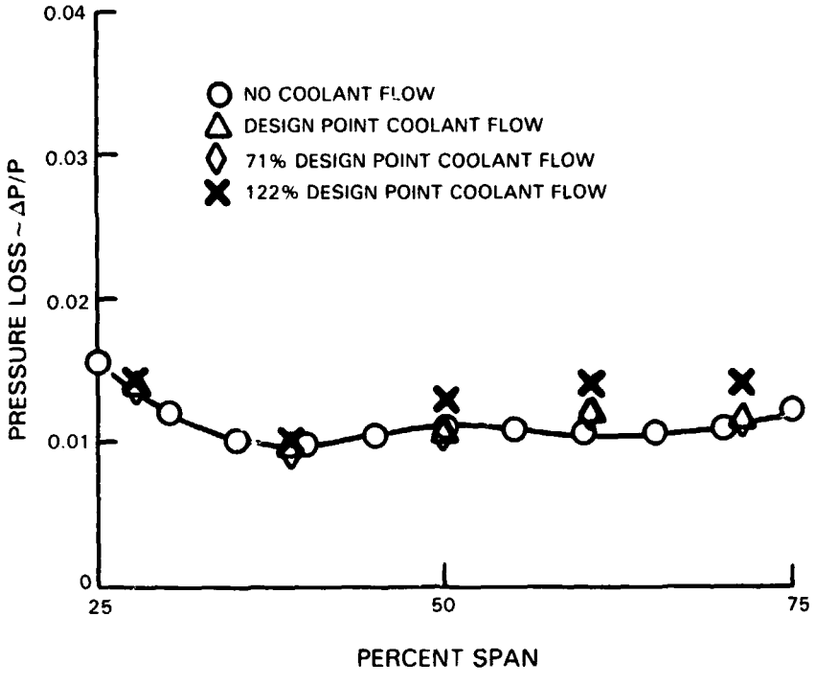

Figure 44 Pressure Loss Effects Due to Pressure Surface Coolant Injection

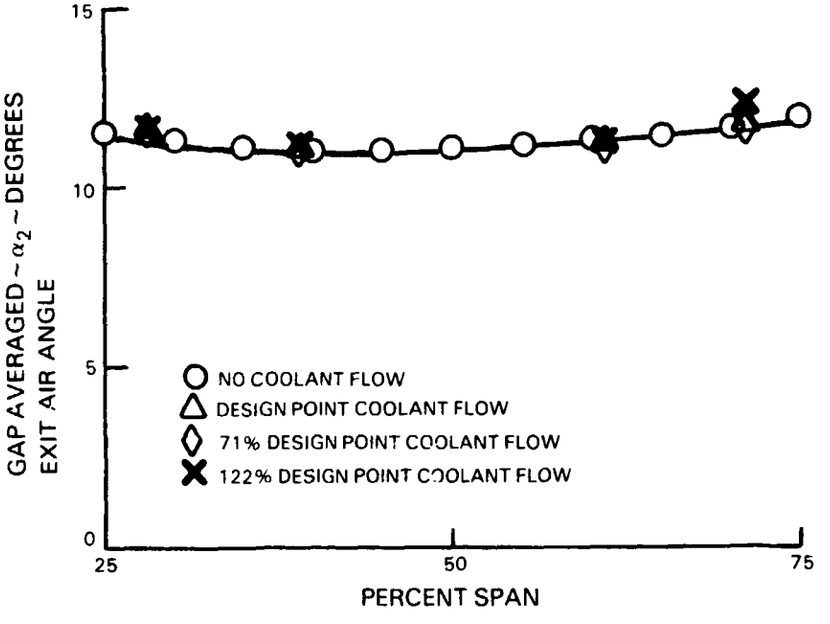

Figure 45 Exit Air Angle Effects Due to Pressure Surface Coolant Injection

ORIGINAL PAGE IS
OF POOR QUALITY

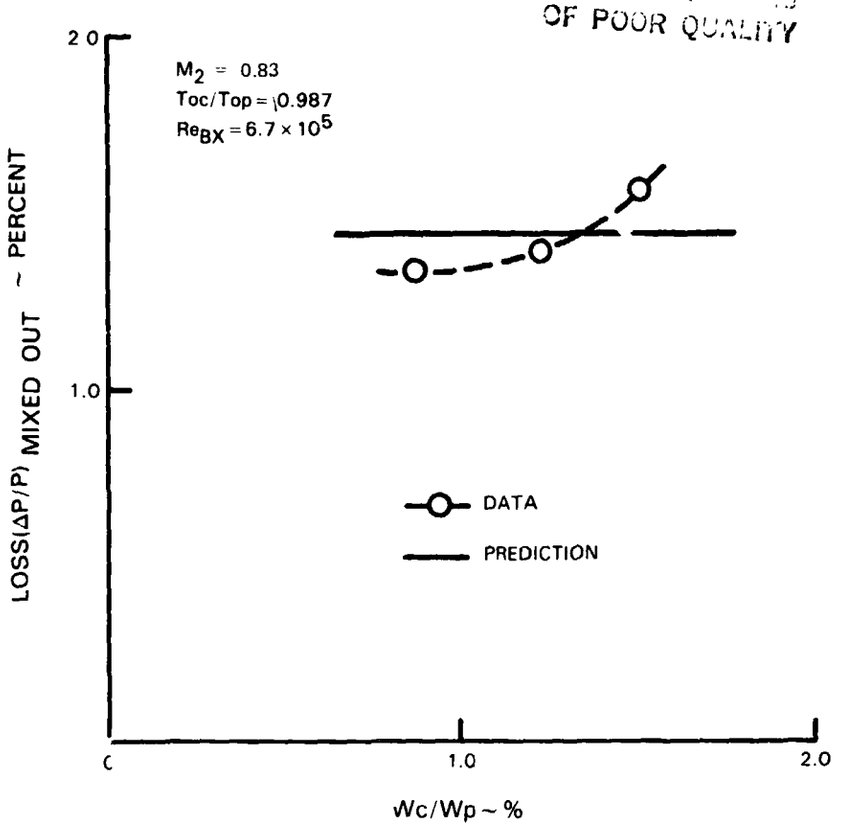

Figure 46 Pressure Loss Effects Due to Pressure Surface Coolant Flow Injection Rate Variation

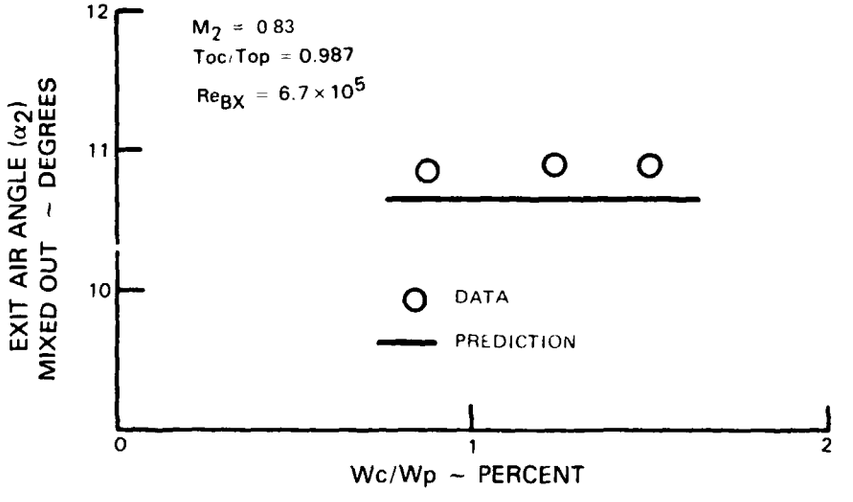

Figure 47 Exit Air Angle Effects Due to Pressure Surface Coolant Flow Injection Rate Variation

ORIGINAL PAGE IS
OF POOR QUALITY

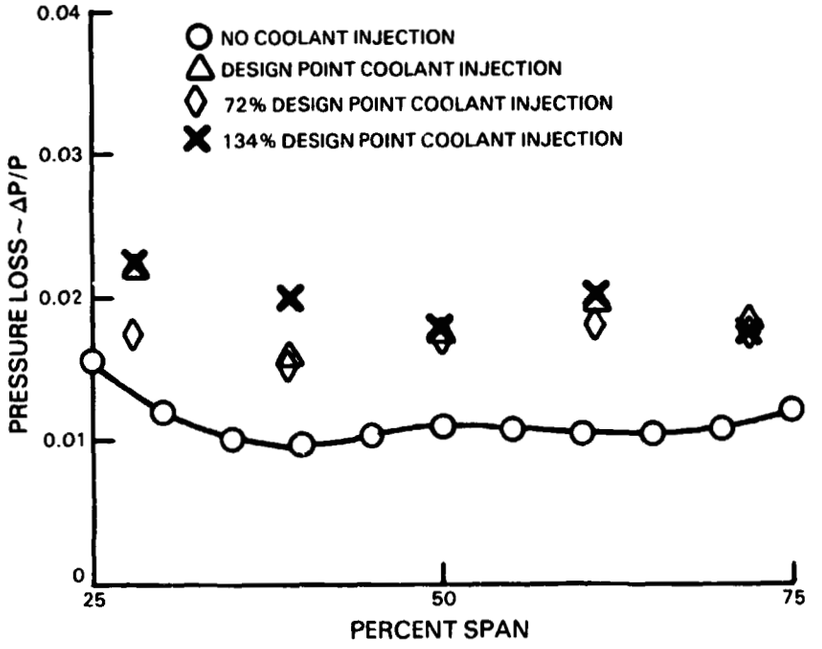

Figure 48 Pressure Loss Effects Due to Suction Surface Coolant Injection

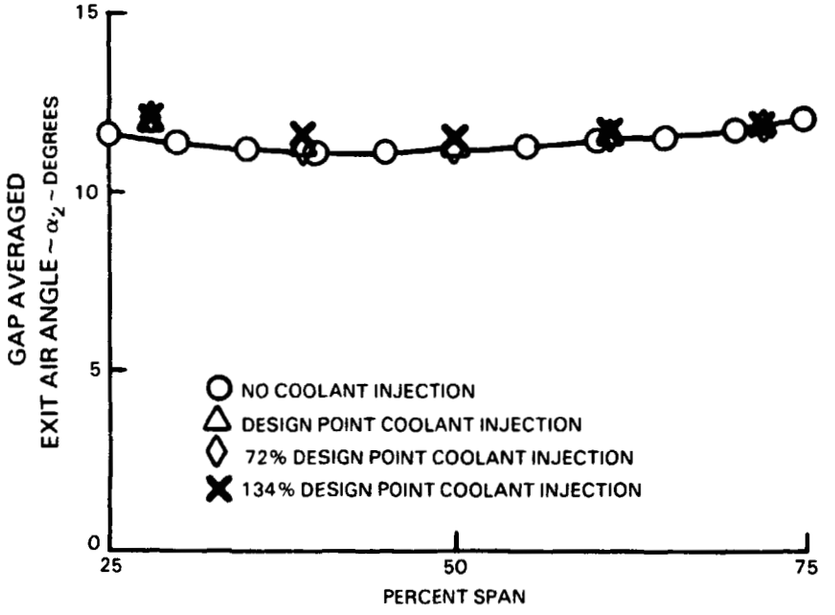

Figure 49 Exit Air Angle Effects Due to Suction Surface Coolant Injection

ORIGINAL PAGE IS
OF POOR QUALITY

"Mixed out" pressure losses were subsequently calculated with the spanwise average values being presented as a function of cooling flow rate in Figure 50 along with a prediction of the data. These results at the design point flow rate are compared with predictions and the measured uncooled cascade losses in Table 14. As the table indicates, suction surface injection is a major contributor to cooling losses for the vane. Figure 51 presents the spanwise average exit air angle as a function of coolant flow rate along with a prediction.

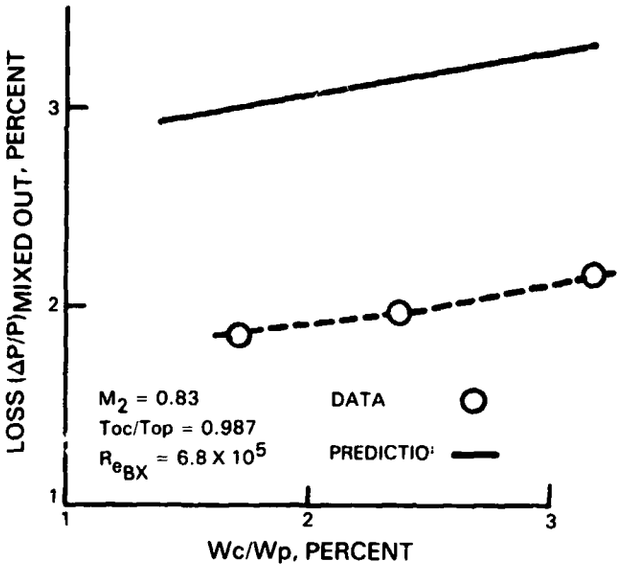

Figure 50 Vane Suction Surface Injection Midspan Loss vs Cooling Flow Rate

TABLE 14
SUCTION SURFACE DISCHARGE
PRESSURE LOSS COMPARISON
(Approx. Design Point)

	Predicted Pressure Loss (ΔP/P)	"Mixed-Out" Pressure Loss (ΔP/P)
Cooled Cascade	0.0315	0.0195
Uncooled Cascade	0.0134	0.0120
Cooling Penalty	0.0181	0.0075

ORIGINAL PAGE IS
OF POOR QUALITY

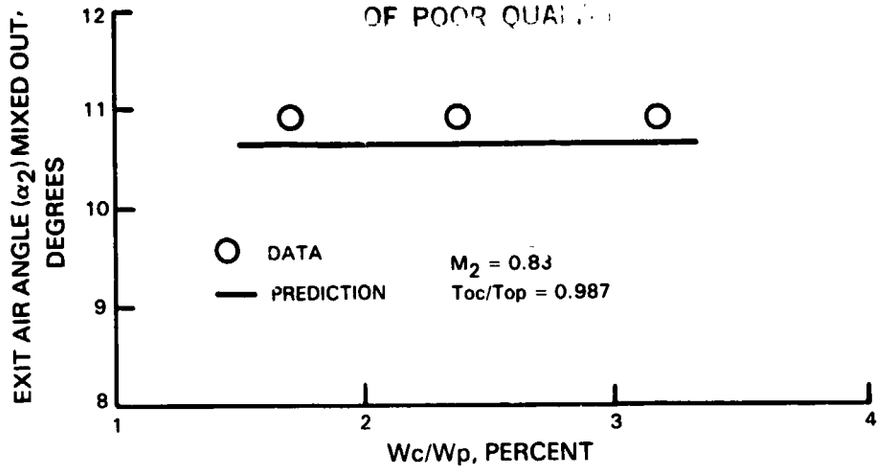

Figure 51 Straight Wall Cascade Exit Air Angle vs Cooling Flow Rate

These results confirm the well-known and expected predominance of suction surface coolant discharge penalty in the overall vane cooling loss penalty. This is best explained by referring to Figure 7(b). Here it can be seen that the coolant flow injected from the trailing edge and pressure surface passages is more nearly aligned with the free-stream flow around the airfoil whereas that injected from the suction surface passages is nearly normal to the free-stream flow. In addition, twice as much coolant flow is injected from the suction surface passages as from either of the other two sites. The prediction was found to considerably overestimate the measured loss level. This result is attributed to the fact that the angle that the cooling holes make with the suction surface is approximately 55 degrees, a configuration outside the data base used in the analytical model. It should be noted, however, that the loss trends with changes in coolant flow rate are well predicted (i.e., compare the slopes of the two curves). Exit air angle results showed that the angle is insensitive to coolant flow rate variations and is well predicted.

3.4.5.5 Effects of Exit Mach Number and Suction Side Coolant Flow Rate Variations on Straight Wall Cascade Performance

As was the case for the uncooled cascade, exit Mach number was increased to simulate flow conditions near the vane root in order to detemine if transonic drag rise might be a problem with a cooled cascade. The suction-side injection case was selected for this evaluation because vane performance was shown to be most sensitive to suction surface injection. Pressure loss and exit air angle measurements were obtained at three cooling flow rates.

"Mixed-out" pressure losses were subsequently calculated from these data with the spanwise average values being presented as a function of cooling flow rate (see Figure 52).

ORIGINAL PAGE IS
OF POOR QUALITY

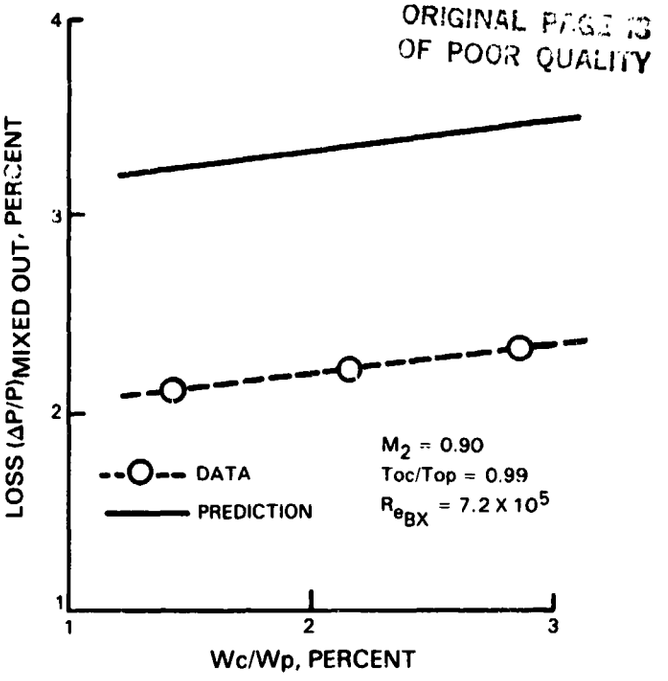

Figure 52 Straight Wall Cascade Pressure Loss vs Suction Surface Coolant Flow Rate at Exit Mach Number Equal to 0.9

As was the case when exit Mach number was 0.83, the analytical prediction considerably overestimates the level of pressure loss, although the change in pressure loss with variations in coolant flow rate agrees quite well with the experimental data (i.e., compare the curve slopes).

Figure 53 presents a comparison of the suction surface injection results for the two exit Mach numbers tested, along with their respective analytical predictions.

Figure 54 presents a comparison of the Mach number sensitivity of the vane section with no coolant flow and flow at the design flow rate. This figure shows that cascade loss increase with Mach number and suction surface coolant discharge is similar to the results obtained with no coolant flow.

Figure 55 compares the measured exit air angle results for the two Mach numbers tested and shows the exit angle to be insensitive to both coolant flow rate and Mach number. A prediction of the data is also presented in this figure, and is in good agreement with the data.

3.4.6 Summary of Vane Cascade Results

3.4.6.1 Uncooled Vane Cascade

Design-point mass averaged pressure losses for the straight wall and S-wall cascades are summarized in Table 15. As noted in the table, profile losses for the two cascades are about the same whereas the secondary losses of the S-wall cascade are considerably lower than for the straight wall cascade. Because of this, the S-wall cascade has a total pressure loss 17 percent lower than the straight wall cascade. This confirms the predicted benefits associated with contoured endwalls in turbine vane cascades.

ORIGINAL
OF POOR

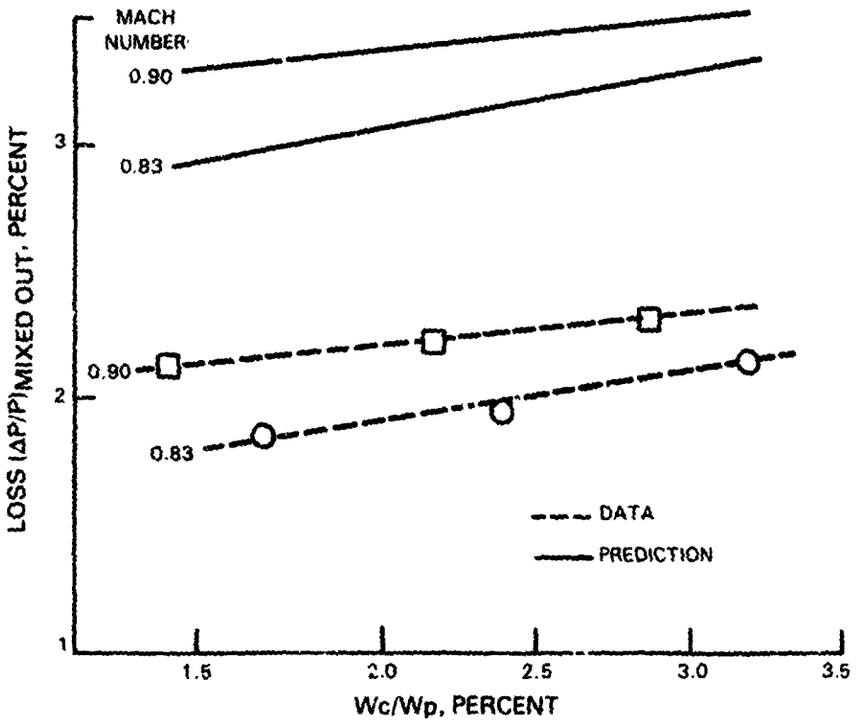

Figure 53 Effects of Changes in Suction Surface Coolant Flow Rate and Exit Mach Number on Cascade Pressure Loss

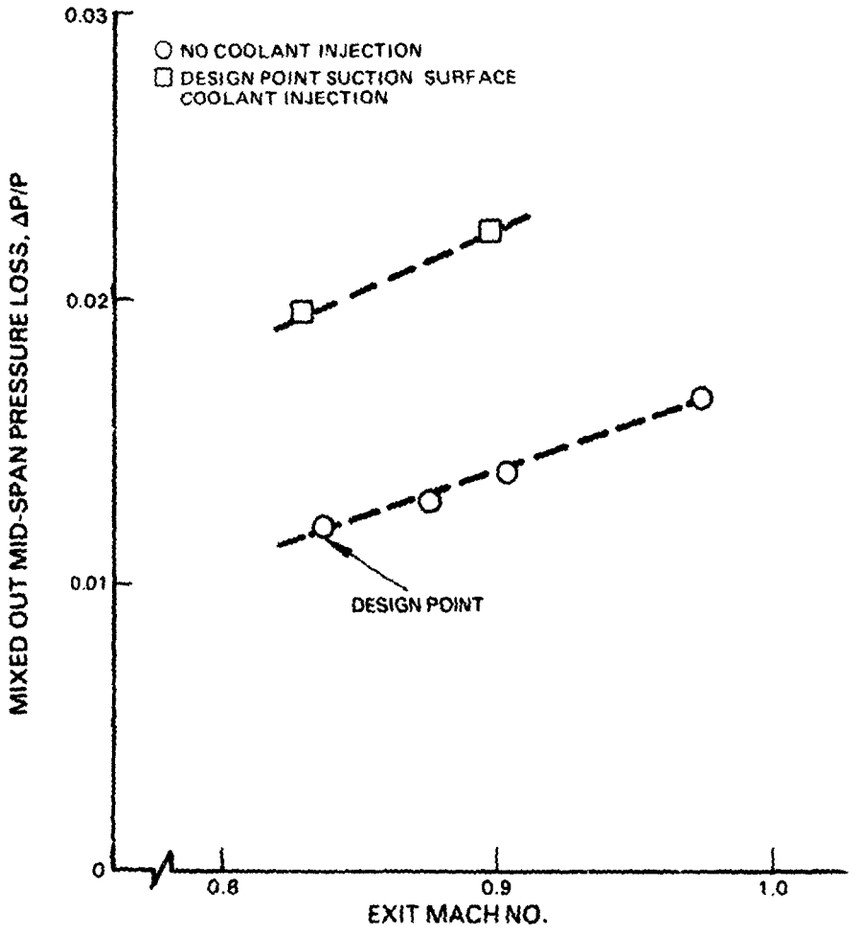

Figure 54 Straight Wall Cascade Midspan Loss vs Mach Number With and Without Design Point Coolant Flow Injection

ORIGINAL PAGE IS
OF POOR QUALITY

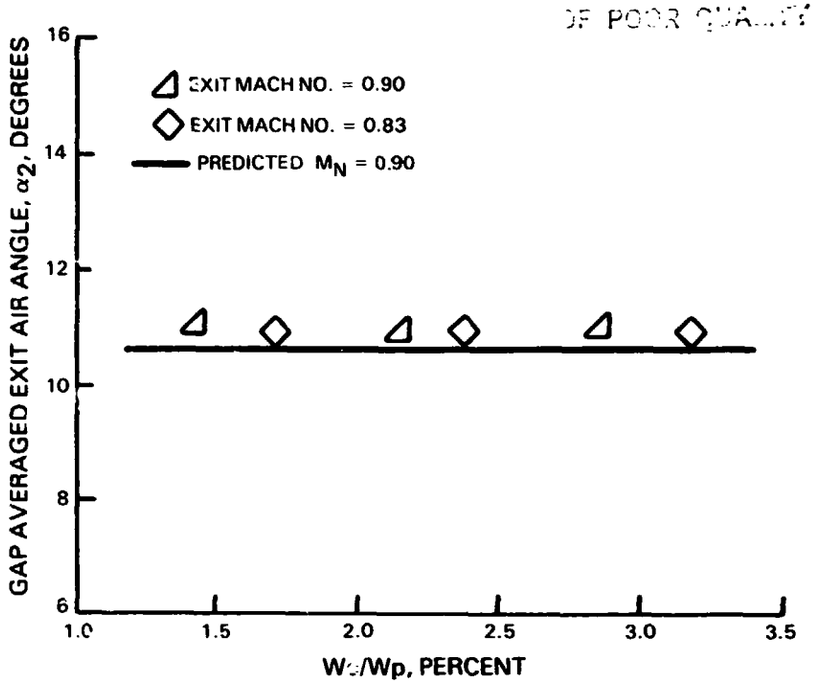

Figure 55 Measured Exit Air Angle as a Function of Suction Surface Coolant Flow Variation for Exit Mach Numbers of 0.83 and 0.9

TABLE 15

UNCOOLED STRAIGHT WALL AND S-WALL VANE CASCADE PRESSURE LOSSES
(Mass Averaged at Exit Mn = 0.84)

	Total Loss ($\Delta P_T/P_T$)	Profile Loss ($\Delta P_T/P_T$)	Secondary Loss ($\Delta P_T/P_T$)
Straight Wall Cascade	0.023	0.011	0.013
S-Wall Cascade	0.019	0.010	0.009
S-Wall Reduction % $\Delta P_T/P_T$	17.4	9.1	30.8

Increasing the exit Mach number in the straight wall cascade increased pressure losses; however, there was no abrupt increase in pressure loss even though the flow approached sonic conditions. This indicated that the component vane design is free of transonic drag rise over the range of intended operating conditions.

Spanwise variations in vane exit yaw angle were essentially similar for the two cascades except near the endwalls.

3.4.6.2 Cooled Vane Cascade

Design-point mass-averaged mid-span pressure losses and coolant flo penalties for the straight wall cascade with coolant flow injection from the airfoil trailing edge, pressure surface, and suction surface are summarized in Table 16. The basic points to be made from this summary are:

(1) The analytical prediction method consistently overestimates the pressure losses.

(2) Design point pressure loss almost doubled when design point coolant flow was injected from all discharge ports. The coolant flow penalty alone is approximately the same as the total profile loss for the uncooled cascade.

(3) Coolant injection penalties associated with trailing edge and pressure surface injection are comparable.

(4) The dominant loss penalty results, as expected, from suction surface coolant flow injection.

(5) Increasing exit Mach number causes an increase in total loss and loss penalty. This is shown by both the measured data and the analytical prediction. This increase is only moderate in the exit Mach number range of interest and confirms that flow within the cascade is free of transonic drag rise.

Predicted and measured exit air angles were in good agreement and proved to be insensitive to coolant flow injection rate changes as well as changes in exit Mach number.

TABLE 16

MID-SPAN PRESSURE LOSSES FOR STRAIGHT WALL CASCADE WITH COOLANT FLOW INJECTION
("Mixed Out" Loss at Design Point Coolant Flows)

	Trailing Edge Injection	Pressure Surface Injection	Suction Surface Injection	Suction Surface Injection	All Ports Flowing
Exit Mach. No.	.83	.83	.83	.90	.83
Measured Loss with Coolant Injection $\Delta P_T/P_T$	.0134	.0139	.0195	.0223	.0210
Measured Loss with No Coolant Injection $\Delta P_T/P_T$	.0120	.0120	.0120	.0140	.0120
Measured Coolant Loss Penalty $\Delta P_T/P_T$	.0014	.0019	.0075	.0083	.0090
Predicted Coolant Loss Penalty $\Delta P_T/P_T$	.0009	.0010	.0181	.0185	.0178
Predicted Total Loss with Coolant Injection $\Delta P_T/P_T$	.0143	.0144	.0315	.0340	.0312

4.0 BLADE CASCADE PROGRAM

4.1 Analysis and Design

Previous in-house studies of turbine blade cascades indicated that airfoil trailing edge base static pressure and cascade total pressure loss could be significantly affected by the distribution of the airfoil surface curvature aft of the throat.

The single stage turbine of the Energy Efficient Engine employs advanced aerodynamic concepts that achieve a high ratio of wheel speed to specific work (velocity ratio), a low ratio of through-flow to wheel tangential velocity (C_x/U) and high AN^2 (product of annulus area and wheel speed squared). The result is a blade airfoil operating at supersonic exit conditions which is different from state-of-the-art multi-stage high-pressure turbine airfoils. The blade design also employs internal conductive and external film cooling. The combination of these factors made it highly desirable to (1) verify that the distribution of curvature selected for the component blade airfoil geometry would achieve design objectives and (2) confirm the predicted effects on cascade performance due to trailing edge coolant flow discharge (i.e., in-house studies have indicated that trailing edge coolant flow discharge effects predominate over effects caused by leading edge film coolant flow discharge). An additional objective was to employ measured data to assess the accuracy of analytical methods and to gain a better understanding of the flow field within the cascade, particularly as it may be affected by trailing edge shocks.

To satisfy these objectives, three blade cascades were designed to model three airfoil geometries chosen for evaluation: (1) base, (2) overcambered, and (3) straightback. The base design represented the 43-percent reaction component blade mean section.

The overcambered airfoil featured more camber toward the trailing edge than the base design; and the straightback design featured a flatter suction surface downstream of the throat than the base airfoil. Cascade geometry design parameters and predicted pressure distributions for these three blade designs are summarized in Figures 56 through 58 respectively. Refer to Appendix A for a listing of the airfoil coordinates used for the base blade (Table A-3), overcambered blade (Table A-4), and the straightback blade (Table A-5).

The base airfoil design was modified to include internal flow passages (see Figure 59). These passages provided simulated cooling airflow for the trailing edge flow discharge tests. These flow passages simulate the cooling air discharge geometry conceived for the high-pressure turbine component blade.

The same analytical methods that were used to design the vane cascades were also employed in the blade cascade design. An existing exit angle deviation system and radial work distribution were modified, using previously generated in-house turbine design correlations, and applied to the blade design. The blade airfoil sections were designed to the same pressure distribution criteria as the vane. The blade suction surface curvature downstream of the throat was further optimized to reduce trailing edge shock losses.

ORIGINAL PAGE IS
OF POOR QUALITY

(43% REACTION BLADE MEAN SECTION)

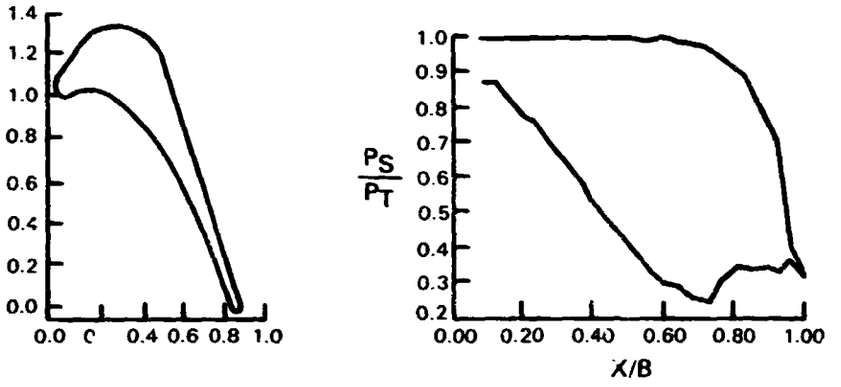

AXIAL CHORD (cm/in.)	2.34 (0.922)	EXIT METAL ANGLE (DEGREE)	17.07
PITCH (cm/in.)	3.45 (1.359)	EXIT WEDGE ANGLE (DEGREE)	2.00
THROAT (cm/in.)	0.940 (0.370)	UNCOVERED TURNING (DEGREE)	6.00
LEADING EDGE RADIUS (cm/in.)	0.155 (0.061)	INLET GAS ANGLE (DEGREE)	45.15
TRAILING EDGE RADIUS (cm/in.)	0.053 (0.021)	EXIT GAS ANGLE (DEGREE)	17.08
INLET METAL ANGLE (DEGREE)	40.15	MAX MACH NO.	1.58
INLET WEDGE ANGLE (DEGREE)	30.00	EXIT MACH NO.	1.22

Figure 56 High-Pressure Turbine Base Blade Design Parameters and Predicted Pressure Distribution

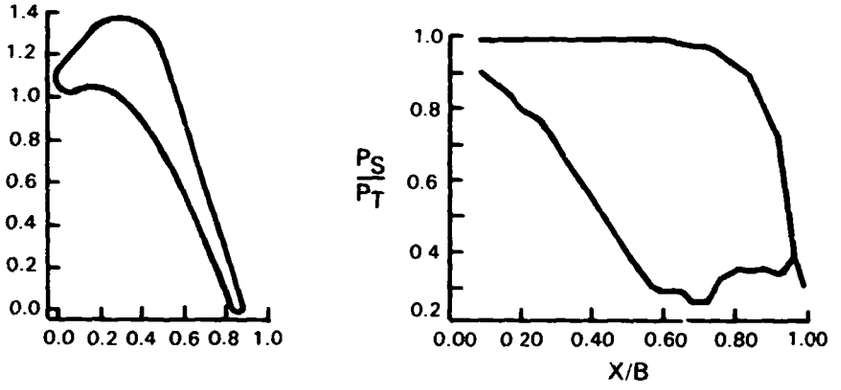

AXIAL CHORD (cm/in.)	2.34 (0.922)	EXIT METAL ANGLE (DEGREE)	15.50
PITCH (cm/in.)	3.45 (1.359)	EXIT WEDGE ANGLE (DEGREE)	2.00
THROAT (cm/in.)	0.940 (0.370)	UNCOVERED TURNING (DEGREE)	6.0
LEADING EDGE RADIUS (cm/in.)	0.155 (0.061)	INLET GAS ANGLE (DEGRFE)	45.15
TRAILING EDGE RADIUS (cm/in.)	0.053 (0.021)	EXIT GAS ANGLE (DEGREE)	17.08
INLET METAL ANGLE (DEGREE)	40.15	MAX MACH NO.	1.53
INLET WEDGE ANGLE (DEGREE)	30.00	EXIT MACH NO.	1.22

Figure 57 High-Pressure Turbine Overcambered Blade Design Parameters and Predicted Pressure Distribution

ORIGINAL PAGE IS
OF POOR QUALITY

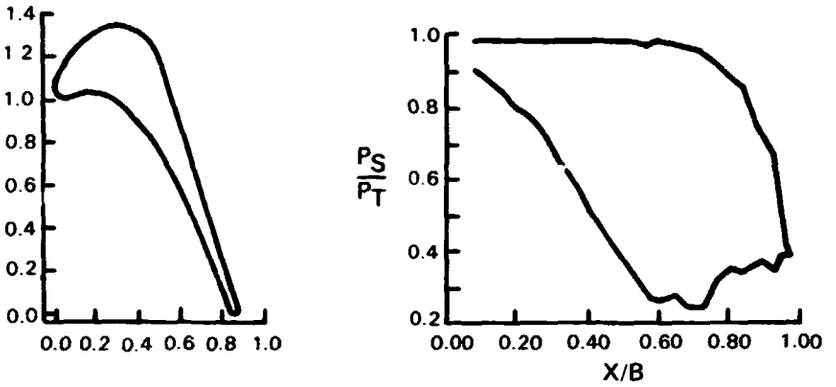

AXIAL CHORD (cm/in.)	2.34 (0.922)	EXIT METAL ANGLE (DEGREE)	17.82
PITCH (cm/in.)	3.45 (1.359)	EXIT WEDGE ANGLE (DEGREE)	2.00
THROAT (cm in.)	0.940 (0.370)	UNCOVERED TURNING (DEGREE)	2.00
LEADING EDGE RADIUS (cm/in.)	0.155 (0.061)	INLET GAS ANGLE (DEGREE)	45.15
TRAILING EDGE RADIUS (cm/in.)	0.053 (0.021)	EXIT GAS ANGLE (DEGREE)	17.08
INLET METAL ANGLE (DEGREE)	40.15	MAX MACH NO.	1.57
INLET WEDGE ANGLE (DEGREE)	30.00	EXIT MACH NO.	1.22

Figure 58 High-Pressure Turbine Straightback Blade Design Parameters and Predicted Pressure Distribution

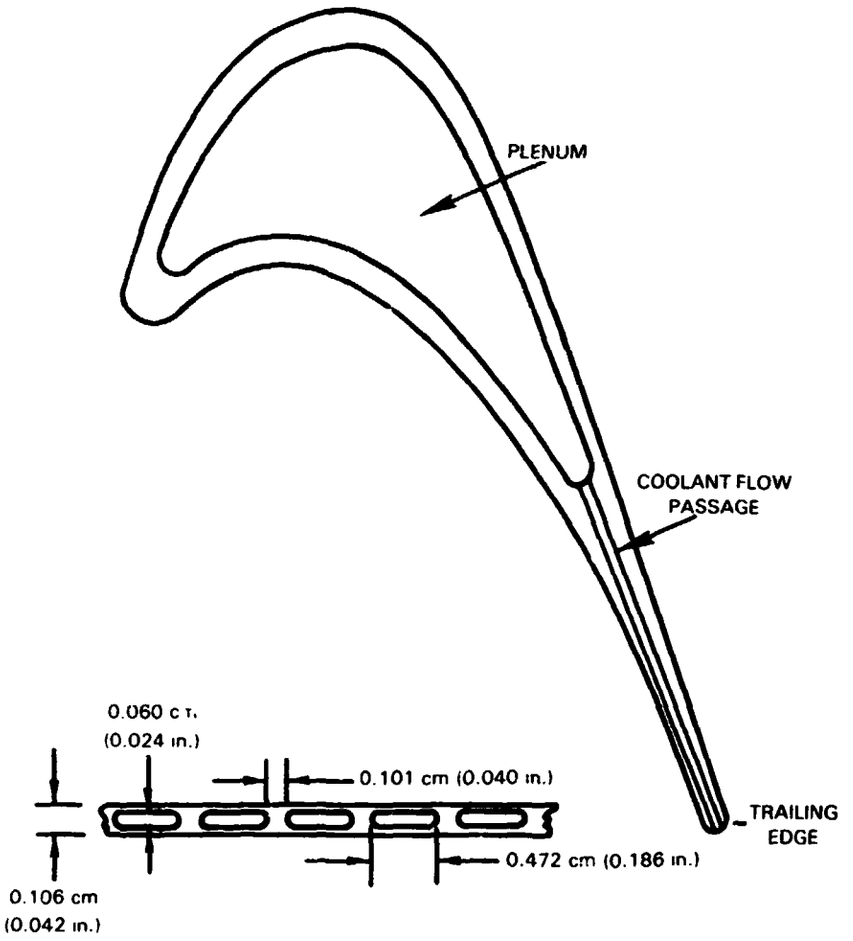

Figure 59 High-Pressure Turbine Base Blade Trailing Edge Coolant Ejection Geometry

4.2 Fabrication and Assembly

Three blade cascade assemblies corresponding to the three airfoil sections being investigated were fabricated for the program. Each cascade assembly consisted of eight constant section airfoils with a span of 10.16 cm (4 in.) and two circular acrylic plastic endwalls (Schlieren windows). These endwalls were free to rotate so that inlet air incidence angle could be varied. The height of the approach duct was also variable so that the walls would approximate the stagnation streamlines of the end airfoils. Two of the eight airfoils were instrumented with static pressure taps. Close tolerance pins at the ends of each airfoil secured the airfoils between the endwalls. In addition, these pins served as conduits for the trailing edge discharge air and the pressure tap leads. For cooled testing, the center four airfoils of the base airfoil cascade were replaced with airfoils fabricated with internal flow passages (see Figure 59) to permit trailing edge ejection of simulated cooling air. This air enters the plenum chamber through a feed tube, which extends through the cascade endwall (schlieren window). From the plenum the flow passes through a restrictor plate (plate with holes in it), which ensures spanwise flow uniformity to the slots that discharge the flow at the trailing edge of the airfoil. A fully instrumentated blade is shown in Figure 60 and Figure 63 shows an assembled blade cascade installed in the test tunnel.

4.3 Testing

4.3.1 General Description

The objective of the blade cascade test program was to evaluate the performance of the base, overcambered, and straightback blade designs. The performance of each of the three airfoil designs was evaluated in terms of total pressure loss, airfoil pressure distribution, base pressure coefficient, shock loss, and exit gas angle. Coolant flow tests focused on determining the effects of trailing edge coolant flow injection on exit gas angle, cascade performance, and cascade flow field.

4.3.2 Test Facility and Instrumentation

4.3.2.1 Test Facility

The United Technologies Research Center (UTRC) variable density supersonic plane cascade wind tunnel, shown schematically in Figure 61, is a steady flow tunnel consisting of a test section, an upstream plenum supplied by a compressor, a heat exchanger system, and a downstream plenum connected to an exhauster system. The test section inlet duct length from the plenum is 91.4 cm (36 in.) long with 2 two-dimensional contractions. The overall contraction ratio is approximately 370 to 1. The inlet duct (airfoil span) is 10.2 cm (4 in.) long, and its height can be varied from about 10.2 cm (4 in.) to 21.6 cm (8.5 in.) as required when the cascade is rotated to change incidence angle. Mach number and Reynolds number can be independently varied by selective control of the compressor and exhauster. Large Plexiglas windows on both sides of the test section are provided for Schlieren photographs of shock waves. Figure 62 provides a schematic representation of the eight blade cascade installation. Figure 63 presents a photograph of the tunnel test section with a cascade installed.

ORIGINAL PAGE IS
OF POOR QUALITY

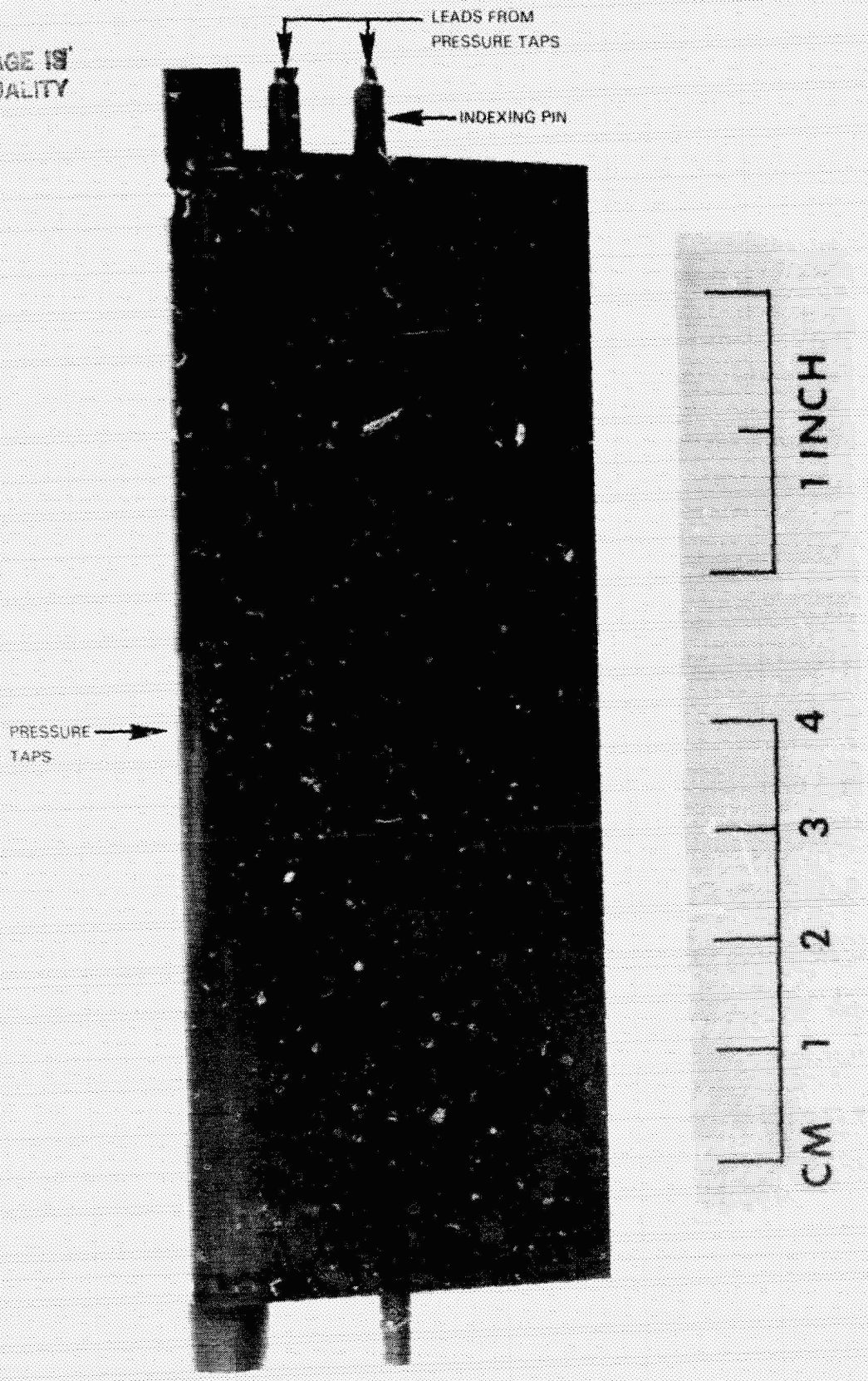

Figure 60 Photograph of Instrumented Blade

ORIGINAL PAGE
BLACK AND WHITE PHOTOGRAPH

ORIGINAL PAGE IS
OF POOR QUALITY

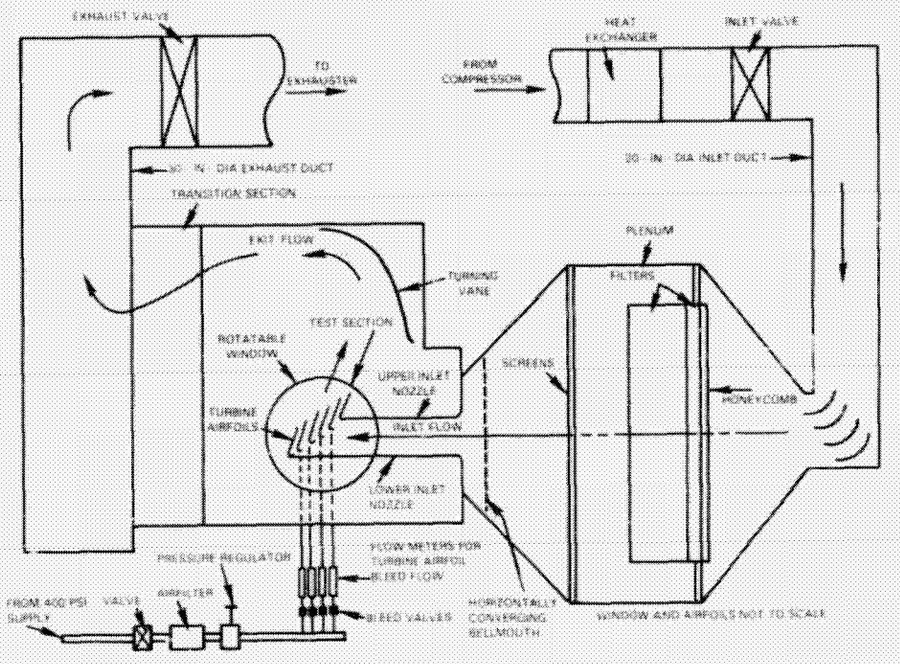

Figure 61 Schematic of UTRC Variable Density Supersonic Cascade Wind Tunnel

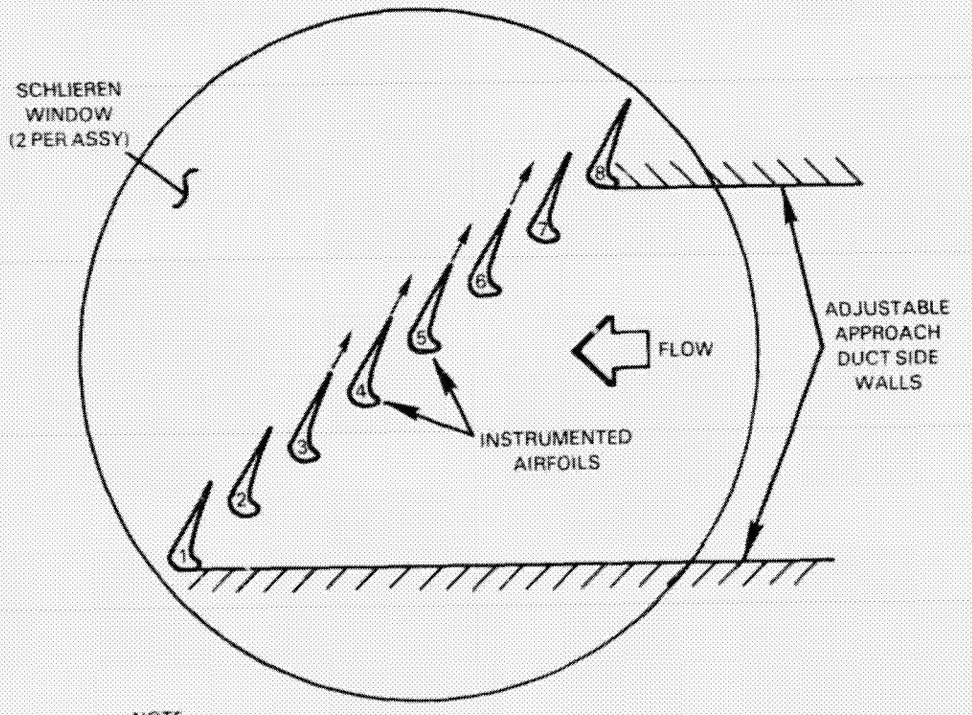

Figure 62 Schematic of Cascade Installation

ORIGINAL PAGE IS
OF POOR QUALITY

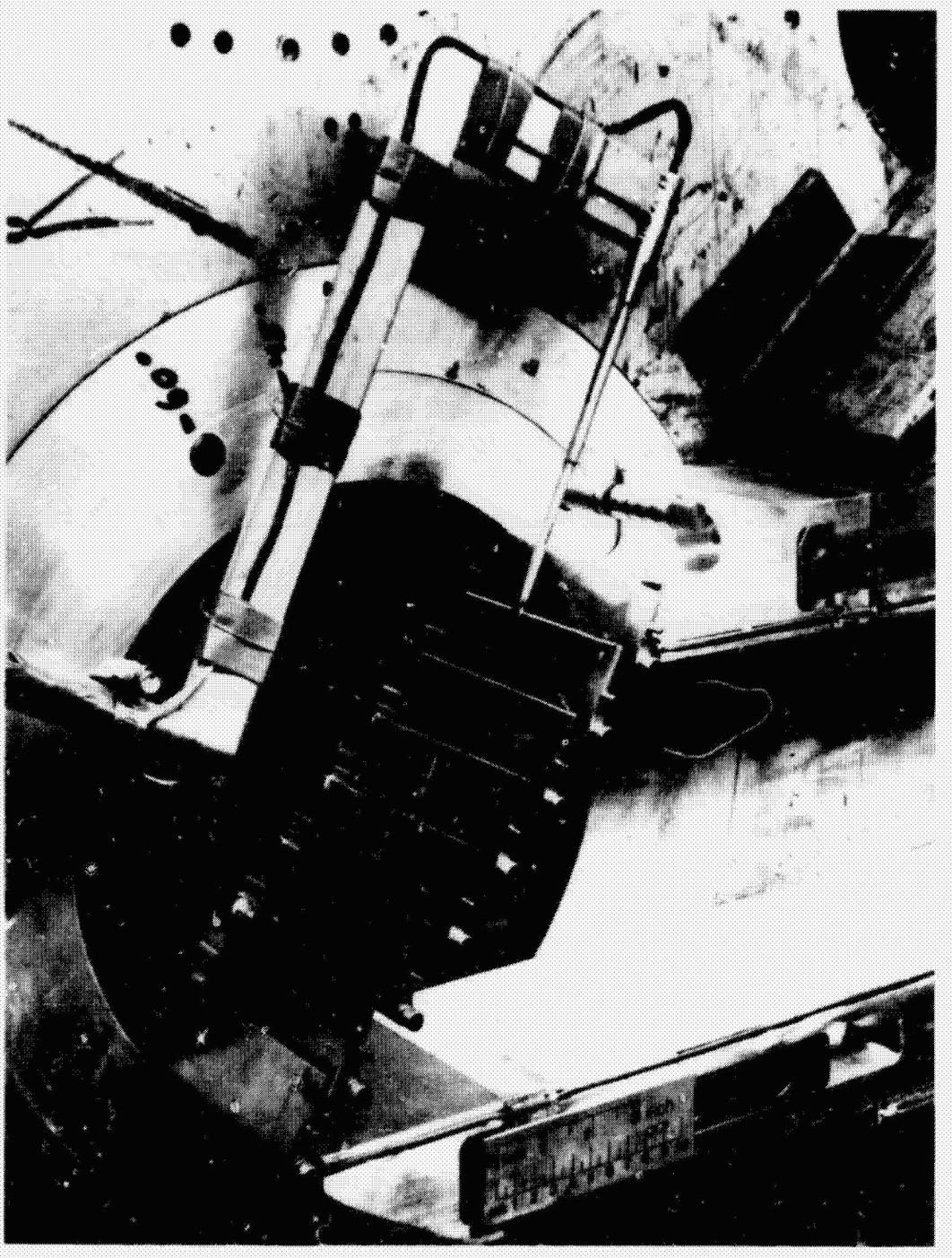

Figure 63 Tunnel Test Section with a Cascade Installed

ORIGINAL PAGE
BLACK AND WHITE PHOTOGRAPH

ORIGINAL PAGE IS
OF POOR QUALITY

A turbulence grid was not employed for blade cascade testing because residual turbulence in the cascade inlet flow, combined with the aerodynamic characteristics of the blade design, precluded the possibility of flow separation problems in the cascade during testing.

The Schlieren system permitted single frame roll film or 16 mm motion picture film to be taken of the blade cascade. Its viewing screen permitted monitoring of the image to be recorded, and its controls were located outside of the test cell. The parabolic mirrors were mounted on large heavy stone and steel piers to minimize the effects of vibration. The light beam in the system was folded to economize on the space available in the test cell. A dual light source, steady and pulsed, provided the illumination. Exposures as short as 1/2 second at rates as high as 4000 exposures per second were made. Both the normal opaque knife edge and the optional color knife edge were operator-adjustable at the camera station for optimum cutoff. Figure 64 presents a schematic representation of the Schlieren system for the blade cascade.

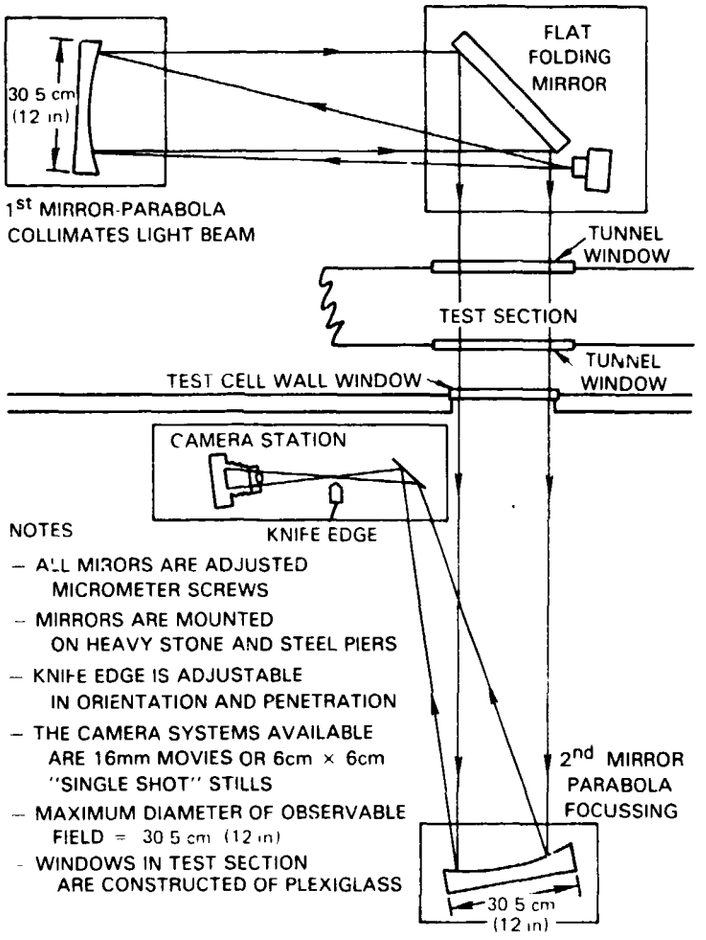

Figure 64 Schematic of Schlieren System

The cascade tunnel is provided with instrumentation that permits setting the cascade expansion ratio and operating Reynolds number. This instrumentation measures the upstream plenum total pressure and temperature and downstream plenum static pressure.

The tunnel is also equipped with a probe system used to obtain flow field performance measurements downstream of the cascade. This probe system consists of a probe drive mechanism, probe drive controller, pressure transducers, and data recording instrumentation. The probe drive mechanism moves the probe to programmed positions on the survey plane downstream of the cascade as indicated by the drive controller. This controller permits both the step size and the dwell time to be set as required for a given test.

The test facility is equipped to provide high-pressure air to the cascade for film cooling purposes. Coolant airflow rates are measured with rotameters. Instrumentation is provided to establish the total temperature and total pressure of the flow provided to the cascade.

4.3.2.2 Instrumentation

The instrumentation required for blade cascade testing is presented in Table 17.

TABLE 17

BLADE INSTRUMENTATION

Location	Measurement	Type	Quantity
Supply Plenum	Total Pressure	Kiel Probe	1
	Total Temperature	Thermocouple	1
Discharge Plenum	Static Pressure	Static Taps	1
Coolant Supply (each airfoil)	Flow Rate	Rotameter	1
	Total Pressure	Pressure Tap	1
	Total Temperature	Thermocouple	1
Survey Plane Downstream of Cascade	Total Pressure	Wedge Probe	1
		Kiel Probe	1
	Static Pressure	Wedge Probe	
	Yaw Angle	Wedge Probe	
Blade Surface	Static Pressure	Static Taps	*15
Cascade Passage	Schlieren Photograph	Schlieren System and Camera	1

*Each Blade: two airfoil's instrumented, as shown in Figure 65

ORIGINAL PAGE IS
OF POOR QUALITY

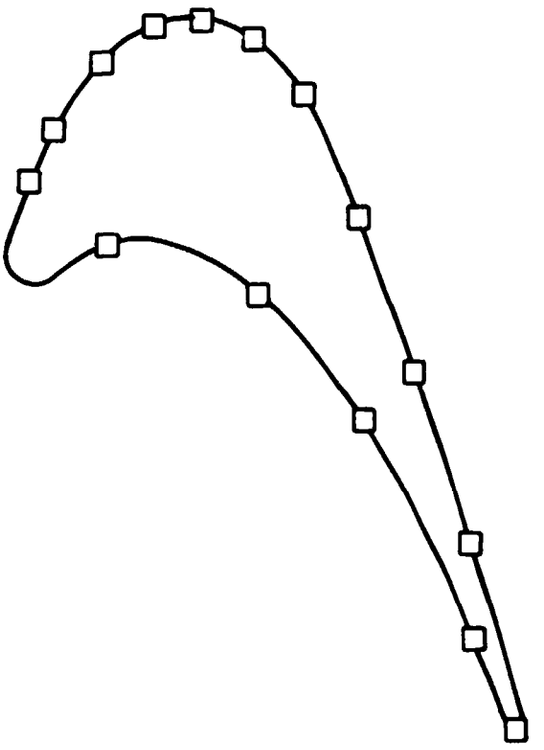

Figure 65 High-Pressure Turbine Blade Cascade Static Pressure Tap Locations

All of the performance data were obtained by using a wedge probe, shown in Figure 66, which consists of a 30-degree included angle wedge mounted on a stem. A pitot tube extends from the center of the wedge and meets flush with the wedge leading edge. Pressure ports for sensing air angle are located on both sides of the wedge. The taps for sensing static pressure are located at the axial location of the angle sensing taps and behind rearward facing steps. Calibration of this probe was accomplished by relating known flow conditions to probe pressure readings to yield calibration curves for total and static pressure and yaw angle. This calibration covered a range of Mach numbers from 0.6 to 1.4.

In addition to the wedge probe, a nineteen-element kielhead probe was used to measure exit total pressure across the blade span in order to determine the region of two-dimensional flow where more precise measurements could be taken with the wedge probe. The elements of this probe covered approximately 75 percent of the blade span, which was sufficient to penetrate the region where endwall effects begin to predominate (see, for example, Figure 76).

ORIGINAL PAGE IS
OF POOR QUALITY

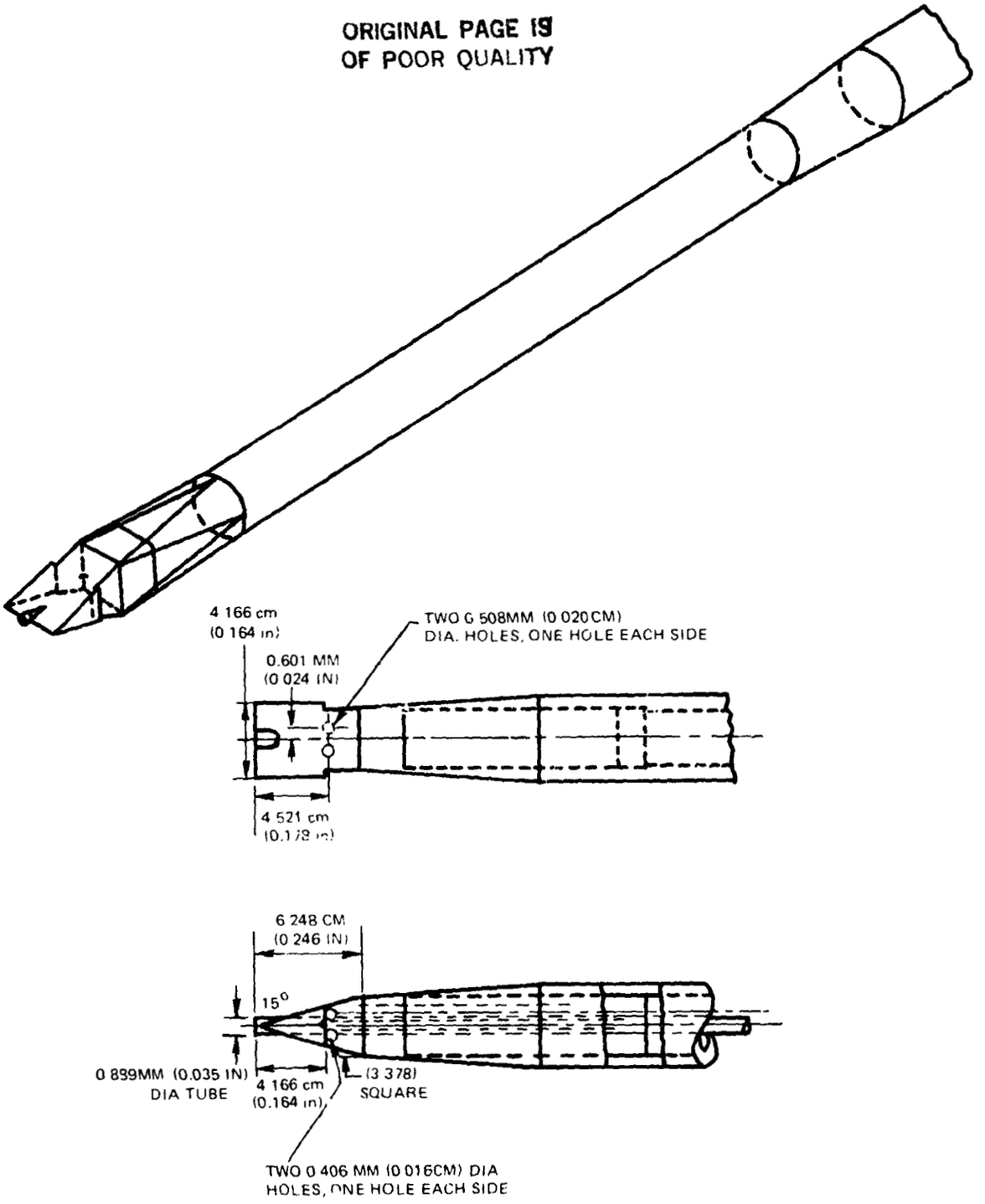

Figure 66 Isometric View of Wedge Probe Tip

4.3.3 Test Procedures

4.3.3.1 Establishing Test Conditions

Test conditions were established to provide a close simulation of engine design point altitude cruise conditions. Engine design point values and the corresponding range of rig test parameters evaluated are shown in Table 18.

TABLE 18

ENGINE DESIGN POINT VALUES AND RIG TEST PARAMETERS

Parameter	Engine	Rig
Exit Mach Number	1.22	0.6 - 1.3
Reynolds Number	6.0×10^6	5.0×10^6*
Inlet Air Angle (Degrees)	45	33 - 58
Coolant Flow (Percent Total)	2.0	1.0 - 3.0

* Although the flight condition Reynolds number was not achievable in the cascade tunnel, the value shown is in a range where pressure loss is relatively insensitive to variation of Reynolds number.

4.3.3.2 Shakedown Testing

Shakedown testing consisted of pressure leak checks and calibration of all instrumentation. A preliminary data point was run to verify performance of the instrumentation and data acquisition systems. The test program was initiated after it was ascertained that all instrumentation and systems were operating properly.

4.3.3.3 Performance Testing

The blade cascade test program was structured to permit performance evaluations over a range of test conditions. These included variations in coolant flow rate for the tests with trailing edge coolant ejection. In addition, the flow characteristics were observed through the use of Schlieren techniques.

Airfoil section pressure performance was measured by traversing the wedge probe in 0.762 mm (0.03 in.) steps in the pitchwise direction at midspan of the blade cascade. A minicomputer was used to control the probe traverse. At each sampling location, total pressure, static pressure, and yaw angle (angle in plane of endwall) were measured by pneumatic-to-electrical transducers. The transducer output corresponding to these measurements was recorded and magnetically stored, and the data were later reduced.

The cooled base airfoils were static tested by flowing air through the internal passages to atmospheric conditions, thereby establishing the total pressure drop between the internal plenum and the trailing edge. During cooled testing, the characteristics of the cooling flow at the exit of the internal passages could be calculated and used in the analytical prediction of performance.

For each test point, the inlet air incidence angle was set by rotating the circular endwalls as required. For each incidence setting, the height of the cascade approach duct was adjusted so that the du wall approximately corresponded to the stagnation streamlines of the outermost airfoils in the cascade.

The desired Mach number and Reynolds number for a test point were set by adjusting cascade tunnel pressures and total temperature to calculated values. Once test conditions were stabilized, the automatic data acquisition sequence was initiated.

Schlieren techniques were used to obtain still photographs which illustrated the cascade shock patterns. In some tests, lampblack and oil were applied to airfoil surfaces to establish surface flow patterns.

4.3.4 Performance Test Plan

The test plan for the blade cascade tests is presented in Table 19.

TABLE 19

ACTUAL BLADE CASCADE TESTS*

Test	Mach Number (Isentropic)	Expansion Ratio(1)	Inlet Air Angle (degrees)	Reynolds Number
1	0.8	0.656	43	5.0×10^5
2	1.0	0.528	43	
3	1.1	0.468	43	
4	1.2	0.412	43	
5	1.3	0.361	43	
6	1.2	0.412	33	
7	1.2	0.412	58	
8	1.4	0.314	43	
9	0.65	0.753	43	4.0×10^5

* The nominal cooling ejection rates were 1, 2, and 3 percent for the base blade cascade.

(1) Exit static-to-inlet total pressure ratio

Each cascade was evaluated over the range of test conditions shown with no trailing edge coolant ejection. In addition, the base blade cascade was tested with trailing edge coolant flow ejection rates of 1, 2, and 3 percent of the total flow to determine the performance impact of coolant flow variations at design point and off-design conditions.

Since actual exit Mach number (M_2) is dependent upon the actual cascade loss, isentropic Mach number (M_{2i}) was used to set the test conditions. The relationship between M_2 and M_{2i} for the cascades tested is shown in Figures 67, 68, 6. and 70.

ORIGINAL PAGE IS
OF POOR QUALITY

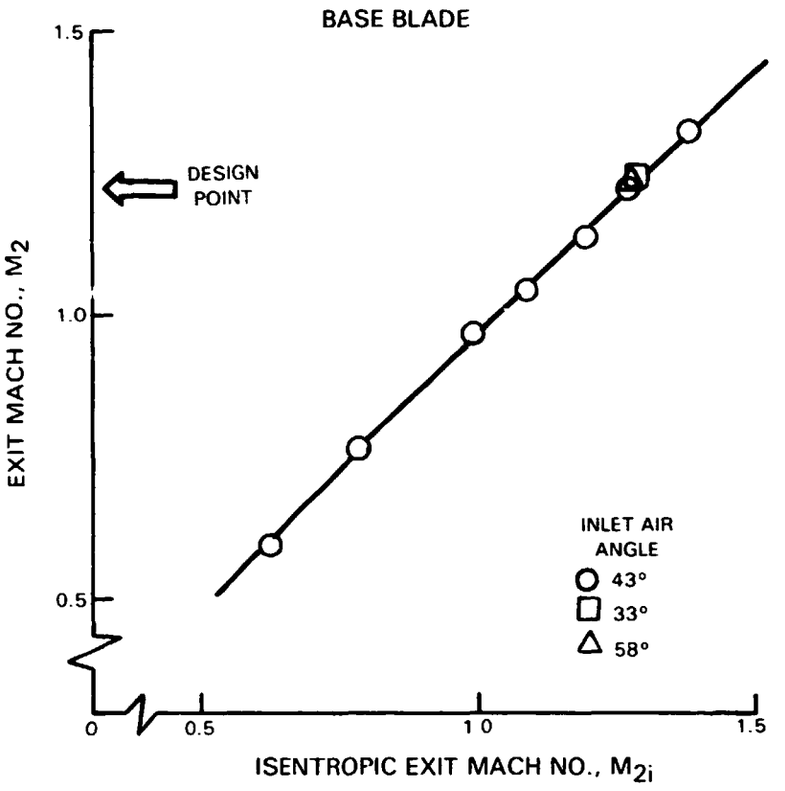

Figure 67 Relationship Between Actual Exit Mach Number and Isentropic Exit Mach Number for the Base Airfoil Cascade

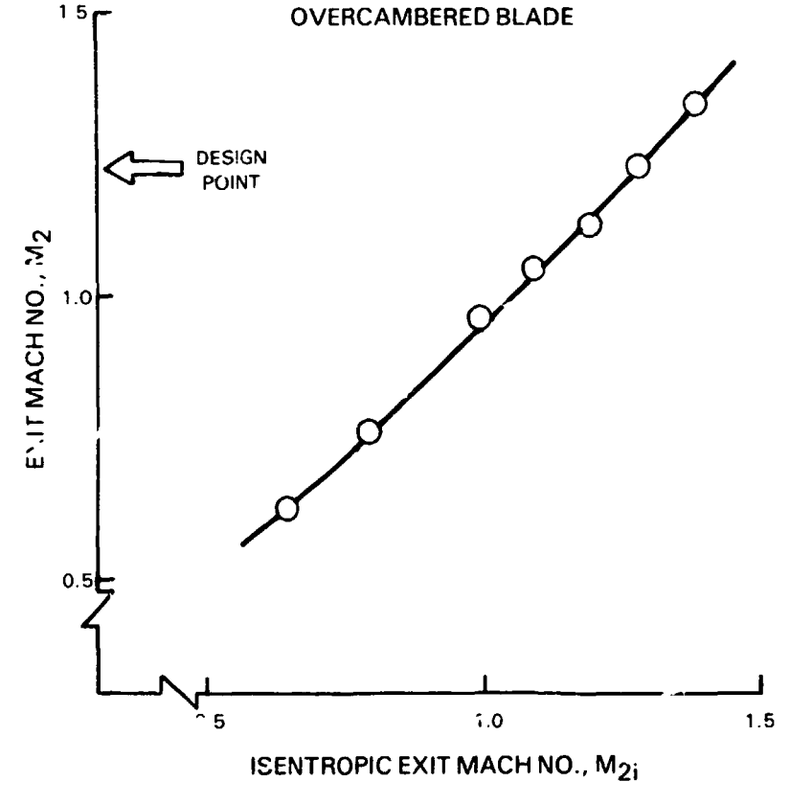

Figure 68 Relationship Between Actual Exit Mach Number and Isentropic Exit Mach Number for the Overcamber Airfoil Cascade

ORIGINAL PAGE IS
OF POOR QUALITY

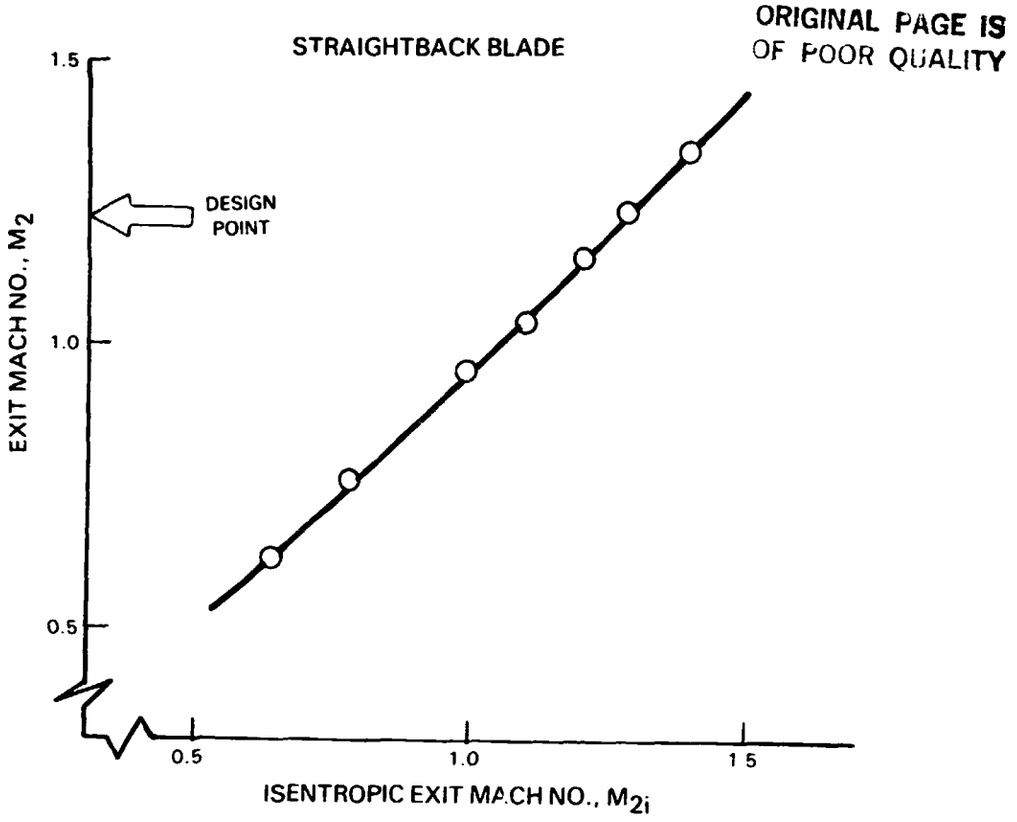

Figure 69 Relationship Between Actual Exit Mach Number and Isentropic Exit Mach Number for the Straightback Airfoil Cascade

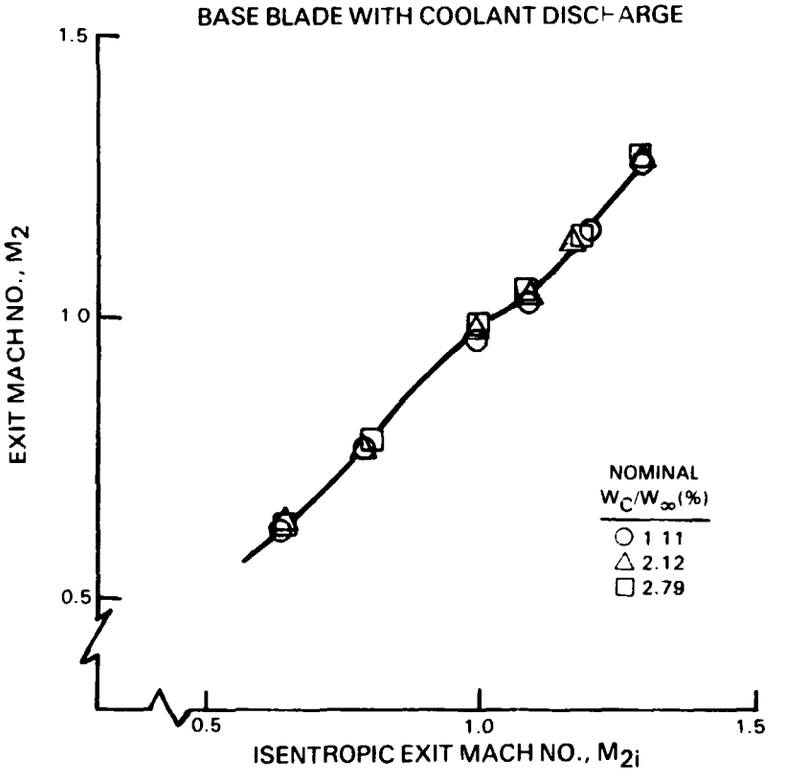

Figure 70 Relationship Between Actual Exit Mach Number and Isentropic Exit Mach Number for the Base Airfoil Cascade with Trailing Edge Coolant Flow Discharge

4.3.5 Data Reduction and Analysis

The data acquisition sequence for the blades in presented in Table 20.

TABLE 20

BLADE DATA ACQUISITION SEQUENCE

Sequence	Data Obtained
1. Apply known pressure to transducers (*)	Transducer calibration
2. Set cascade expansion ratio	None
3. Set coolant flow rates	Primary flow inlet total pressure Primary flow temperature Cell static pressure Airfoil static pressures Coolant total pressures Coolant flow rates
4. Program probe controller and start data acquisition sequence	Local total pressure, static pressure, and yaw angle for the mid-span exit plane traverse of two pitches
5. Check cascade expansion ratio and coolant flow rates; to be repeated periodically during data acquisition sequence	Check for drift of test conditions; test ended if significant drift occurs

(*) Transducers are periodically calibrated against reference pressures during data acquisition.

The data obtained from the test program were analyzed in detail to permit the verification of design concepts and the development of information useful in executing the design of the high-pressure turbine component. This data analysis included the following:

1. Comparison of measured airfoil static pressures with analytical predictions.

2. Comparison of measured total pressure losses with analytical predictions.

3. Comparison of measured exit air angle with analytical predictions.

4. Determination of the performance sensitivity to incidence angle variations.

5. Determination of performance sensitivity to coolant flow rates.

6. Determination of the variation of base pressure coefficient with exit Mach number.

7. Determination of shock wave locations.

Pressure loss and exit air angle data for each individual cascade are mass-averaged. Summary data used in the airfoil performance comparisons are an arithmetic average of the airfoil 4 and 5 mass-averaged data measured at each test condition. This is done to partially account for the difference in measured data between airfoils 4 and 5 which was due to non-periodicity in the cascades at transonic and supersonic Mach numbers.

4.3.6 Experimental Uncertainty

Experimental uncertainty for the results obtained are estimated to be ± 0.02 P/PT for surface static data; ± 2.5 degrees for gap averaged exit air angle (β_2) and $\pm .01$ isentropic exit Mach number; ± 8 percent $\backslash P_T/P_T$ at subsonic exit Mach numbers and ± 22 percent $\backslash P_T/P_T$ at supersonic exit Mach numbers.

4.4 Results

Analysis of the blade cascade data. described in sections 4.4.3 and 4.4.4 was divided into two major categories: (1) that associated with the uncooled tests (section 4.4.3) and (2) that associated with trailing edge cooling flow discharge tests (section 4.4.4).

4.4.1 Flow Visualization

As with the vane cascades, surface flow visualizations were conducted prior to performance testing to establish if any flow separation problems existed. These flow visualizations were made by applying a mixture of lampblack and oil to the airfoil surfaces and subsequently operating the cascade tunnel at test point conditions for about one minute. In addition, because at design point conditions part of the flow field is supersonic, Schlieren photographs were obtained to detail the shock structure.

A typical airfoil suction surface flow pattern at design point conditions (inlet gas angle of 43 degrees and exit Mach number of 1.25) is shown in Figure 71. This pattern was observed to be quantitively and qualitively similar for the base, overcamber, and straightback airfoils.

Referring to Figure 71, two separation bubble regions were observed in the flow visualizations; one at X/BX of approximately 0.6, which was about 0.25 cm (0.1 in.) wide and which was also found to occur for both subsonic and supersonic exit flows, and a second at X/BX of approximately 0.7, which was also about 0.25 cm (0.1 in.) wide but occurred only for supersonic exit flows. The more forward separation bubble is attributed to a laminar separation resulting from the start of the adverse pressure gradient on the suction surface (see, for example, Figure 82). Boundary layer calculations indicated that the boundary layer was laminar at this point on the suction surface. The second separation bubble region indicated further aft on the suction surface is attributed to an oblique shock-boundary layer interaction. This is

ORIGINAL PAGE
BLACK AND WHITE PHOTOGRAPH

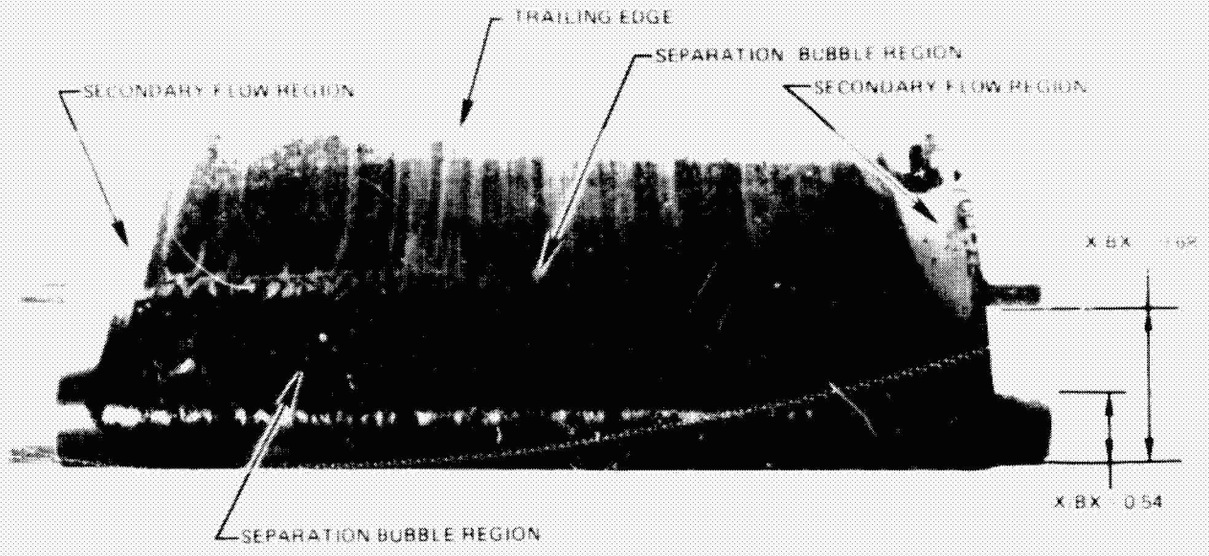

Figure 71 Flow Visualization Photograph of Airfoil Suction Surface for an Isentropic Exit Mach Number of 1.3

supported by the Schlieren photograph obtained for design point conditions (Figure 72) which shows the pressure surface trailing edge shock impinging on the adjacent airfoil surface at approximately X/BX = 0.7. The two reflected shocks characterize the formation of a small separation bubble as depicted in the schematic of the shock impingement region shown in Figure 73. A further discussion and presentation of the schlieren photographs obtained for the three airfoil sections tested are presented in the following sections of this report.

4.4.2 Periodicity and Two-Dimensionality Evaluation

Periodicity (i.e., the degree to which flow characteristics are identical between blade passages, and the degree to which two-dimensional flow was achieved at cascade mid-span were assessed at both subsonic and supersonic exit Mach number conditions. Valid comparisons between analytical predictions and airfoil section performance require that these conditions be met. The base airfoil cascade was used for this assessment. For the purpose of making this assessment these conditions are judged to have been achieved when identical two-dimensional flow conditions exist within the mid-span region of the central airfoil passages of the cascade. This means that adjacent airfoils have equal surface static pressure distributions and a spanwise pitch average downstream total pressure loss distribution which is flat in the mid-span region.

In the overall assessment of cascade periodicity, good airfoil-to-airfoil surface static pressure agreement was achieved for the center airfoils (airfoils 4 and 5) of the cascades tested at subsonic Mach numbers. Some scatter in the data was observed in the suction-surface recompression region at transonic and supersonic exit Mach numbers. This was attributed to non-periodicity of the suction surface shock-boundary layer interaction. Data for all test points run are presented and discussed in the airfoil pressure distribution sections for the respective configurations.

ORIGINAL PAGE
BLACK AND WHITE PHOTOGRAPH

ORIGINAL PAGE IS
OF POOR QUALITY

Figure 72 Schlieren Observation of Oblique Shock Wave - Boundary Layer Interaction on Blade Suction Surface

ORIGINAL PAGE IS
OF POOR QUALITY

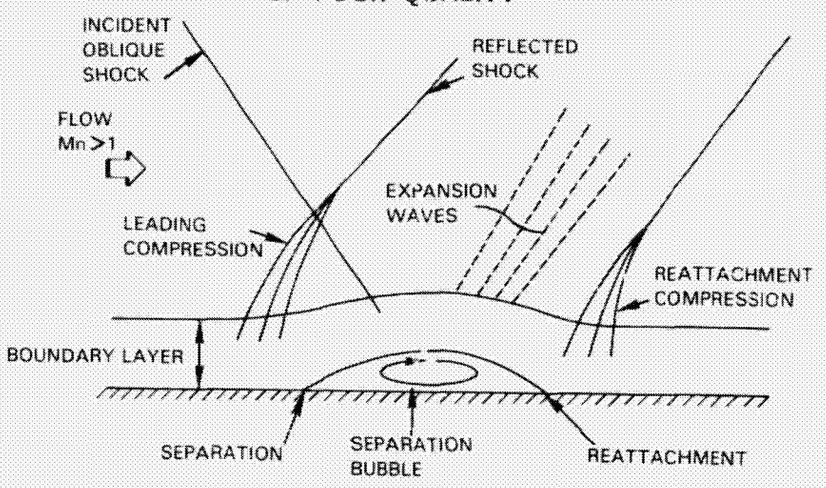

Figure 73 Depiction of Shock Boundary Layer Interaction

The measurement of airfoil mid-span total pressure losses was obtained from a wedge probe traverse downstream of airfoils 2 through 6 (i.e., the region where two-dimensional flow was anticipated). Results of this traverse are shown in Figure 74. For subsonic flow (M_{2i} = 0.8), the data indicate that the loss is relatively constant across airfoils 3 through 6, with cascade end effects beginning to show up at airfoils 2 and 7. Pressure losses for airfoils 4 and 5 were essentially identical. For supersonic flow, the individual airfoil data indicate that the losses are not as periodic as for subsonic conditions. It was also found that the data for airfoils 4 and 5 were not repeatable, the measured variations being approximately +10 percent. It should be pointed out that when the loss was high for airfoil 4, it was low for airfoil 5, and vice versa, indicating that the losses for these airfoils may not be independent of each other.

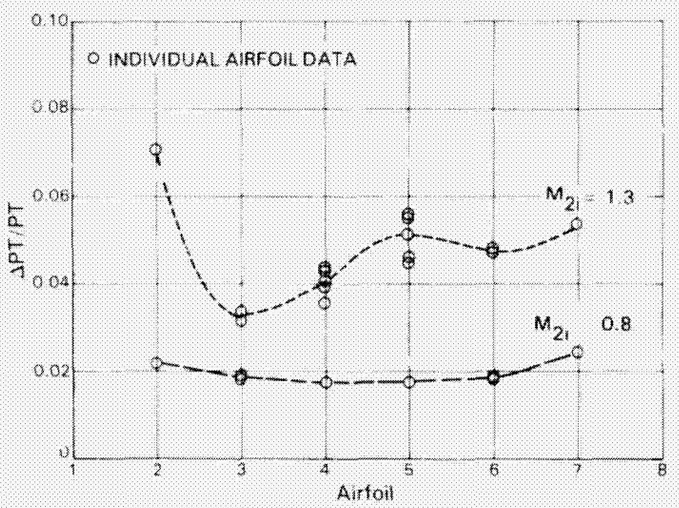

Figure 74 Loss for Individual Base Airfoils In Supersonic and Subsonic Flow

The non-periodicity of the loss data between airfoils 4 and 5 at supersonic conditions may at least partially result from the non-periodic structure of the shock system reflected from the free shear layer. This non-periodic shock structure is evident in the Schlieren photograph shown in Figure 75. The lack of repeatibility in the loss data for the individual airfoils is unexplained at this time but is most probably related to the downstream shock system having a number of differing stable modes.

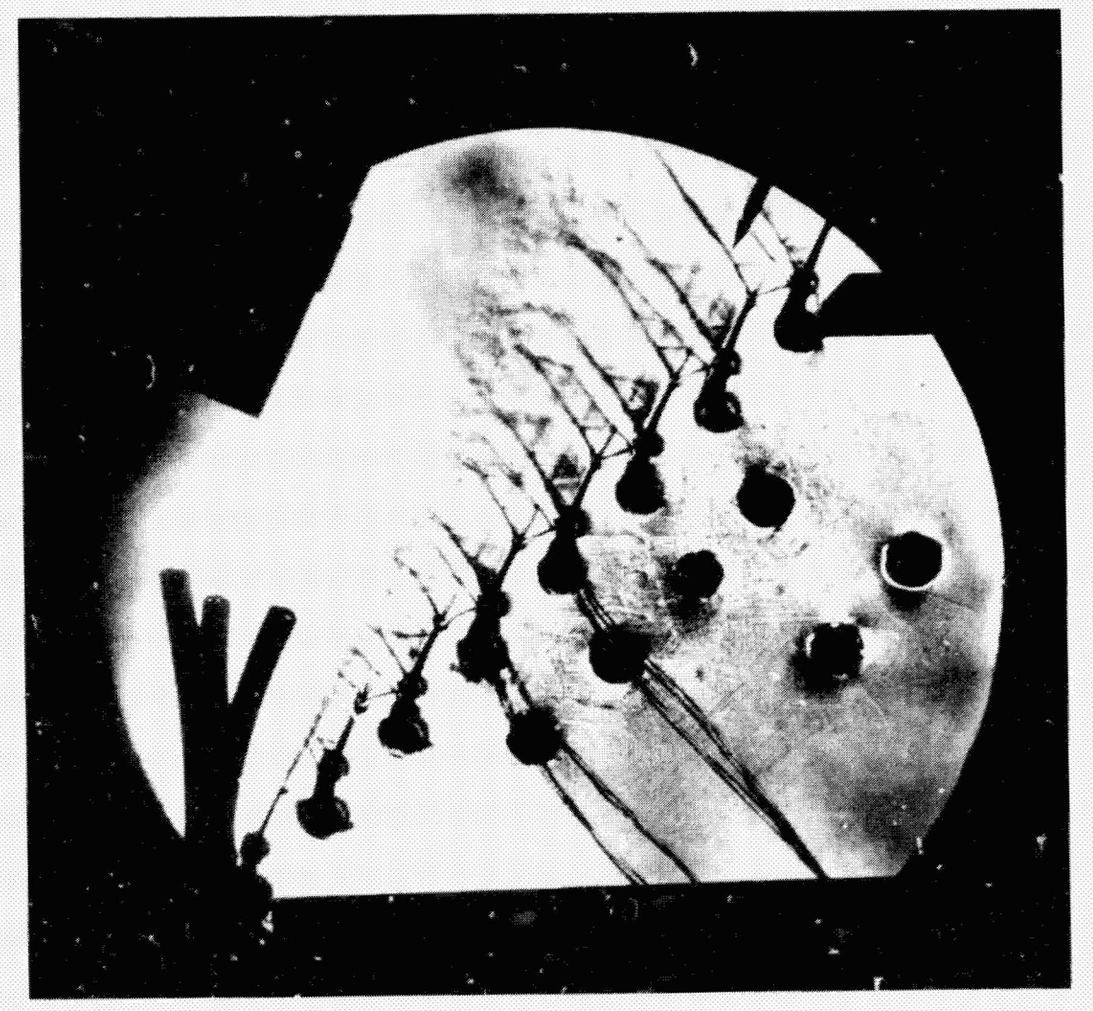

Figure 75 Schlieren Photograph Showing Flow Structure with Reflected Shocks

ORIGINAL PAGE
BLACK AND WHITE PHOTOGRAPH

ORIGINAL PAGE IS
OF POOR QUALITY

The distribution of spanwise total pressure loss data used to assess mid-span two-dimensionality was obtained with a 19-element kielhead rake. These data are presented in Figure 76 for two subsonic Mach numbers and one supersonic Mach number and show that a relatively flat profile was achieved between 25 percent and 75 percent of the span. This indicates that reasonably good two-dimensionality was achieved. The mid-span loss level measured with the wedge probe at the same Mach numbers shows good agreement with the kielhead probe data at the subsonic Mach numbers and at the supersonic Mach number when the kielhead data are corrected for the probe bow shock.

The lack of periodicity in the cascade flow field at transonic and supersonic exit Mach numbers makes precise quantitative comparisons between data and analytical predictions difficult. The same holds true for the comparison of data between cascades. However, the level of data accuracy still permits meaningful conclusions to be drawn relative to component development objectives.

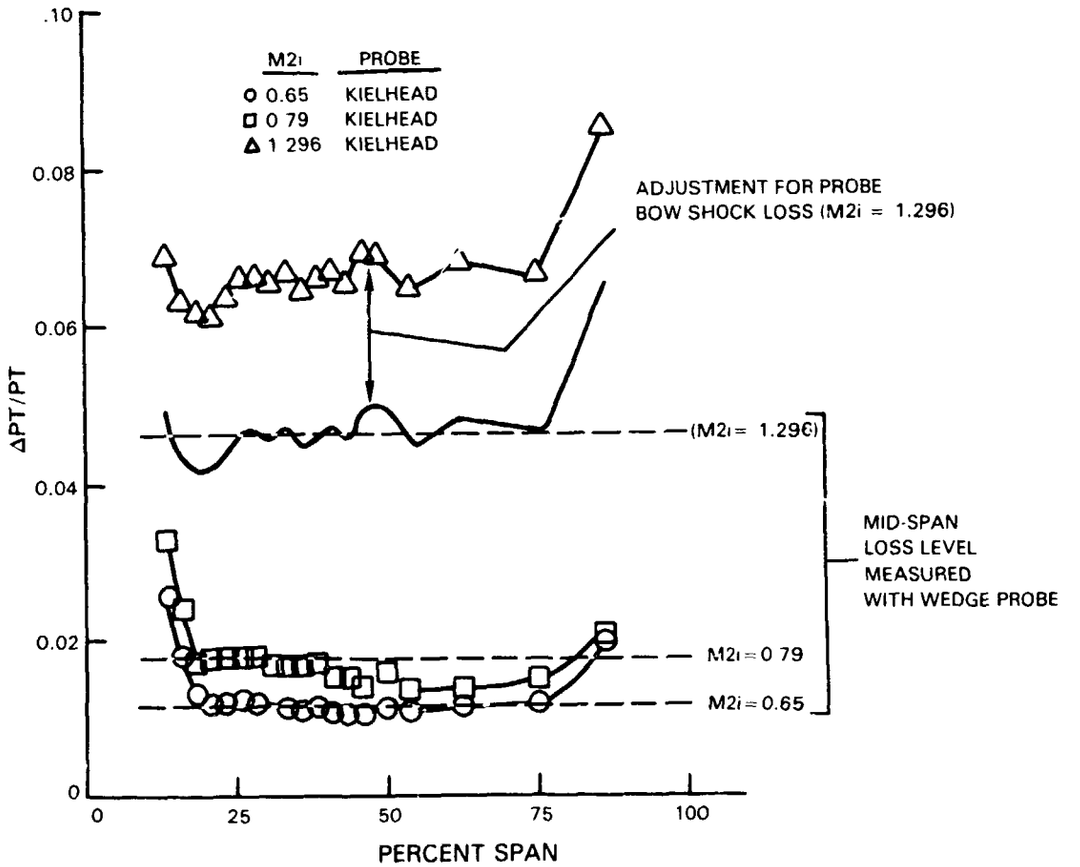

Figure 76 Spanwise Variation of Total Pressure Loss for Base Airfoil at 0.65, 0.79 and 1.3 Exit Mach Numbers

4.4.3 Uncooled Cascade Results

Test and analytical results obtained for the uncooled base, overcambered, and straightback blade designs are presented in this section. Predicted and measured pressure distributions and cascade losses are compared, and airfoil trailing edge base pressure and exit gas angle are assessed.

4.4.3.1 Base Airfoil Evaluation

4.4.3.1.1 Airfoil Pressure Distributions

Predicted and measured base airfoil surface static pressure distributions for the range of subsonic exit Mach numbers tested are shown in Figures 77 through 79. Agreement between the measured subsonic data and predictions was excellent. Pressure distributions for supersonic exit Mach numbers are shown in Figures 80 through 83. Pressure distributions for off-design inlet gas angles of 33 and 58 degrees at a nominal isentropic exit Mach number of 1.3 are shown in Figures 84 and 85. Agreement between predictions and the measured data for the supersonic exit conditions was good except for the recompression region where the measured data were scattered around the prediction The variability in the data from airfoil to airfoil in the recompression region is attributed to non-periodicity of the flow field, as discussed in Section 4.4.2 of this report.

4.4.3.1.2 Schlieren Observations

Schlieren photographs of the flow structure for the base airfoil over the range of isentropic exit Mach numbers tested are shown in Figure 86 through 89. These photographs illustrate that the strength and number of shocks which affect the loss increased with increasing Mach number. Also, the non-periodicity effect of the shocks reflected from the shear layer can be seen.

The double reflected shock shown results from the interaction of a trailing edge shock with the suction surface boundary layer. This is discussed in more detail in Section 4.4.1. The double shock pattern is most noticeable at the higher values of M_{2i}.

4.4.3.1.3 Total Pressure Loss Assessment

The variation of base blade total pressure loss with M_{2i} at the design inlet gas angle of 43 degrees for airfoils 4 and 5 is shown in Figure 90. The total pressure losses for the inlet gas angles of 33 and 58 degrees at M_{2i} = 1.3 (design point Mach number) are also presented in this figure and show that the loss changes little with incidence indicating that the design has good incidence range.

Predicted losses which were calculated employing the measured base pressure coefficients, C_{PB}, are compared with measured losses in Figure 90. This figure shows that the prediction is in good agreement with measured losses at subsonic Mach numbers and underestimate the losses at supersonic Mach numbers.

ORIGINAL PAGE IS
OF POOR QUALITY

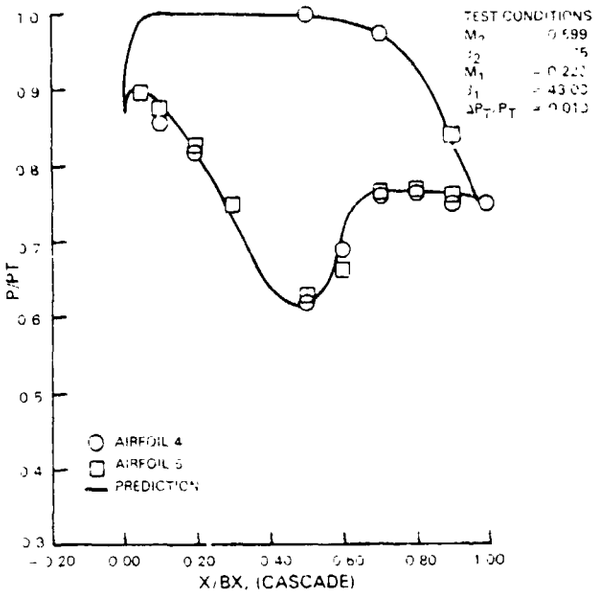

Figure 77 Uncooled Cascade Test (Base Blade Section) Pressure Distribution at 0.599 Exit Mach Number

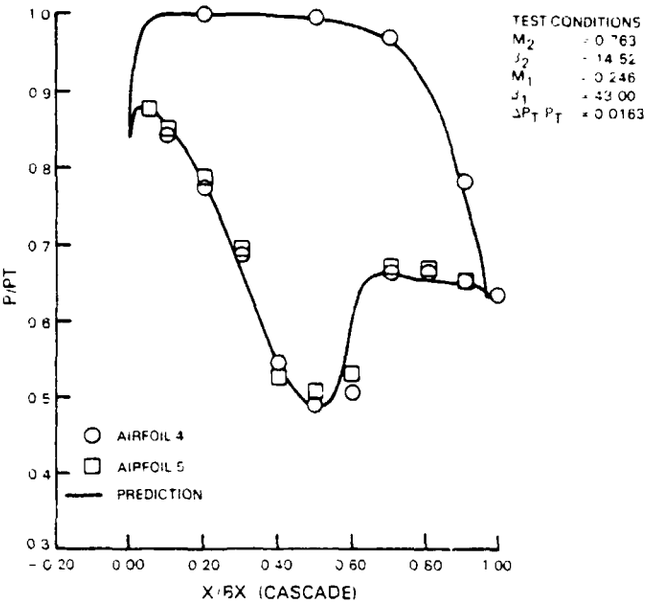

Figure 78 Uncooled Cascade Test (Base Blade Section) Pressure Distribution at 0.763 Exit Mach Number

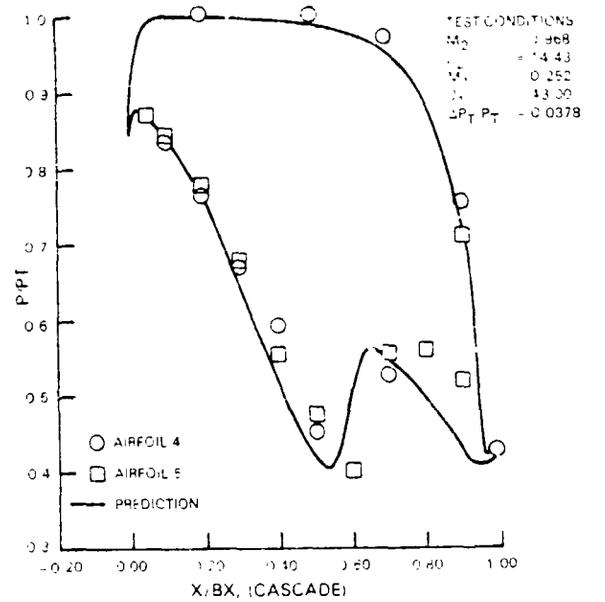

Figure 79 Uncooled Cascade Test (Base Blade Section) Pressure Distribution at 0.968 Exit Mach Number

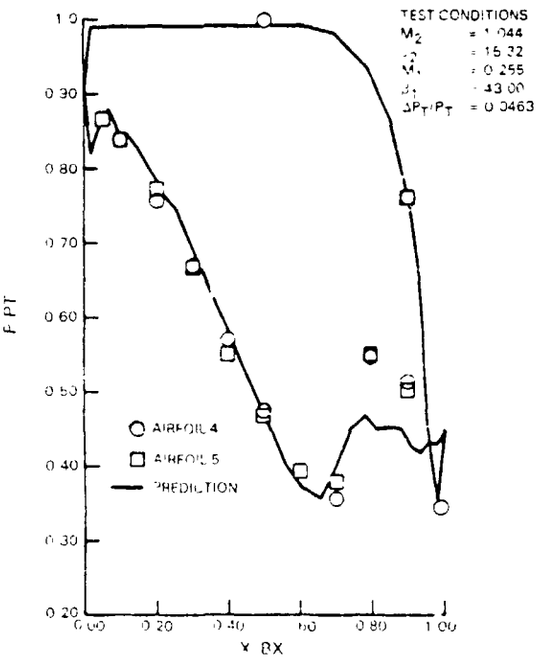

Figure 80 Uncooled Cascade Test (Base Blade Section) Pressure Distribution at 1.044 Exit Mach Number

ORIGINAL PAGE IS
OF POOR QUALITY

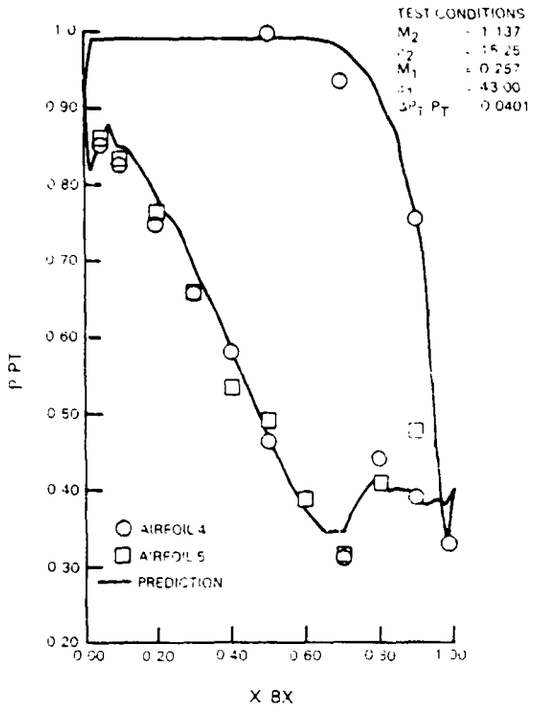

Figure 81 Uncooled Cascade Test (Base Blade Section) Pressure Distribution at 1.137 Exit Mach Number

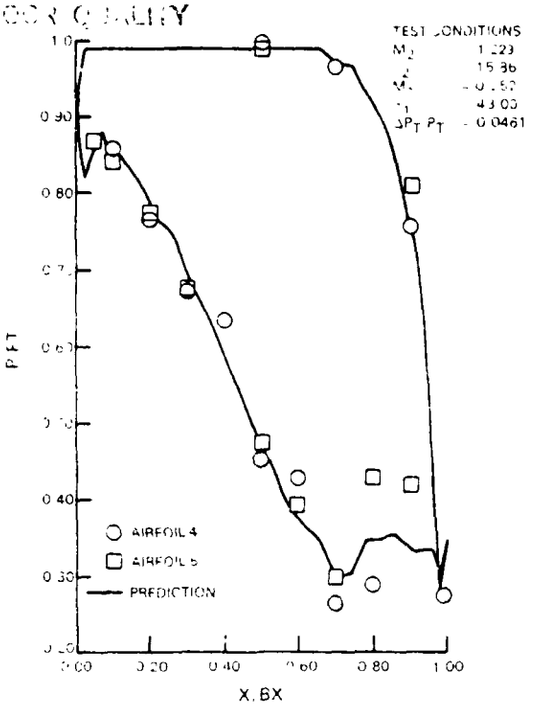

Figure 82 Uncooled Cascade Test (Base Blade Section) Pressure Distribution at 1.229 Exit Mach Number

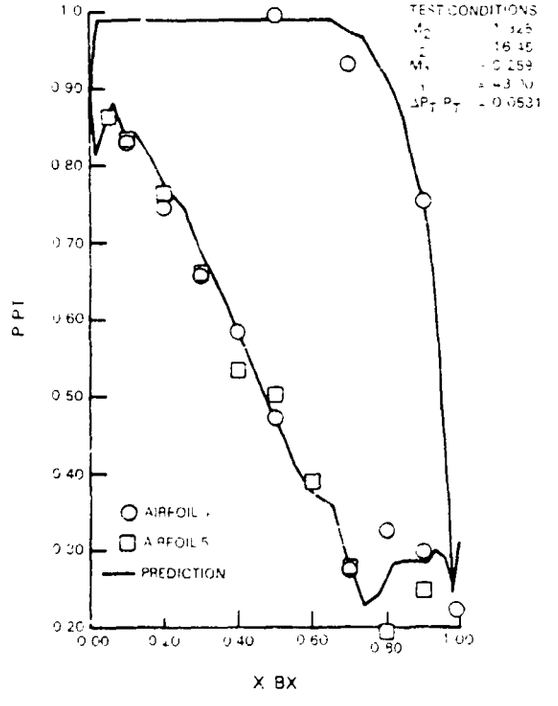

Figure 83 Uncooled Cascade Test (Base Blade Section) Pressure Distribution at 1.325 Exit Mach Number

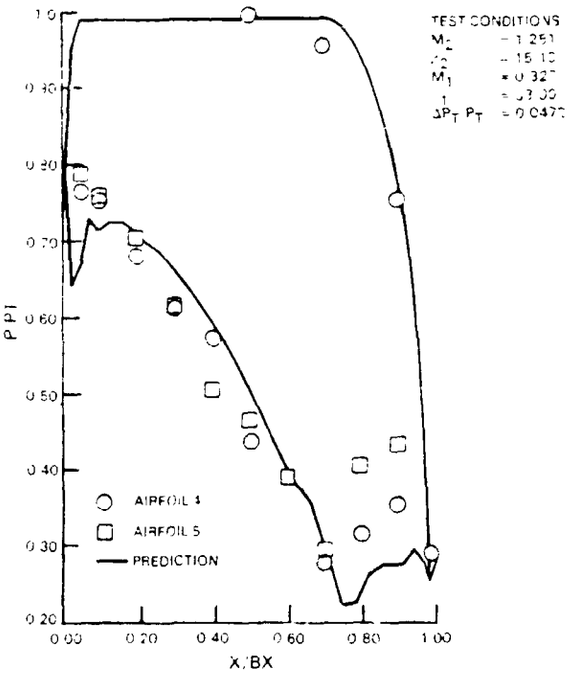

Figure 84 Uncooled Cascade Test (Base Blade Section) Pressure Distribution at 1.251 Exit Mach Number - Inlet Gas Angle of 33 degrees

ORIGINAL PAGE IS
OF POOR QUALITY

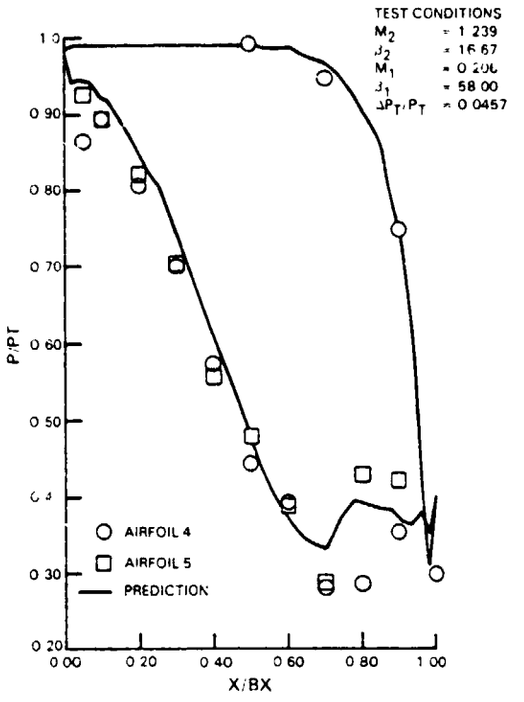

Figure 85 Uncooled Cascade Test (Base Blade Section) Pressure Distribution at 1.239 Exit Mach Number - Inlet Gas Angle of 58 degrees

4.4.3.1.4 Base Pressure Coefficient

The variation of "base" airfoil base pressure coefficient, C_{PB}, with isentropic exit Mach number, M_{2i}, is presented in Figure 91. Base pressure coefficients obtained at M_{2i} of 1.3 and off-design inlet gas angles of 33 and 58 degrees are also presented in Figure 91 and are seen to be approximately equal to the value obtained at the design inlet gas angle of 43 degrees. A curve faired through the data shows a local maximum near the design exit Mach number, which indicates that the design intent was achieved.

4.4.3.1.5 Exit Gas Angle

The variation of exit air angle, β_2, with M_{2i} for the base airfoil is presented in Figure 92. The predicted exit air angle is consistently 1.5 to 2 degrees higher than actual data over the range of Mach numbers investigated. The explanation for this difference is not known but is reasoned to be related to the measured angle. Continuity checks and measured airfoil loadings indicated that the predicted value is more nearly correct. Adjusting the measured angles upward by a nominal 1.70 degrees as indicated by these checks, would place the predicted and actual trends with Mach number in reasonable agreement.

Exit air angles obtained at the design point Mach number and off-design inlet gas angles of 33 and 58 degrees are shown in Figure 92. Changes in inlet gas angle would not be expected to have much of an effect on exit air angle. This proved to be the case for the inlet gas angle of 58 degrees where the exit air angle remained essentially the same as the design exit air angle. However, for the inlet gas angle of 33 degrees, the exit air angle was about 2 degrees less than the design inlet angle. This deviation is thought to have been caused by experimental inaccuracies.

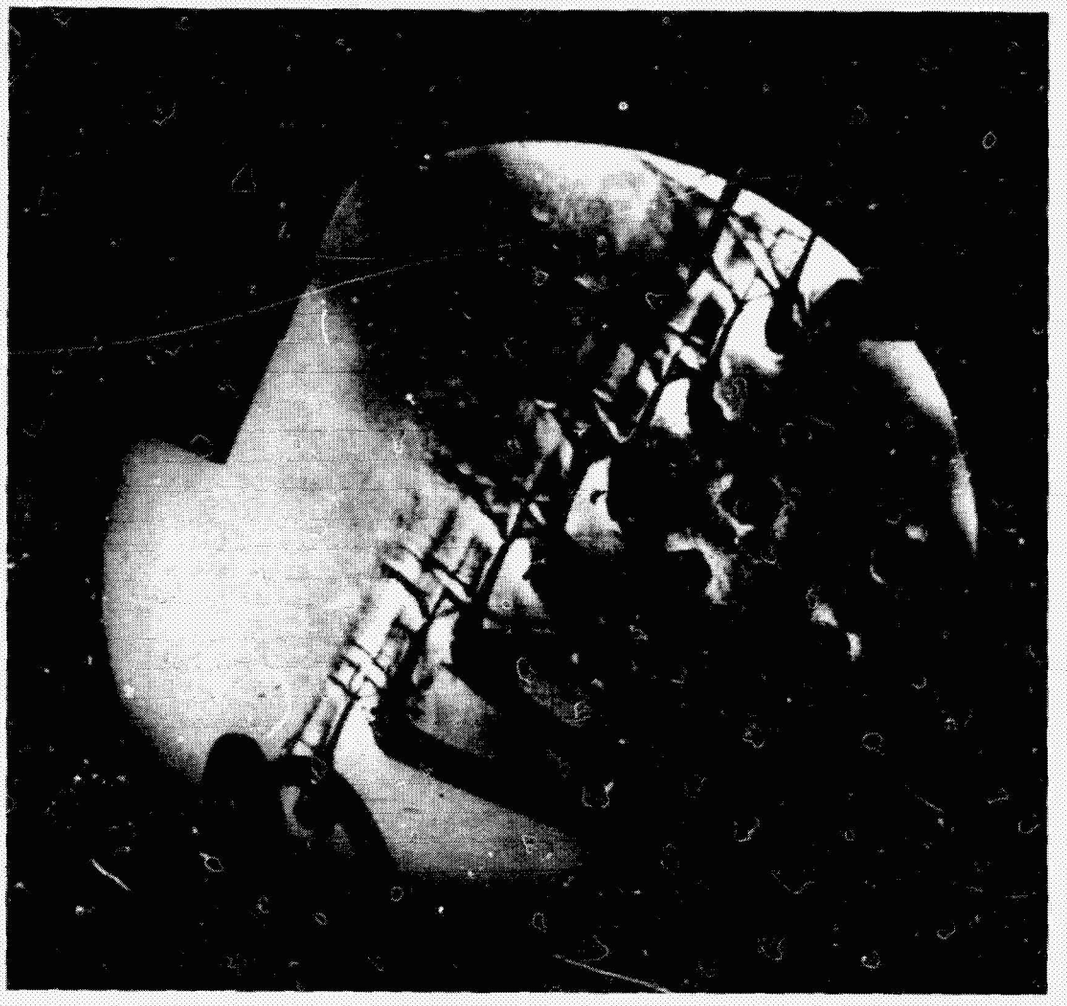

$M_{2_i} = 1.099 \quad \beta_1 = 43.0$

Figure 86 Schlieren Photograph of Base Blade Mean Section at 1.1 Isentropic Exit Mach Number

ORIGINAL PAGE
BLACK AND WHITE PHOTOGRAPH

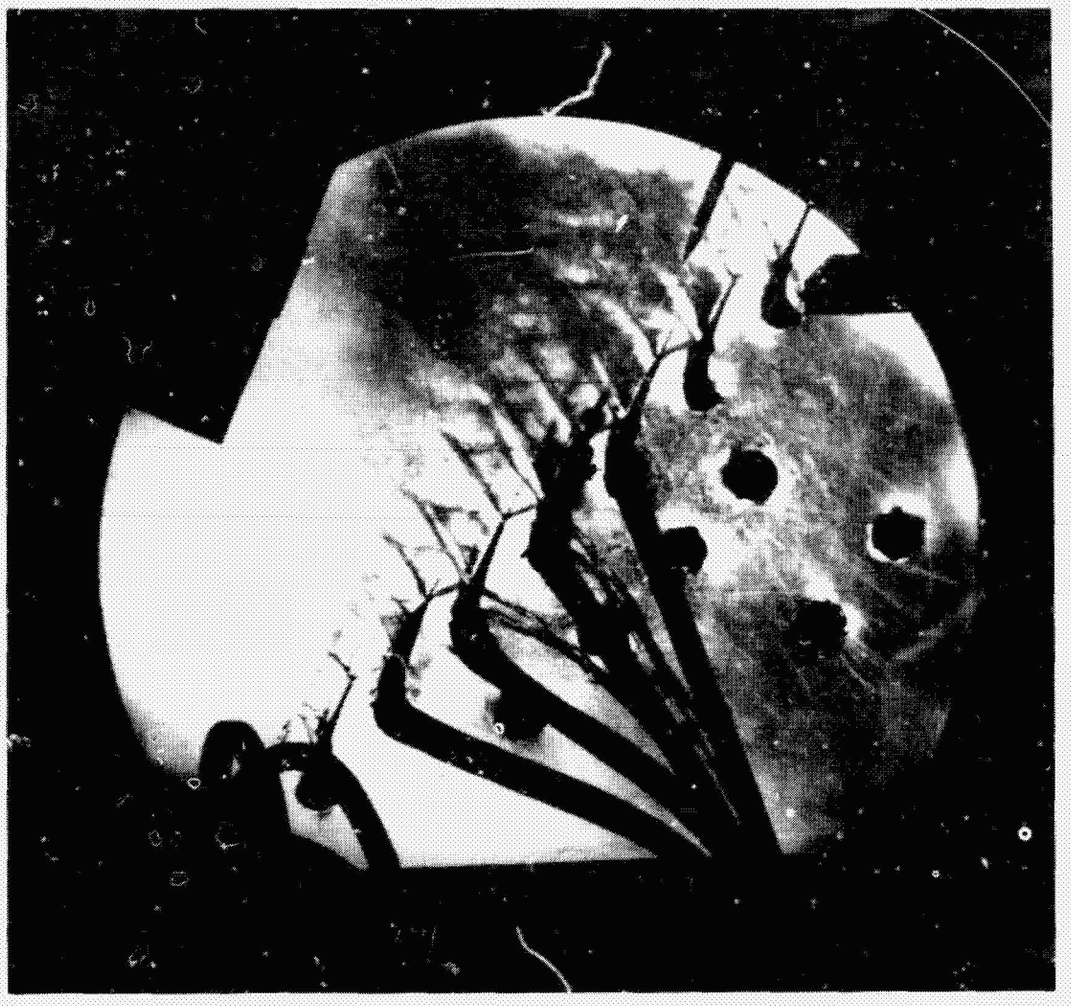

$M_{2_i} = 1.201 \quad \beta_1 = 43.0$

Figure 87 Schlieren Photograph of Base Blade Mean Section at 1.2 Isentropic Exit Mach Number

ORIGINAL PAGE
BLACK AND WHITE PHOTOGRAPH

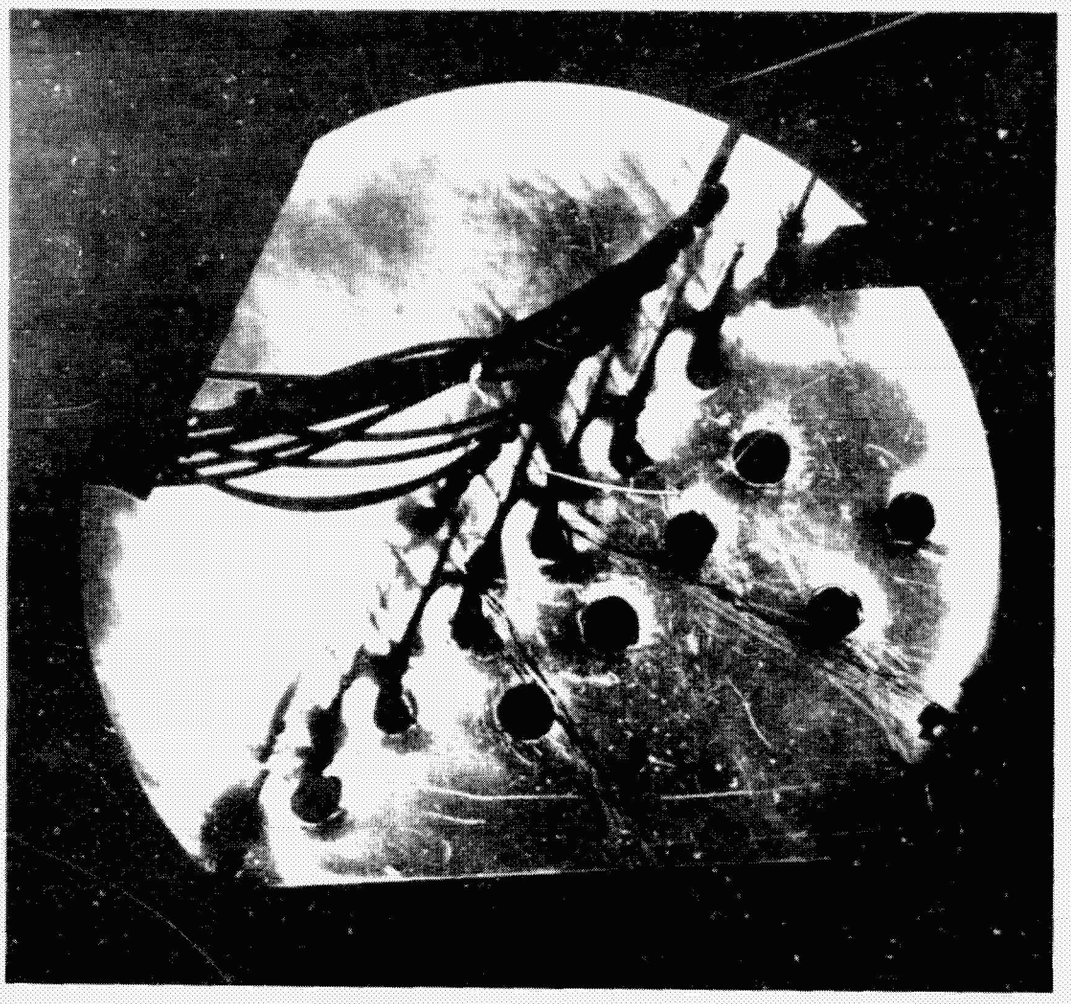

$M_{2_i} = 1.272 \quad \beta_1 = 43.0$

Figure 88 Schlieren Photograph of Base Blade Mean Section at 1.27 Isentropic Exit Mach Number

ORIGINAL PAGE
BLACK AND WHITE PHOTOGRAPH

ORIGINAL PAGE
BLACK AND WHITE PHOTOGRAPH

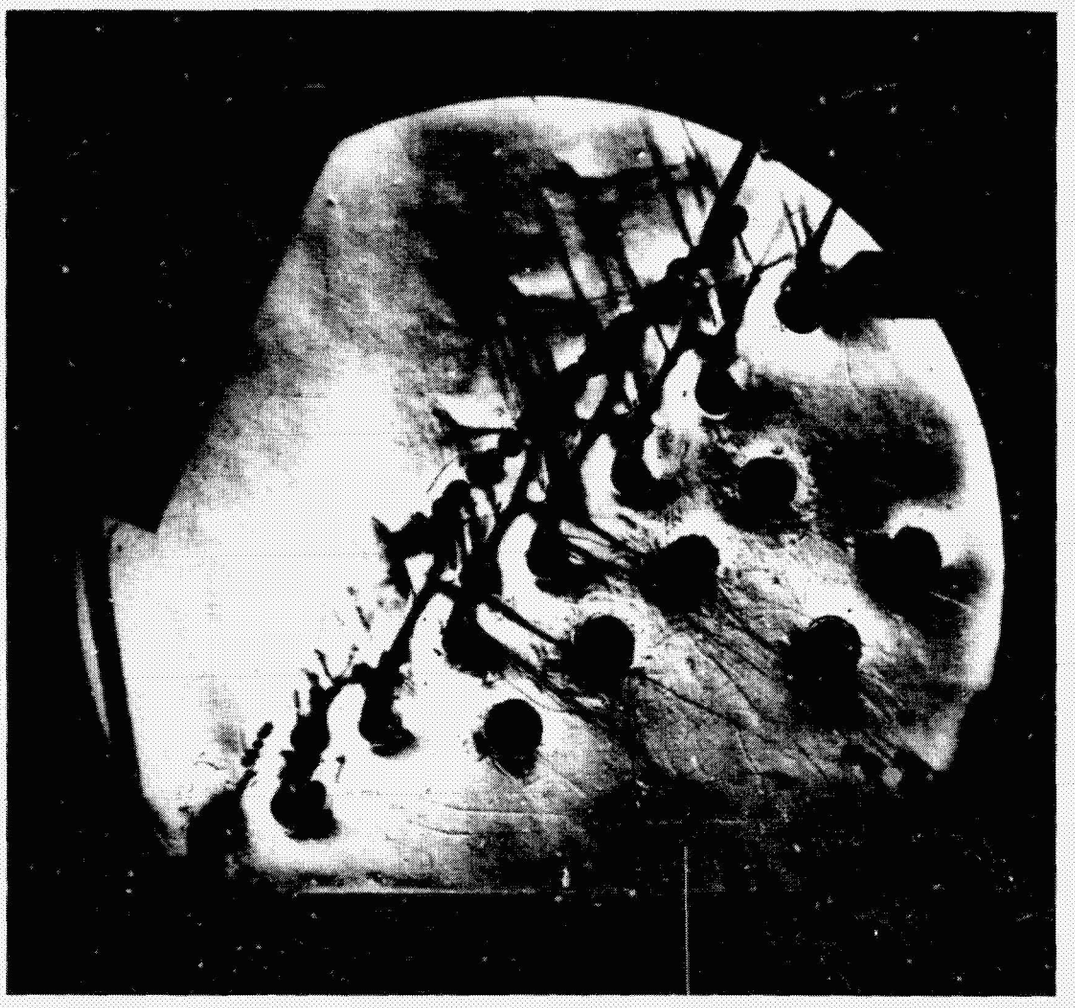

$M_{2_i} = 1.397 \quad \beta_1 = 43.0$

Figure 89 Schlieren Photograph of Base Blade Mean Section at 1.4 Isentropic Exit Mach Number

ORIGINAL PAGE IS
OF POOR QUALITY

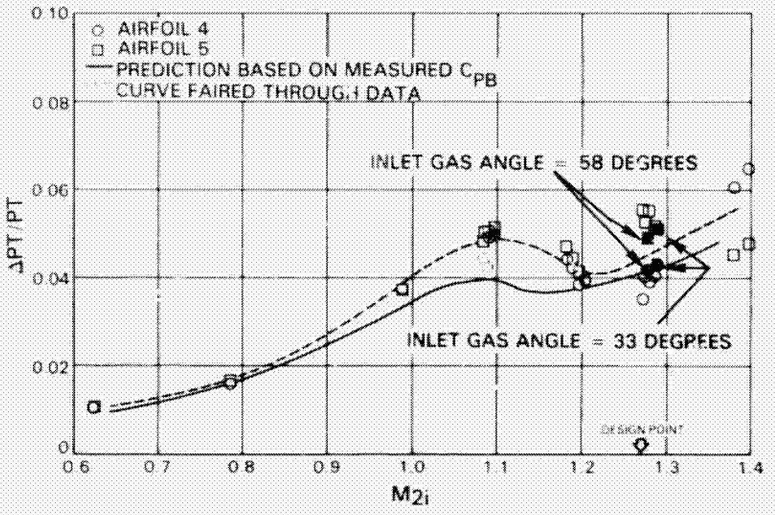

Figure 90 Individual Airfoil Total Pressure Loss vs Exit Isentropic Mach Number Base Blade

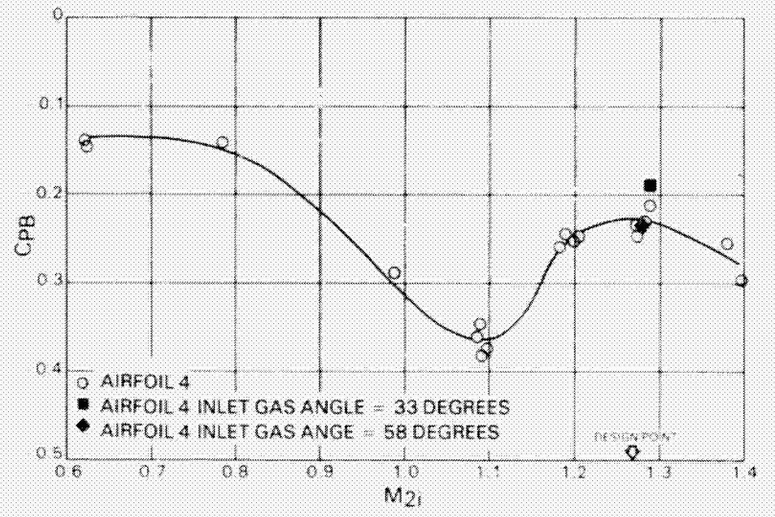

Figure 91 Individual Airfoil Base Pressure vs Exit Isentropic Mach Number Base Blade

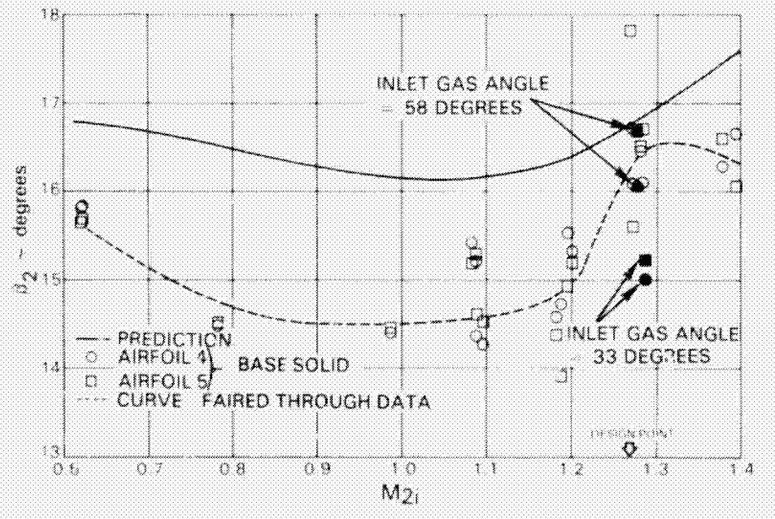

Figure 92 Individual Airfoil Exit Air Angle vs Exit Isentropic Mach Number Base Blade

4.4.3.2 Overcambered Airfoil Evaluation

4.4.3.2.1 Airfoil Pressure Distributions

Predicted and measured airfoil surface static pressure distributions for the range of test subsonic and supersonic exit Mach numbers are presented in Figures 93 through 99. As in the base airfoil cases, the agreement between the measured and predicted pressure distributions at subsonic exit Mach number conditions was excellent. Likewise, agreement between the prediction and the measured pressure distribution data at supersonic exit Mach numbers was good except in the recompression region where the measured data were scattered around the predictions.

4.4.3.2.2 Schlieren Observations

Visual representation of the shock structure for the overcambered airfoil cascade in a range of isentropic exit Mach numbers from 1.08 to 1.39 is shown in Figures 100 through 103. The shock structure depicted in these photographs is very similar to that obtained for the base airfoil which was discussed in sections 4.3.3.1.2. and 4.4.1.

4.4.3.2.3 Total Pressure Loss Assessment

The variations of total pressure loss with M_{2i} for individual overcambered airfoils 4 and 5 are shown in Figure 104. The individual airfoil losses for a test point are essentially the same for subsonic Mach numbers but differ appreciably at supersonic Mach numbers.

Predicted losses, which were calculated employing the measured base pressure coefficient, are also presented in Figure 104 and are seen to be in very good agreement with measured data at subsonic Mach numbers but underestimate the measured losses at supersonic Mach numbers.

4.4.3.2.4 Base Pressure Coefficient

The variation of overcambered airfoil base pressure coefficient with M_{2i} is presented in Figure 105. In general, the overcambered airfoil base pressure coefficient exhibits the same variation with M_{2i} as that of the base airfoil discussed in Section 4.3.3.1.4.

4.4.3.2.5 Exit Gas Angle

The variation of exit air angle β_2, with M_{2i} for the overcambered airfoil is presented in Figure 106. The variation was similar to that obtained for the base airfoil, with β_2 decreasing with a nominal 1.2 degree difference between the predicted and measured data. As with the base blade data, the explanation for this difference is reasoned to be related to the measured angle. Continuity checks and measured airfoil loadings indicated that the predicted value is more nearly correct. Adjusting the measured angles upward by the nominal 1.2 degree difference places the predicted and actual trends with Mach number in reasonable agreement.

ORIGINAL PAGE IS
OF POOR QUALITY

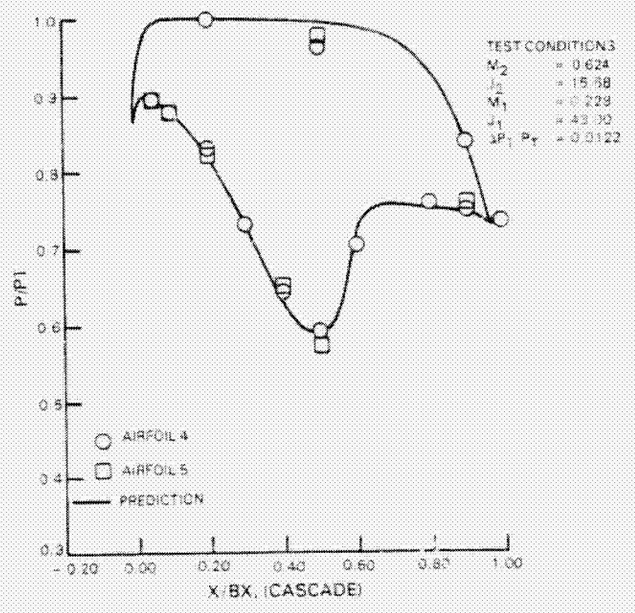

Figure 93 Uncooled Cascade Test Overcambered Blade Section Pressure Distribution at 0.624 Exit Mach Number

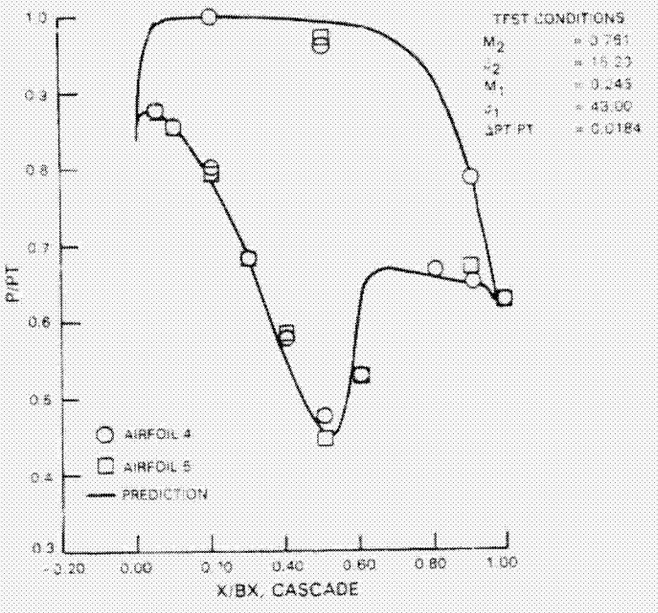

Figure 94 Uncooled Cascade Test Overcambered Blade Section Pressure Distribution at 0.761 Exit Mach Number

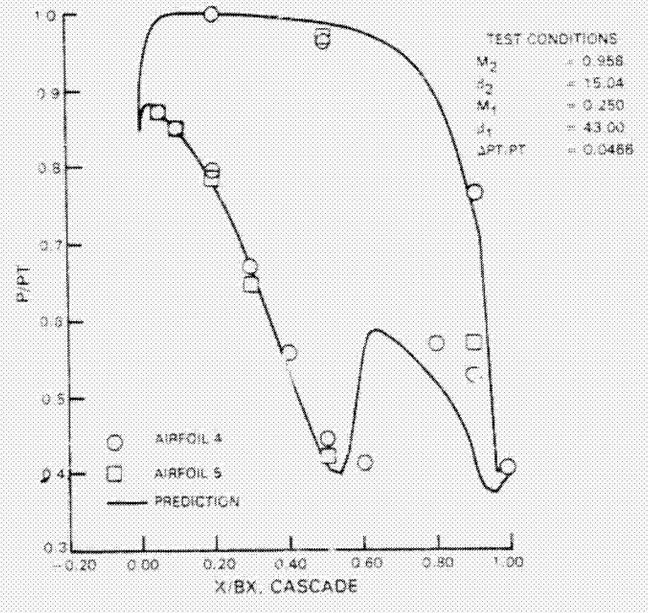

Figure 95 Uncooled Cascade Test Overcambered Blade Section Pressure Distribution at 0.958 Exit Mach Number

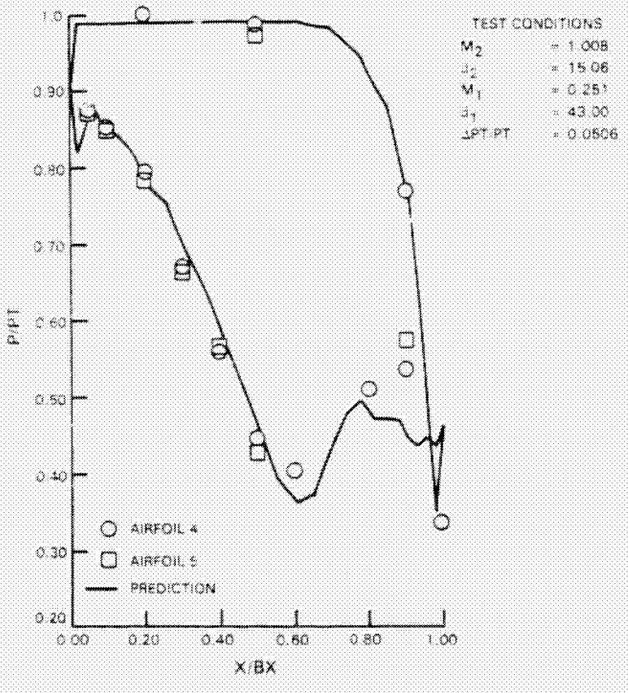

Figure 96 Uncooled Cascade Test Overcambered Blade Section Pressure Distribution at 1.008 Exit Mach Number

ORIGINAL PAGE IS
OF POOR QUALITY

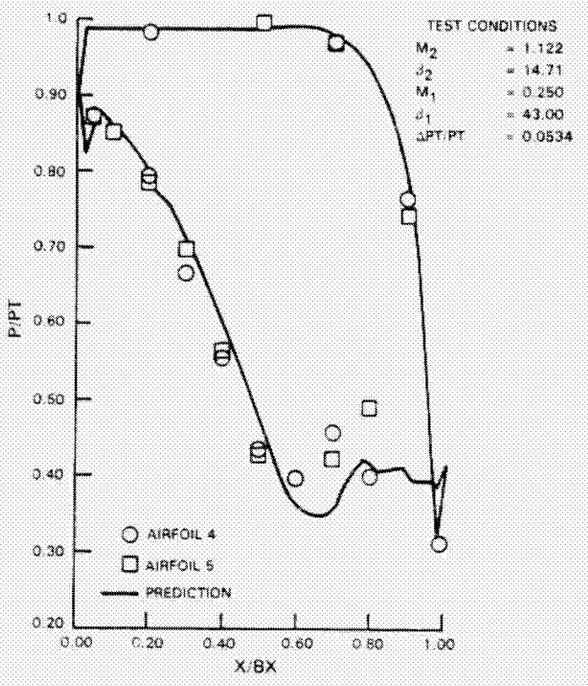

Figure 97 Uncooled Cascade Test Overcambered Blade Section Pressure Distribution at 1.122 Exit Mach Number

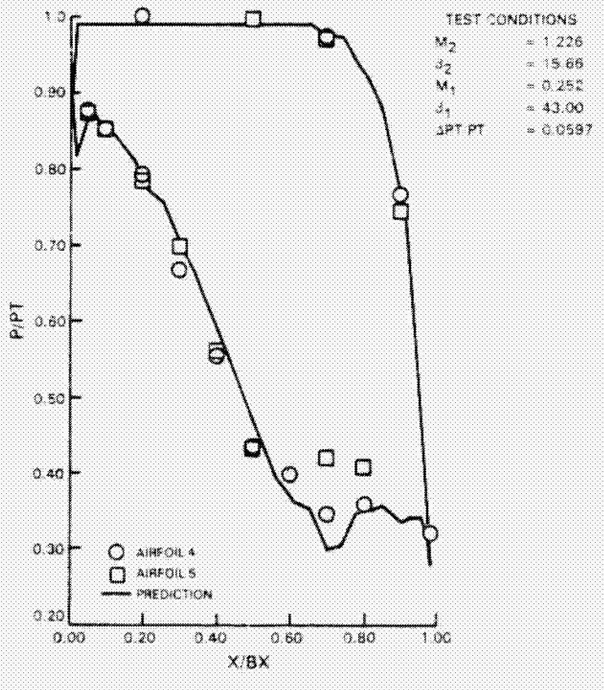

Figure 98 Uncooled Cascade Test Overcambered Blade Section Pressure Distribution at 1.226 Exit Mach Number

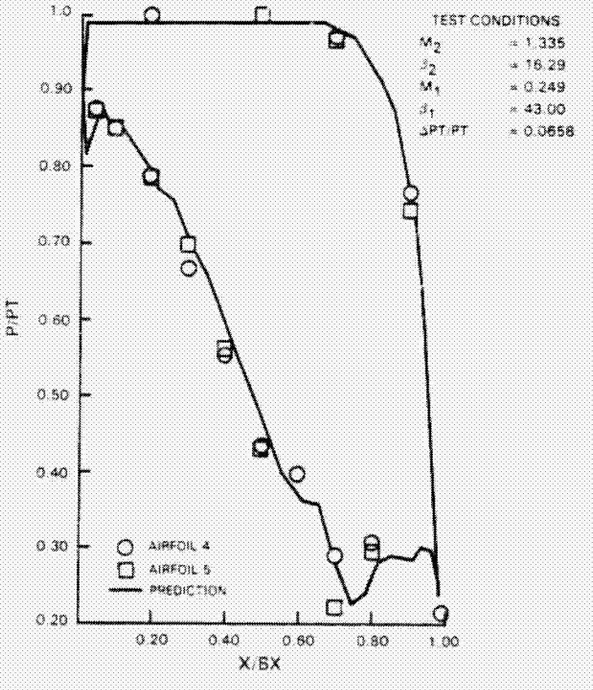

Figure 99 Uncooled Cascade Test Overcambered Blade Section Pressure Distribution at 1.335 Exit Mach Number

ORIGINAL PAGE
BLACK AND WHITE PHOTOGRAPH

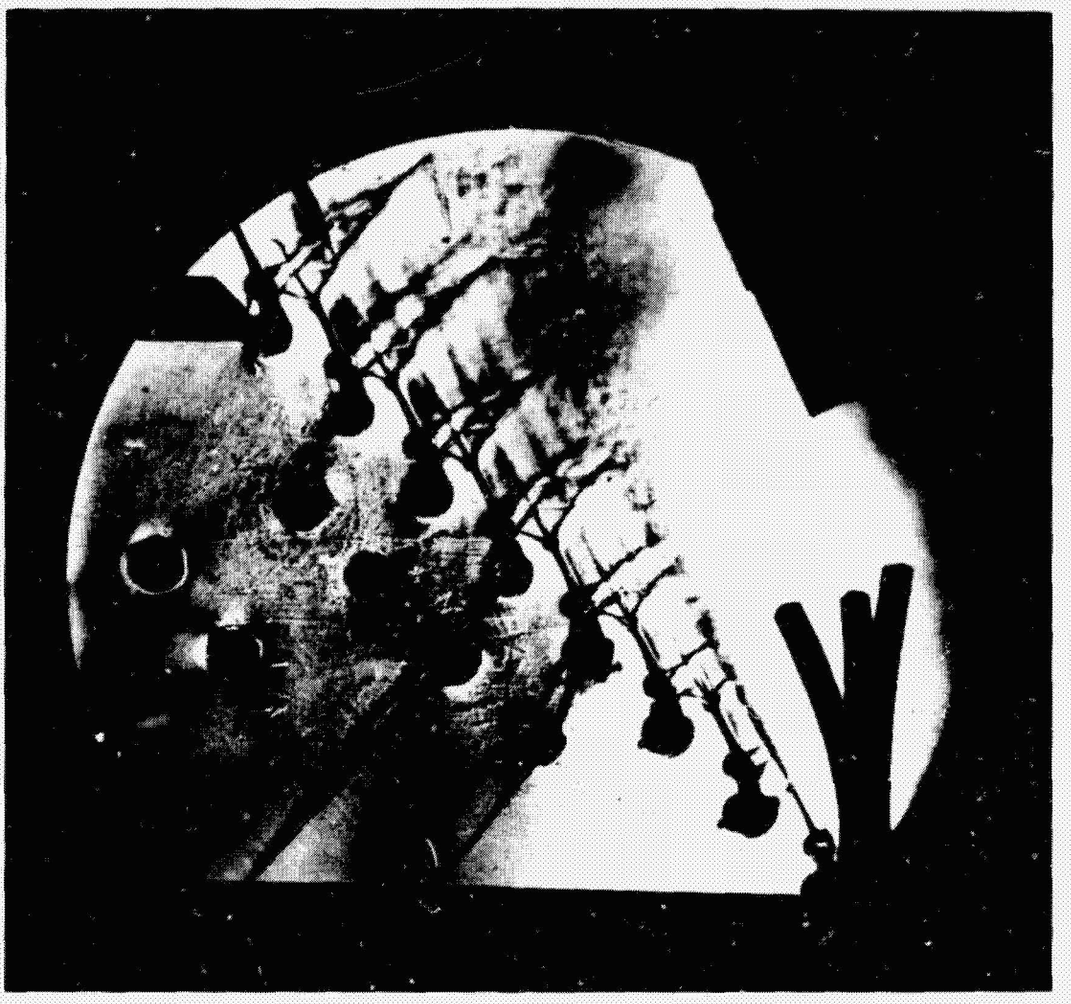

$M_{2_i} = 1.083 \quad \beta_1 = 43.0$

Figure 100 Schlieren Photograph of Overcambered Blade Mean Section at 1.08 Isentropic Exit Mach Number

ORIGINAL PAGE
BLACK AND WHITE PHOTOGRAPH

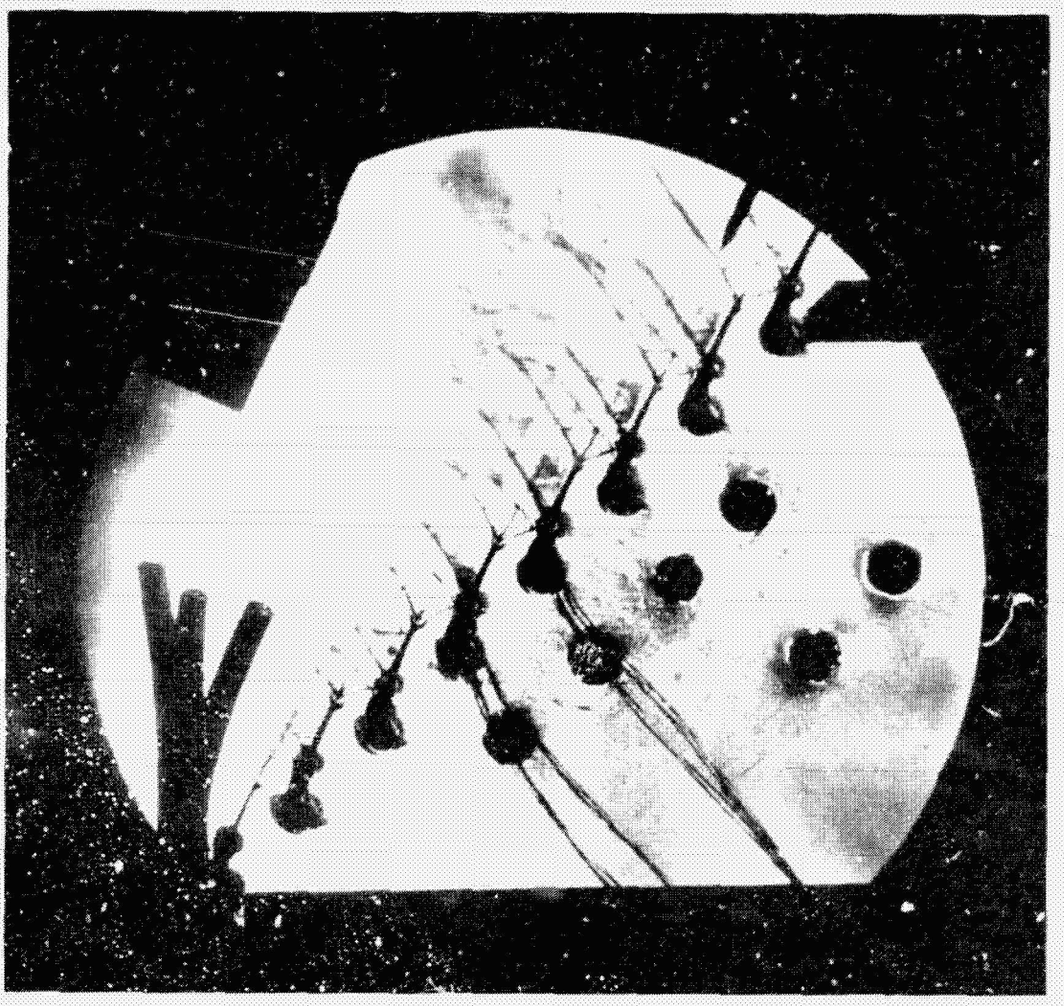

$M_{2_i} = 1.187 \quad \beta_1 = 43.0$

Figure 101 Schlieren Photograph of Overcambered Blade Mean Section at 1.19 Isentropic Exit Mach Number

ORIGINAL PAGE
BLACK AND WHITE PHOTOGRAPH

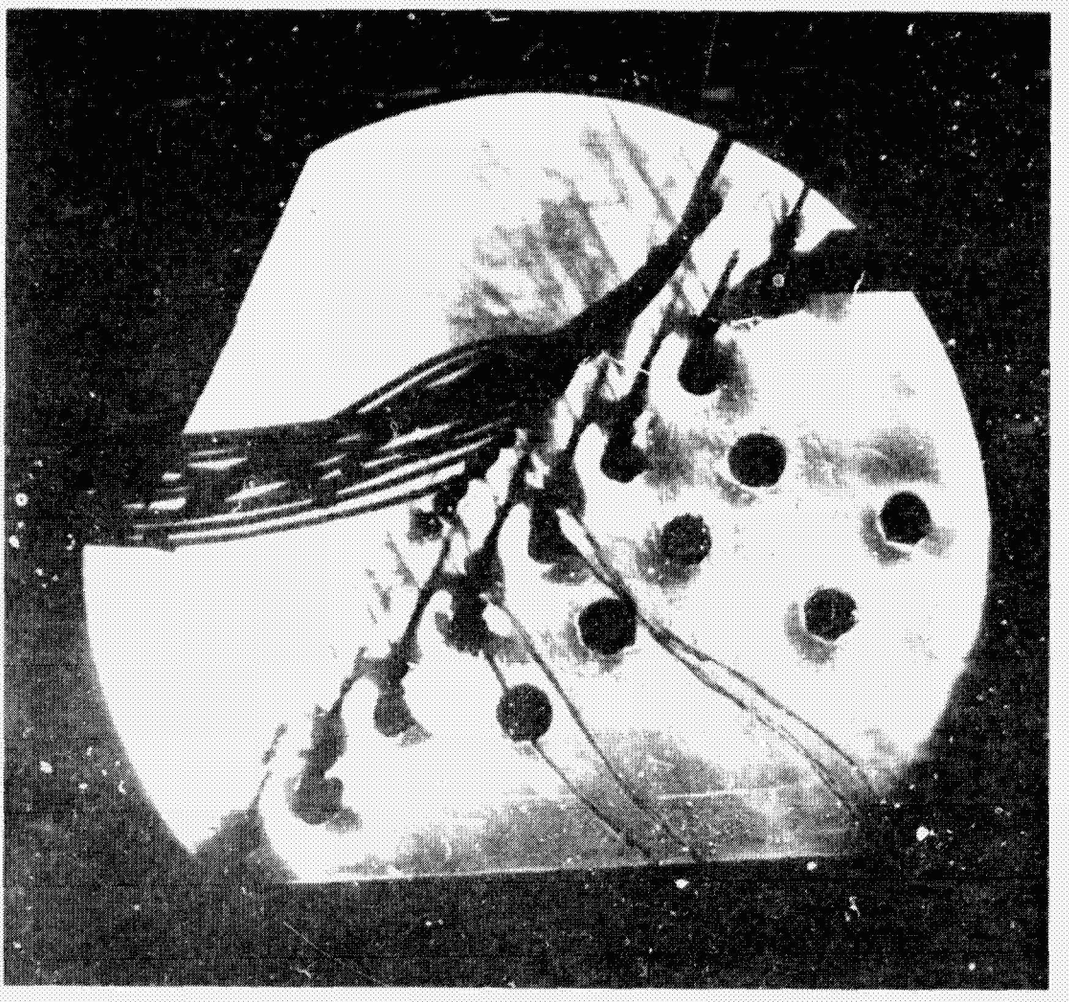

$M_{2_i} = 1.282 \quad \beta_1 = 43.0$

Figure 102 Schlieren Photograph of Overcambered Blade Mean Section at 1.28 Isentropic Exit Mach Number

ORIGINAL PAGE
BLACK AND WHITE PHOTOGRAPH

$M_{2_i} = 1.388 \quad \beta_1 = 43.0$

Figure 103 Schlieren Photograph of Overcambered Blade Mean Section at 1.39 Isentropic Exit Mach Number

ORIGINAL PAGE IS
OF POOR QUALITY

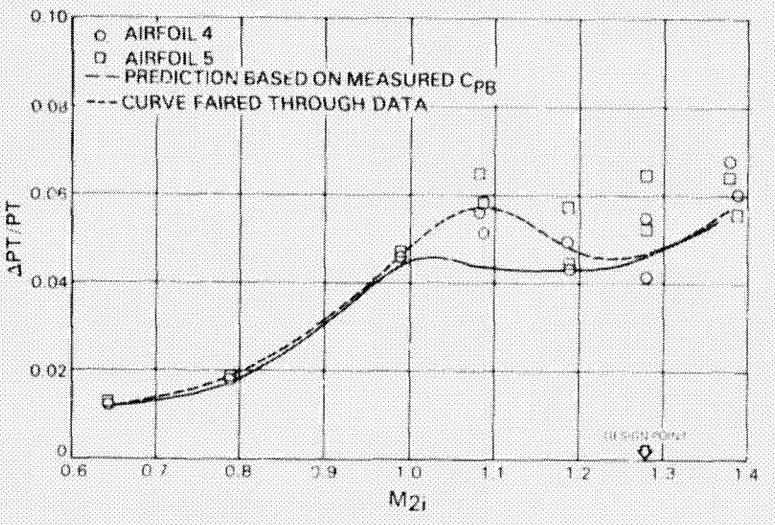

Figure 104 Individual Airfoil Mass Averaged Total Pressure Loss vs Exit Isentropic Mach Number

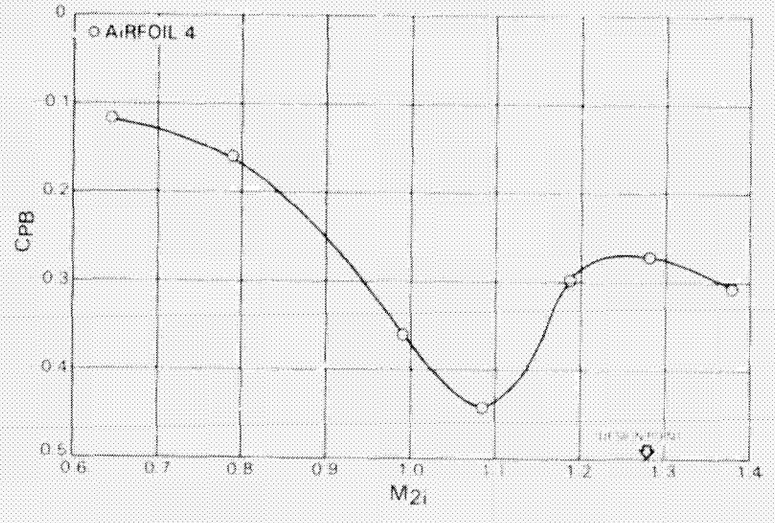

Figure 105 Individual Airfoil Base Pressure vs Exit Isentropic Mach Number

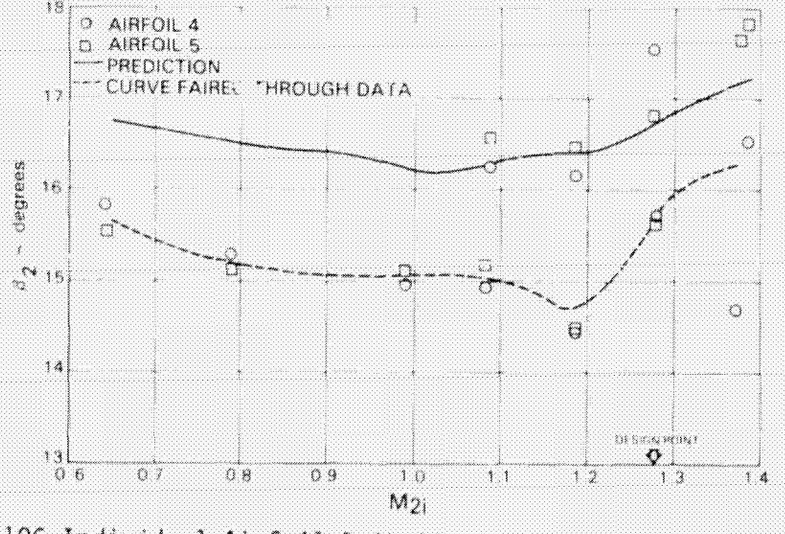

Figure 106 Individual Airfoil Exit Air Angle vs Exit Isentropic Mach Number Overcambered Blade

4.4.3.3 Straightback Airfoil Evaluation

4.4.3.3.1 Airfoil Pressure Distributions

Predicted and measured airfoil surface static pressure distributions for the range of subsonic exit Mach numbers tested are shown in Figures 107 through 109. Pressure distributions for transonic and supersonic exit Mach numbers are shown in Figures 110 through 113. Agreement between the measured and predicted subsonic data is excellent. The predictions at supersonic exit Mach numbers are in good agreement with the measured data except in the recompression region where the data were scattered. Due to an equipment failure, surface static pressure for airfoil 5 were not obtained for Mach numbers greater than 1.1.

4.4.3.3.2 Schlieren Observations

The flow structure for the straightback airfoil cascade in the range of isentropic exit Mach numbers from 1.10 to 1.35 is shown in Figures 114 through 117. The shock structure depicted in these photographs is similar to that observed for the base and overcambered airfoils.

4.4.3.3.3 Total Pressure Loss Assessment

The variations of total pressure loss with M_{2i} for individual straightback airfoils 4 and 5 are shown in Figure 118. The individual airfoil losses are almost the same for subsonic Mach numbers and somewhat different at supersonic Mach numbers.

Predicted losses which were calculated employing the measured base pressure coefficient values are also compared with measured losses in Figure 118. The prediction is in very good agreement with measured values at subsonic Mach numbers and is in fair agreement with the losses at supersonic Mach numbers.

4.4.3.3.4 Base Pressure Coefficient

The variation of straightback airfoil base pressure coefficient with M_{2i} is presented in Figure 119. Generally, the straightback airfoil base pressure coefficient exhibits the same variation with M_{2i} as the base and overcamber designs. The one significant difference is that the base pressure coefficient shows continued improvement with increasing supersonic Mach number and does not "peak out" at the design point Mach number. This suggests that the straight-back design approach might provide improved performance for airfoils whose design point Mach number is greater than 1.3.

4.4.3.3.5 Exit Gas Angle

The variation of exit air angle, β_2, with M_{2i} for the straightback airfoil is presented in Figure 120 and is similar to that obtained for the base and overcambered airfoils. The overall agreement between predicted and measured values is reasonably good. The reason for the spread in the measured data at M_{2i} of 0.8 is not known.

ORIGINAL PAGE IS
OF POOR QUALITY

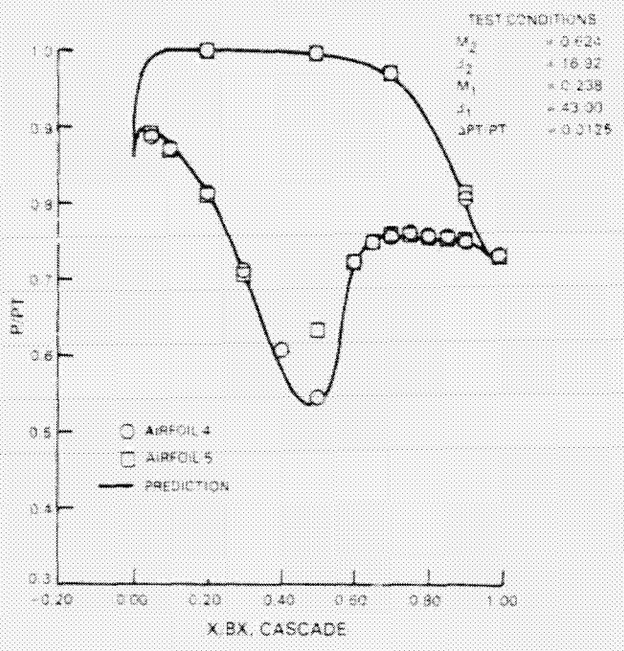

Figure 107 Uncooled Cascade Test Straightback Blade Section Pressure Distribution at 0.624 Exit Mach Number

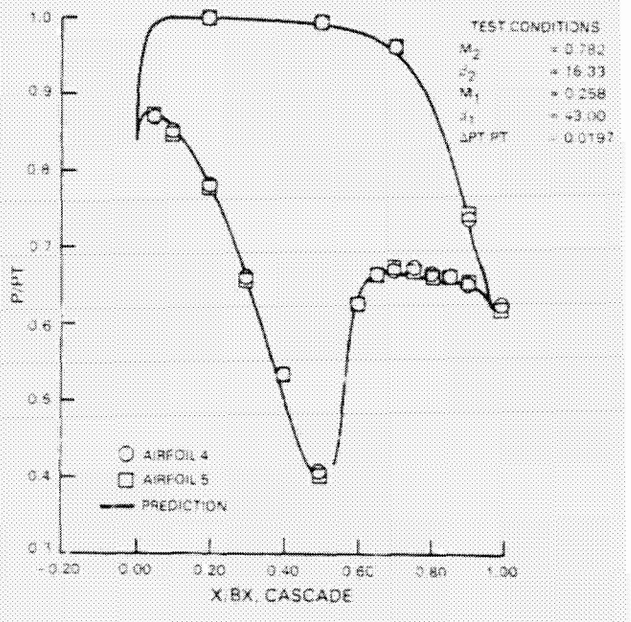

Figure 108 Uncooled Cascade Test Straightback Blade Section Pressure Distribution at 0.782 Exit Mach Number

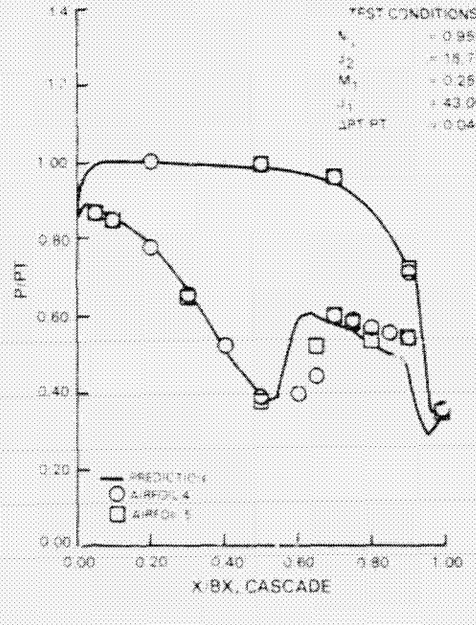

Figure 109 Uncooled Cascade Test Straightback Blade Section Pressure Distribution at 0.956 Exit Mach Number

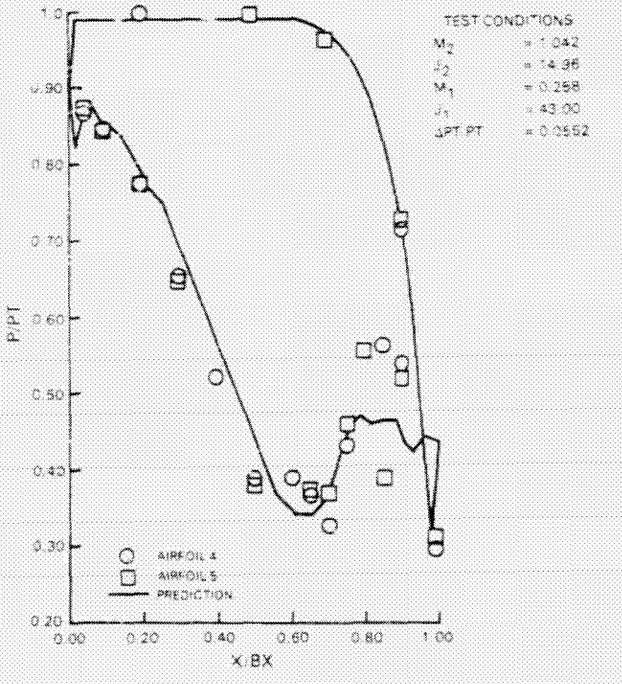

Figure 110 Uncooled Cascade Test Straightback Blade Section Pressure Distribution at 1.042 Exit Mach Number

ORIGINAL PAGE IS
OF POOR QUALITY

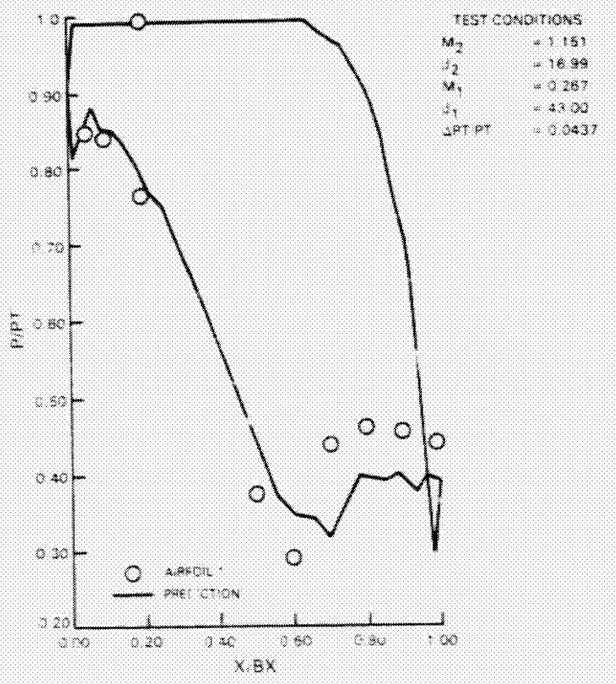

Figure 111 Uncooled Cascade Test Straightback Blade Section Pressure Distribution at 1.151 Exit Mach Number

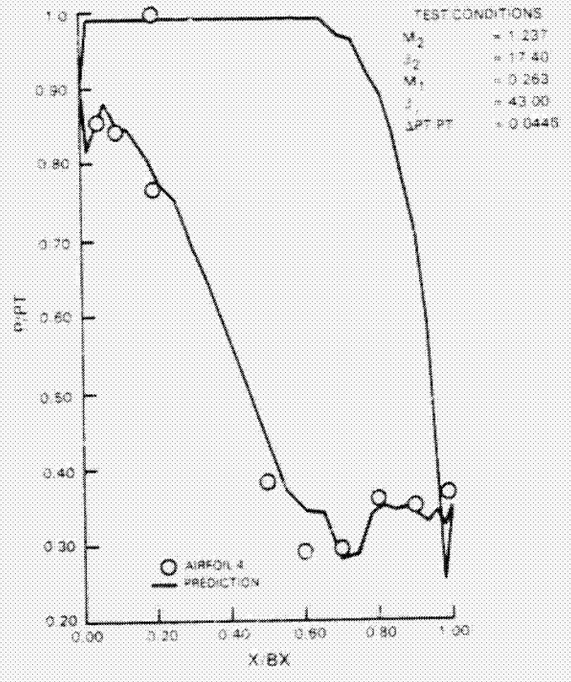

Figure 112 Uncooled Cascade Test Straightback Blade Section Pressure Distribution at 1.237 Exit Mach Number

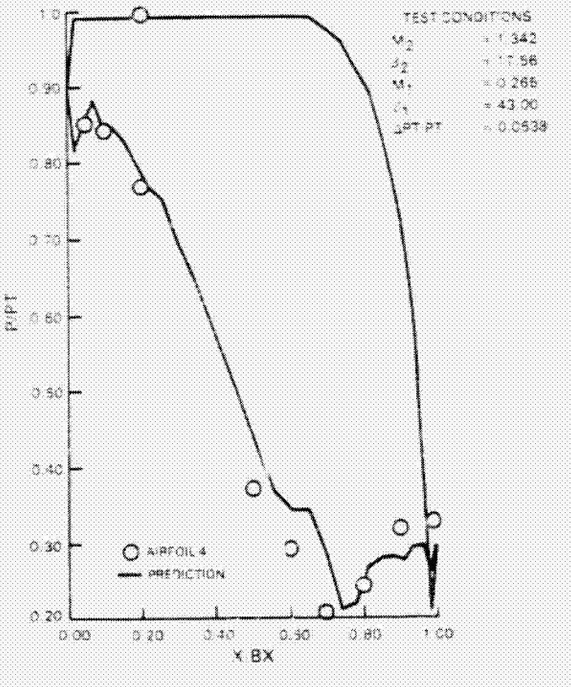

Figure 113 Uncooled Cascade Test Straightback Blade Section Pressure Distribution at 1.342 Exit Mach Number

ORIGINAL PAGE
BLACK AND WHITE PHOTOGRAPH

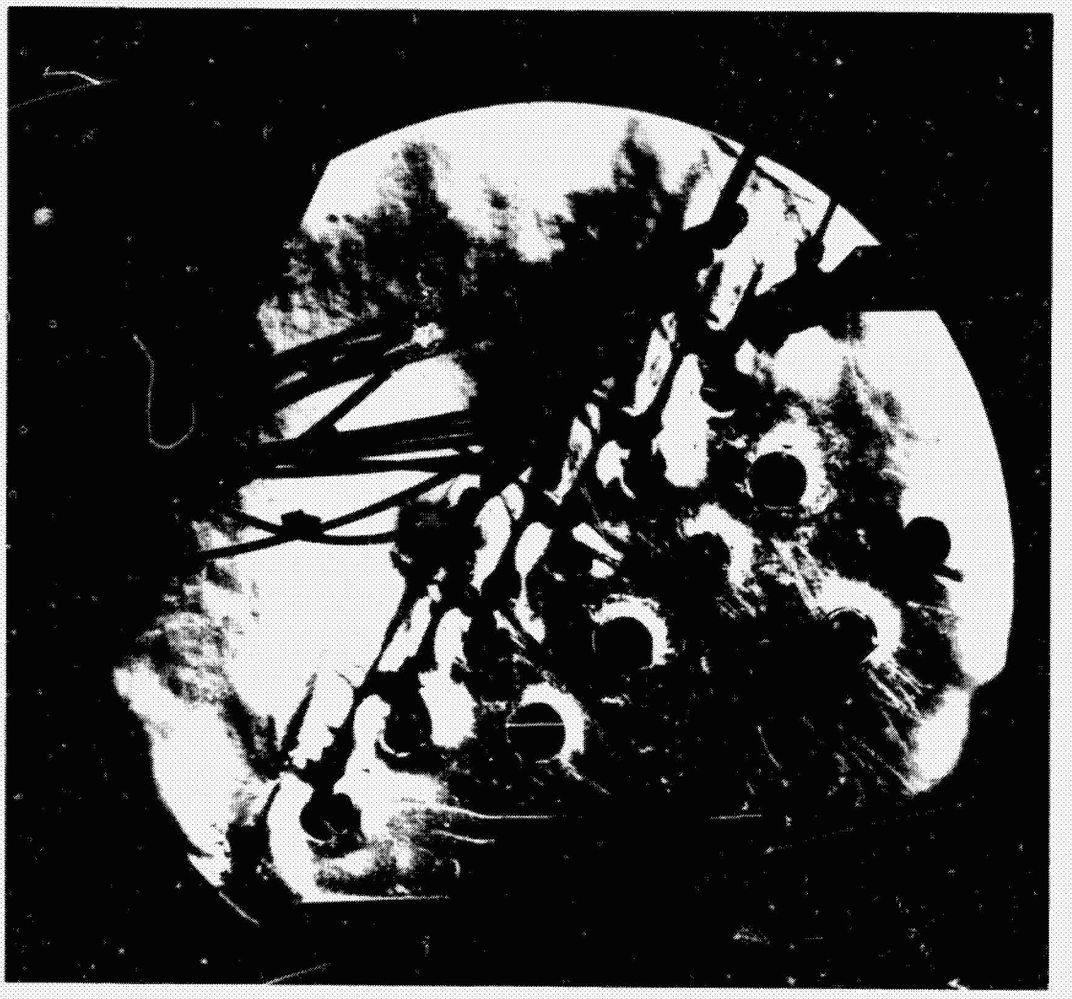

$M_{2_i} = 1.096 \quad \beta_1 = 43.0$

Figure 114 Schlieren Photograph of Straightback Blade Mean Section at 1.10 Isentropic Exit Mach Number

ORIGINAL PAGE
BLACK AND WHITE PHOTOGRAPH

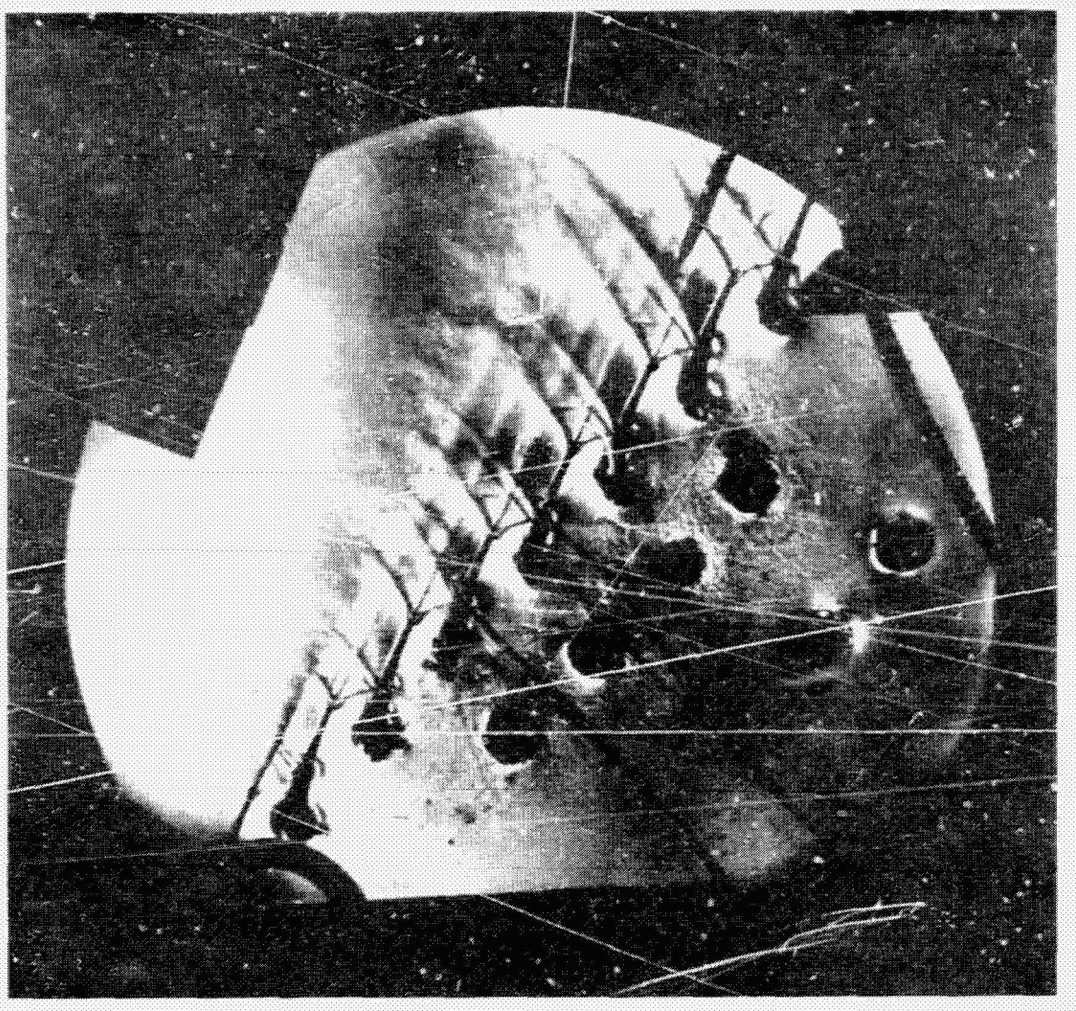

$M_{2_i} = 1.190 \quad \beta_1 = 43.0$

Figure 115 Schlieren Photograph of Straightback Blade Mean Section at 1.19 Isentropic Exit Mach Number

ORIGINAL PAGE
BLACK AND WHITE PHOTOGRAPH

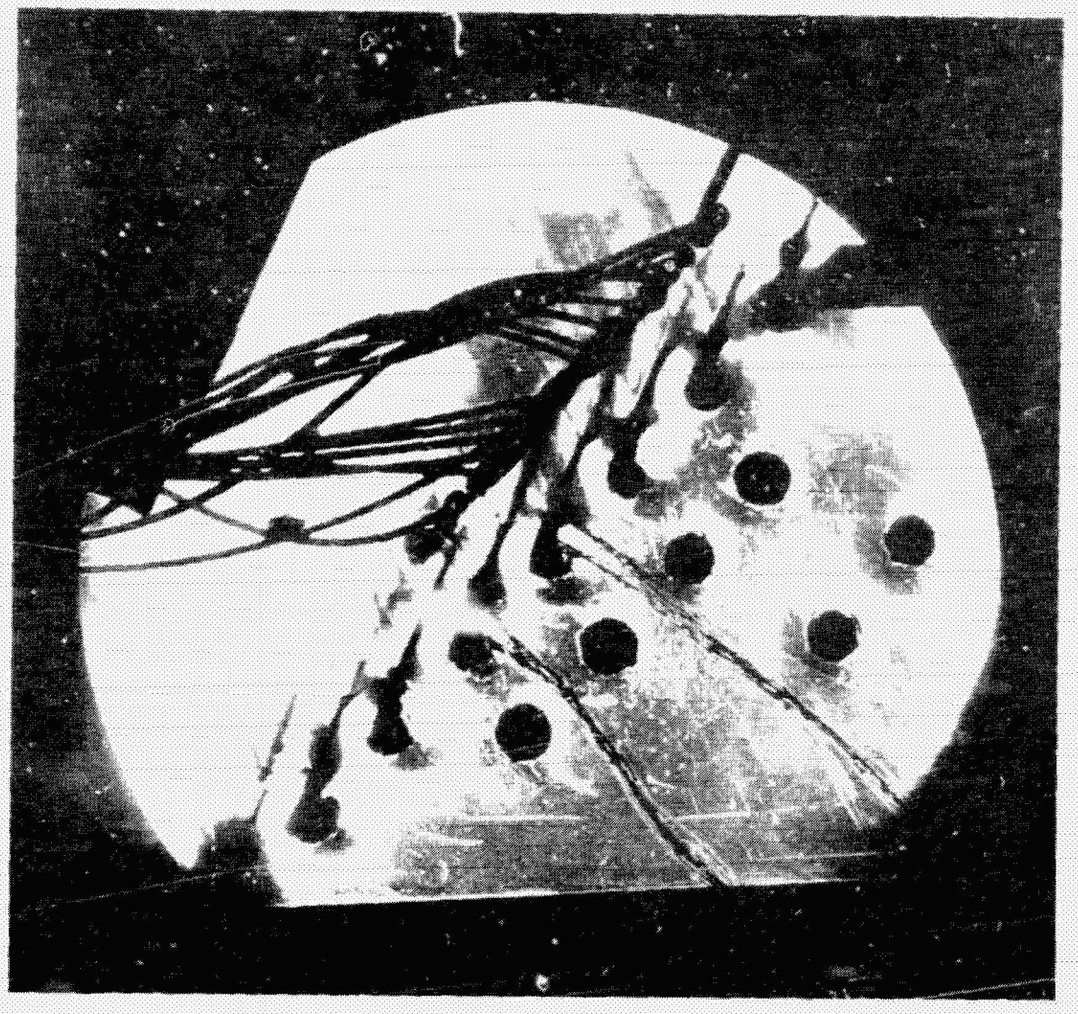

$M_{2_i} = 1.285 \quad \beta_1 = 43.0$

Figure 116 Schlieren Photograph of Straightback Blade Mean Section at 1.29 Isentropic Exit Mach Number

ORIGINAL PAGE
BLACK AND WHITE PHOTOGRAPH

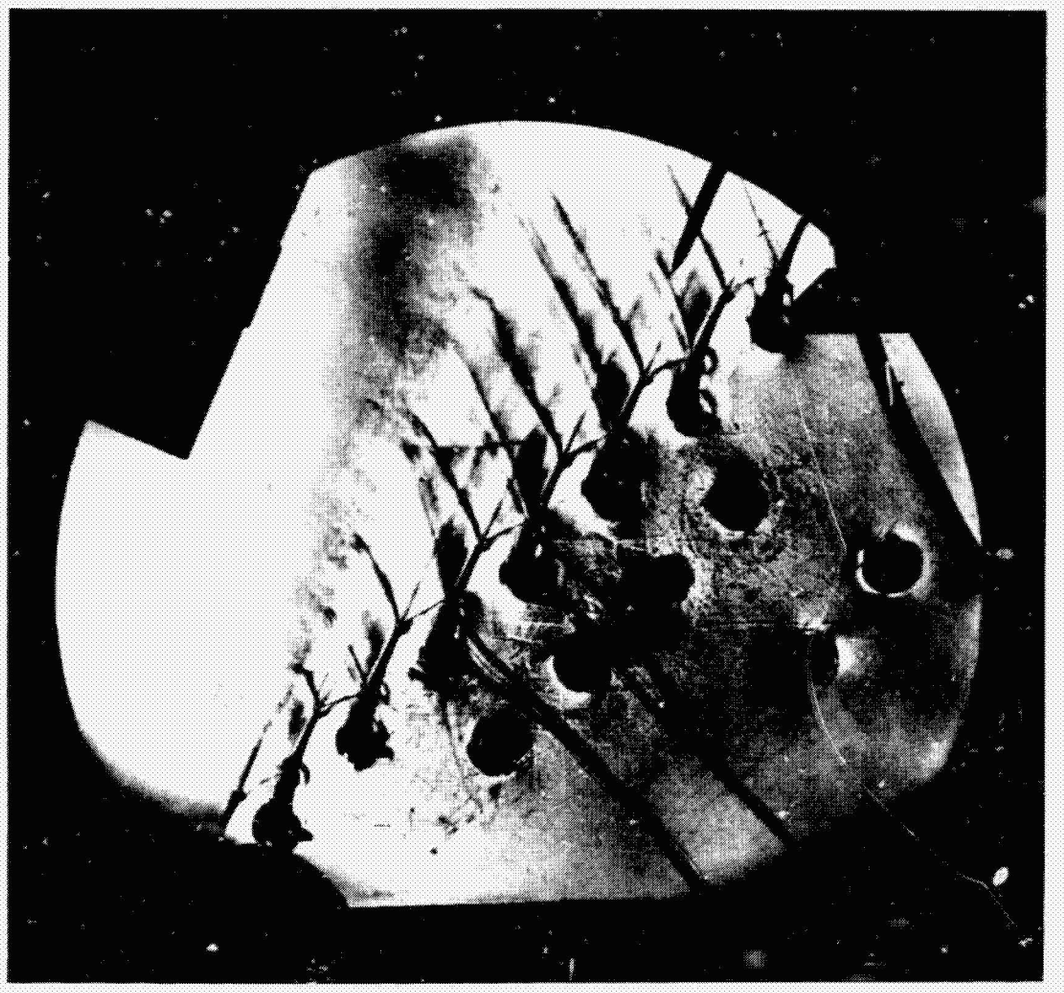

$M_{2_i} = 1.354 \qquad \beta_1 = 43.0$

Figure 117 Schlieren Photograph of Straightback Blade Mean Section at 1.35 Isentropic Exit Mach Number

ORIGINAL PAGE IS
OF POOR QUALITY

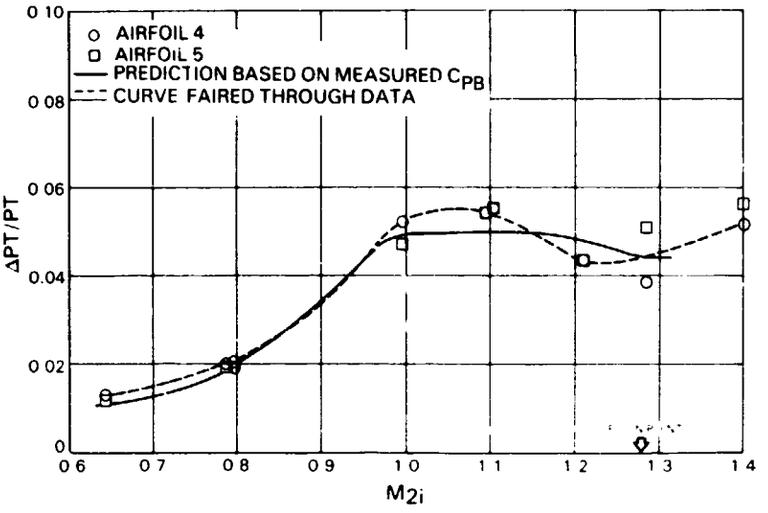

Figure 118 Individual Airfoil Mass Averaged Total Pressure Loss vs Exit Isentropic Mach Number

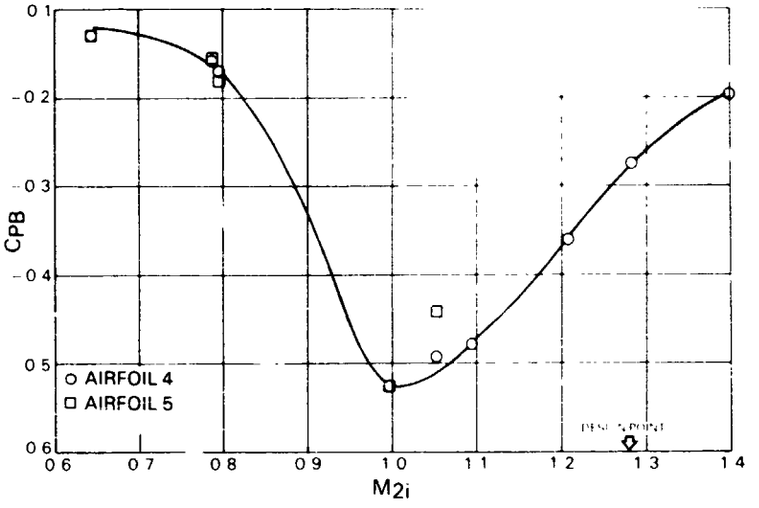

Figure 119 Individual Airfoil Base Pressure vs Exit Isentropic Mach Number

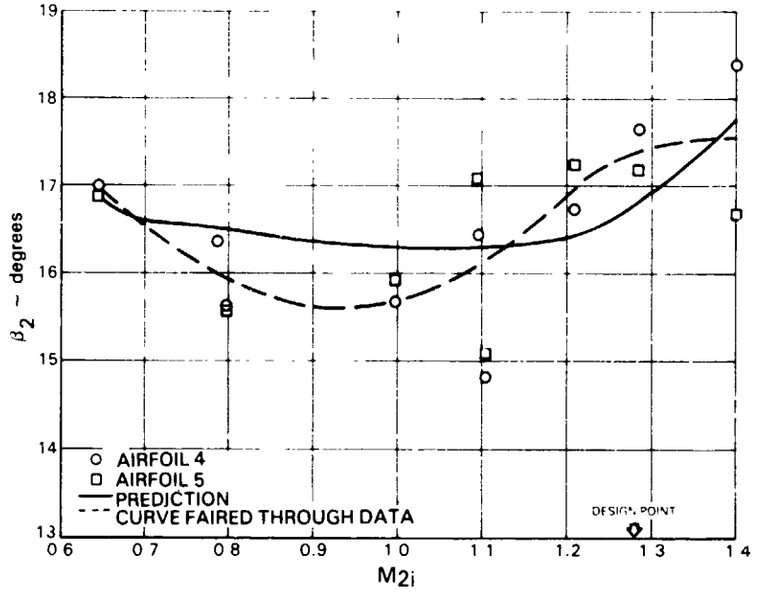

Figure 120 Individual Airfoil Mass Averaged Exit Air Angle vs Exit Isentropic Mach Number

4.4.4 Cooled Cascade Results

Test and analytical results obtained for the base blade with trailing edge coolant ejection are presented in this section. Nominal coolant flow ejection rates were 1, 2, and 3 percent of cascade primary flow, although in one case a flow rate of 0.4 percent (Figure 134) was evaluated. As was the case with the uncooled cascade, predicted and measured pressure distributions and cascade losses are compared and airfoil trailing edge base pressure, and exit gas angles assessed.

4.4.4.1 Airfoil Pressure Distributions

Predicted and measured airfoil surface static pressure distributions for the range of cooling flow rates at subsonic exit Mach numbers are shown in Figures 121 through 126. Pressure distributions for transonic and supersonic exit Mach numbers and various cooling flow rates are shown in Figures 127 through 136. The predicted distributions for subsonic Mach numbers are in excellent agreement with the measured data. Agreement between the measured data and the predictions for supersonic Mach numbers is generally good. A comparison of measured static pressures obtained for approximately the same M_{2i} and different coolant ejection rates (see Figures 122, 123, 125 and 130) indicates that coolant ejection had a very small effect on the distribution. In fact, the pressure distributions were nearly identical with those obtained without coolant flow ejection (see Figures 77 through 83).

4.4.4.2 Schlieren Observations

The shock structure for the base airfoil at the design isentropic exit Mach number and four trailing edge coolant ejection rates is presented in Figures 136-139. A comparison of the shock patterns at the different coolant ejection rates indicates no significant change in shock pattern with changes in flow rate. This could lead to the conclusion that shock losses are relatively unaffected by trailing edge coolant ejection. As is discussed in Section 4.4.4.5, this does not appear to be the case because shock losses were found to be noticably affected by trailing edge coolant ejection, as determined from exit plane wake traverses.

4.4.4.3 Base Pressure Coefficient

Base pressure coefficients are compared with those obtained without coolant ejection in Figure 140. As indicated, trailing edge coolant ejection resulted in base pressure coefficients which increased (became more favorable) with increasing trailing edge flow. For example, 1 percent trailing edge bleed flow increased the base pressure coefficient, C_{PB}, by as much as 0.17 at M_{2i} of 1.3. Increasing the bleed flow to 2 or 3 percent resulted in approximately an additional 0.07 increase in C_{PB} at M_{2i} of 1.3; reducing CP_B to approximately zero.

ORIGINAL PAGE IS
OF POOR QUALITY

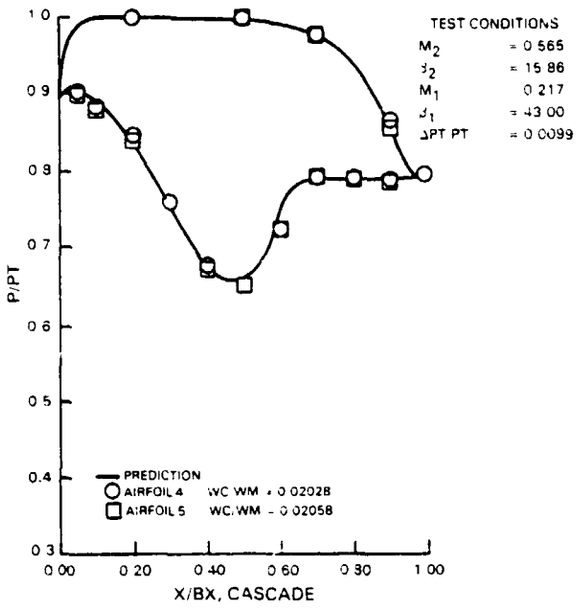

Figure 121 Cooled Cascade Test Base Blade Section Pressure Distribution at 0.565 Exit Mach Number

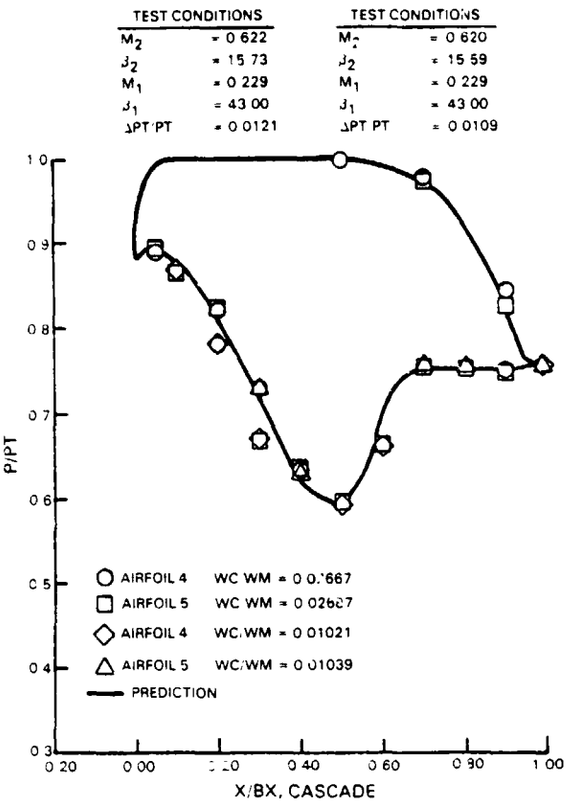

Figure 122 Cooled Cascade Test Base Blade Section Pressure Distribution at 0.62 Exit Mach Number

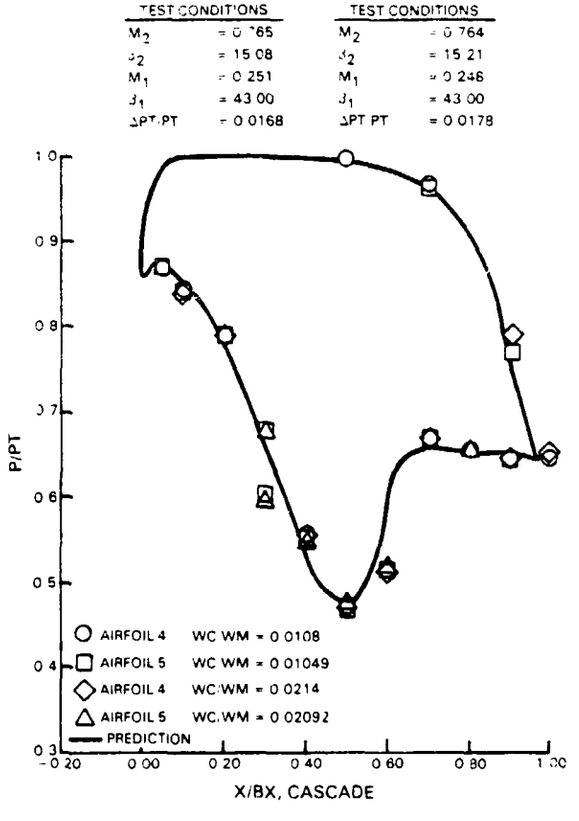

Figure 123 Cooled Cascade Test Base Blade Section Pressure Distribution at 0.765 Exit Mach Number

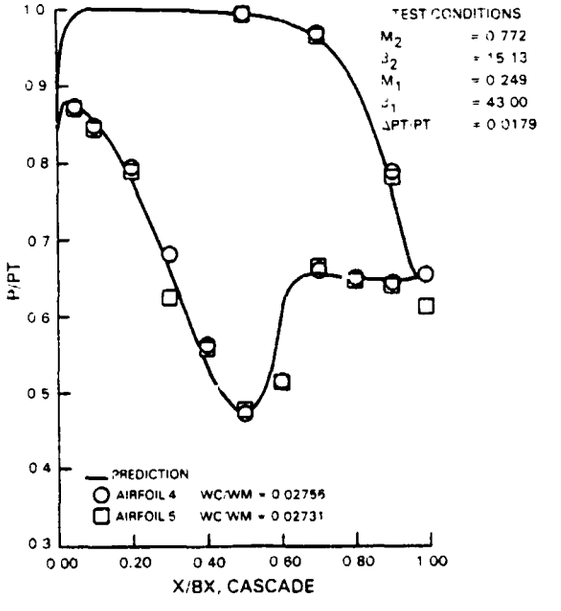

Figure 124 Cooled Cascade Test Base Blade Section Pressure Distribution at 0.772 Exit Mach Number

ORIGINAL PAGE IS
OF POOR QUALITY

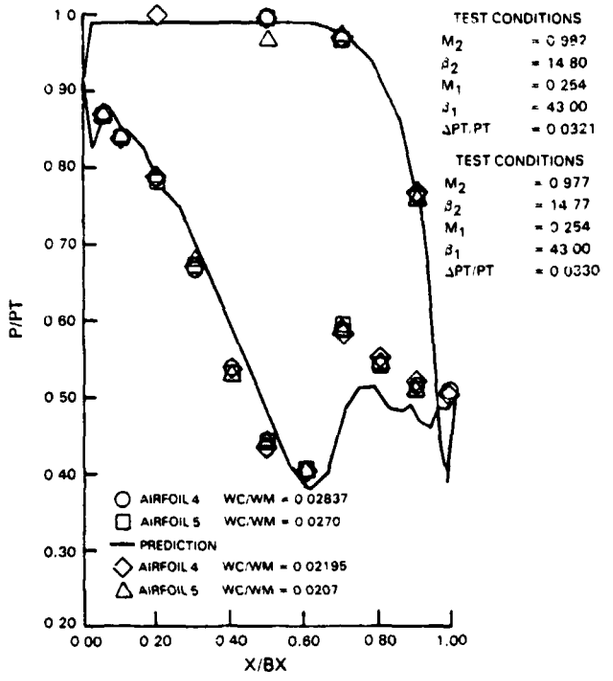

Figure 125 Cooled Cascade Test Base Blade Section Pressure Distribution at 0.98 Exit Mach Number

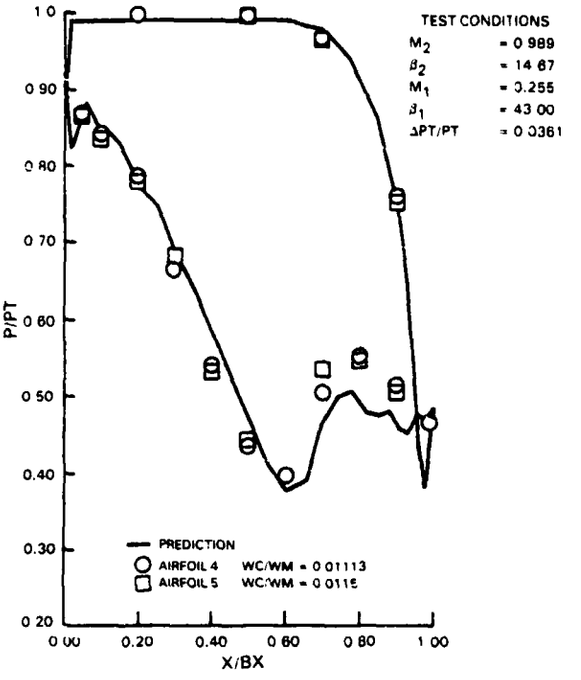

Figure 126 Cooled Cascade Test Base Blade Section Pressure Distribution at 0.989 Exit Mach Number

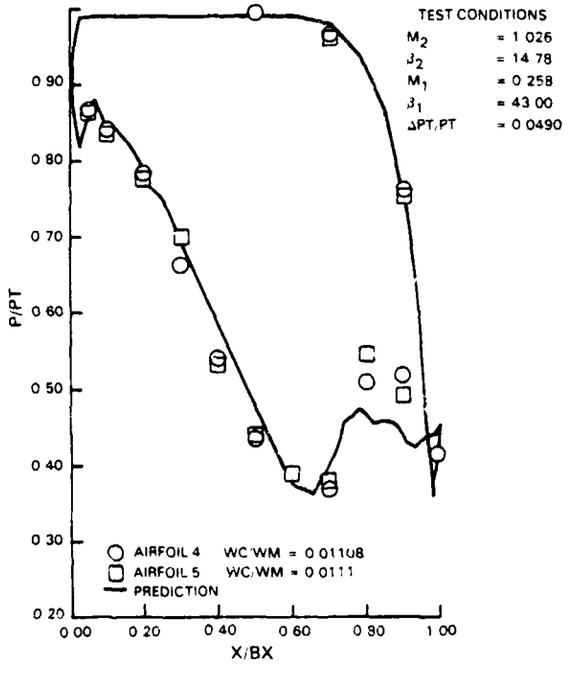

Figure 127 Cooled Cascade Test Base Blade Section Pressure Distribution at 1.026 Exit Mach Number

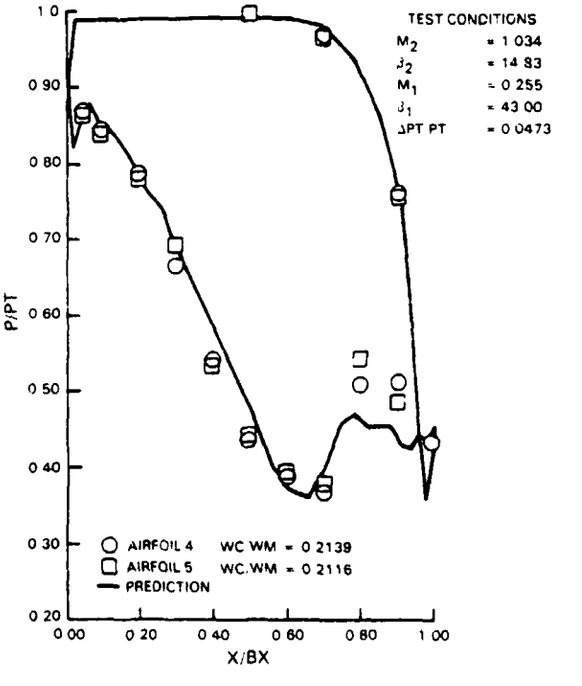

Figure 128 Cooled Cascade Test Base Blade Section Pressure Distribution at 1.034 Exit Mach Number

ORIGINAL PAGE IS
OF POOR QUALITY

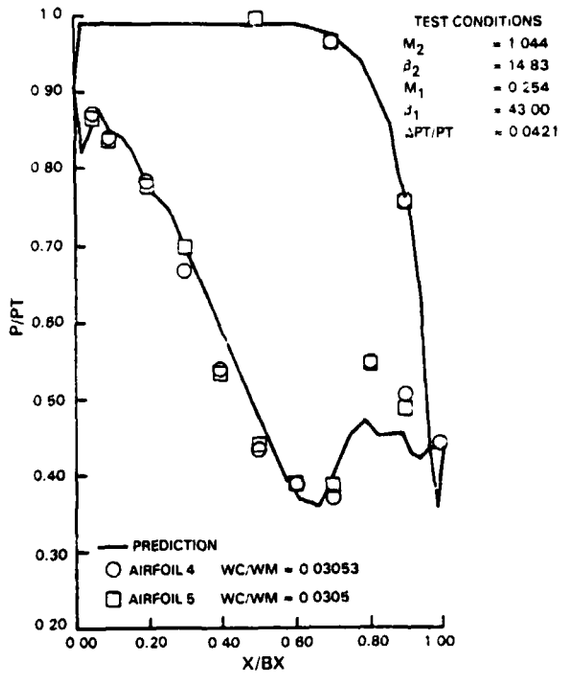

Figure 129 Cooled Cascade Test Base Blade Section Pressure Distribution at 1.044 Exit Mach Number

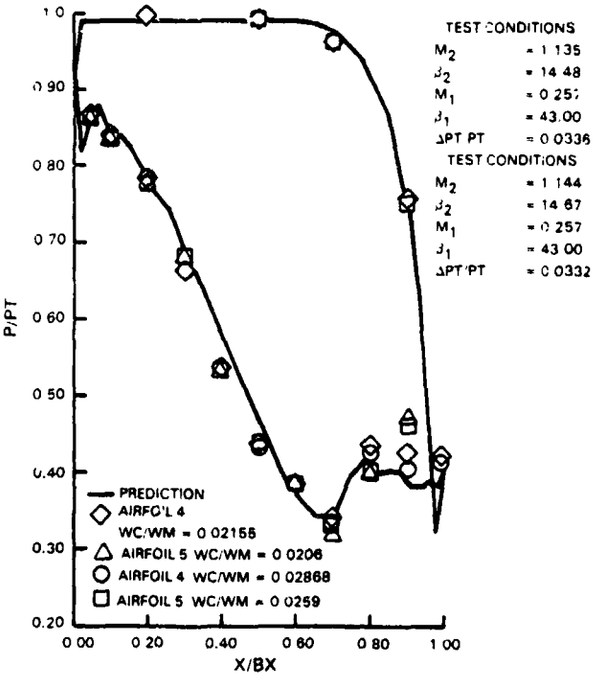

Figure 130 Cooled Cascade Test Base Blade Section Pressure Distribution at 1.14 Exit Mach Number

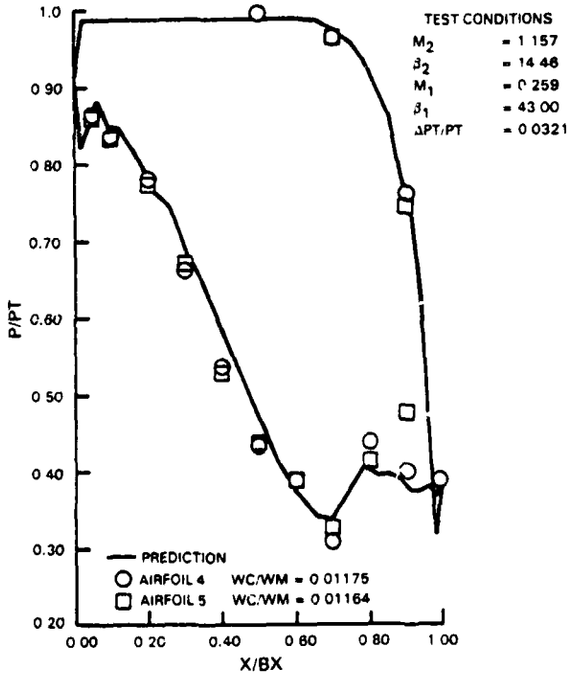

Figure 131 Cooled Cascade Test Base Blade Section Pressure Distribution at 1.157 Exit Mach Number

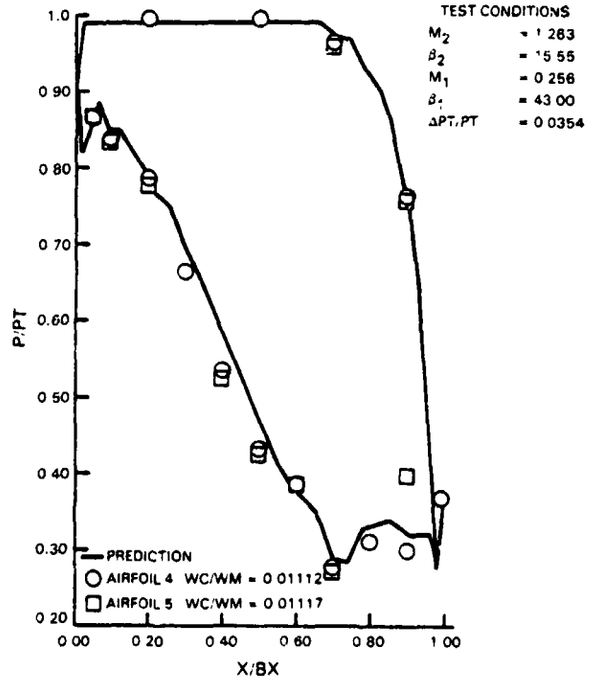

Figure 132 Cooled Cascade Test Base Blade Section Pressure Distribution at 1.263 Exit Mach Number

ORIGINAL PAGE IS
OF POOR QUALITY

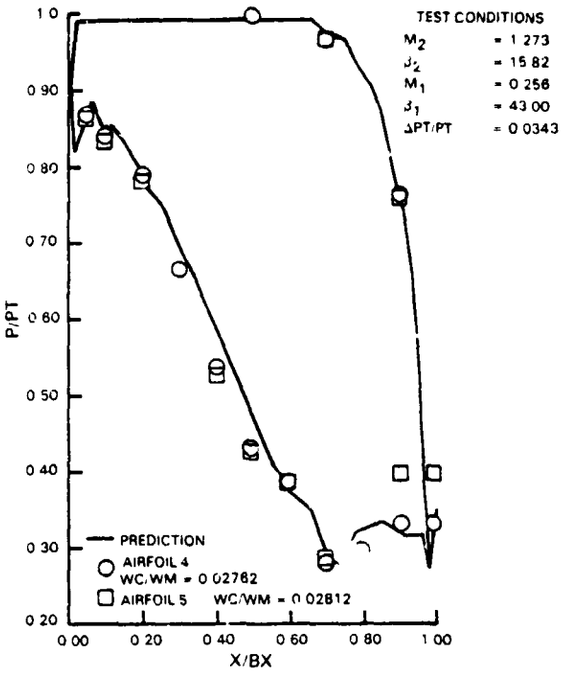

Figure 133 Cooled Cascade Test Base Blade Section Pressure Distribution at 1.273 Exit Mach Number

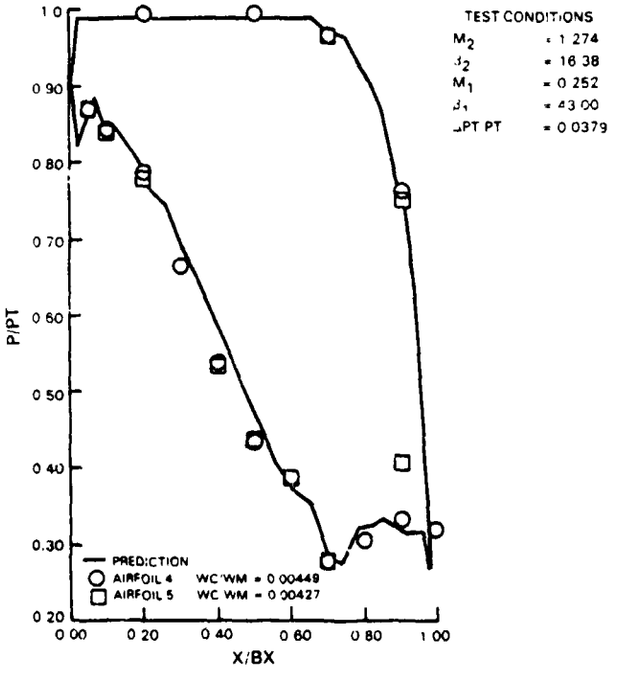

Figure 134 Cooled Cascade Test Base Blade Section Pressure Distribution at 1.274 Exit Mach Number

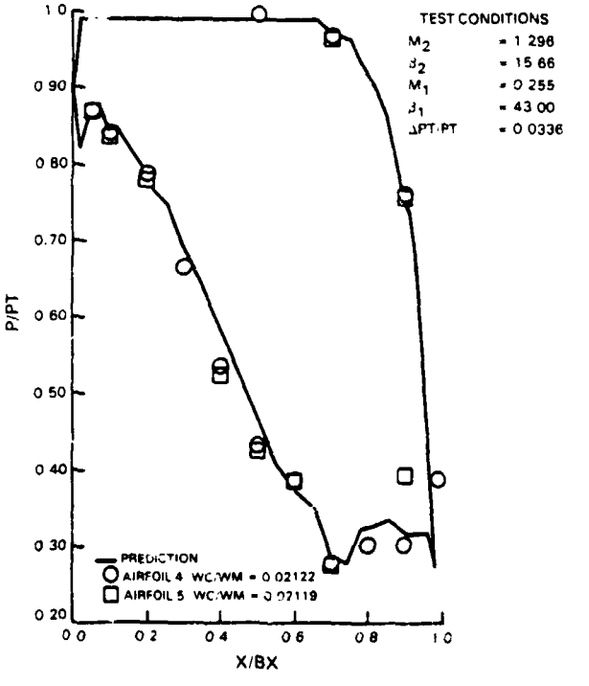

Figure 135 Cooled Cascade Test Base Blade Section Pressure Distribution at 1.296 Exit Mach Number

ORIGINAL PAGE
BLACK AND WHITE PHOTOGRAPH

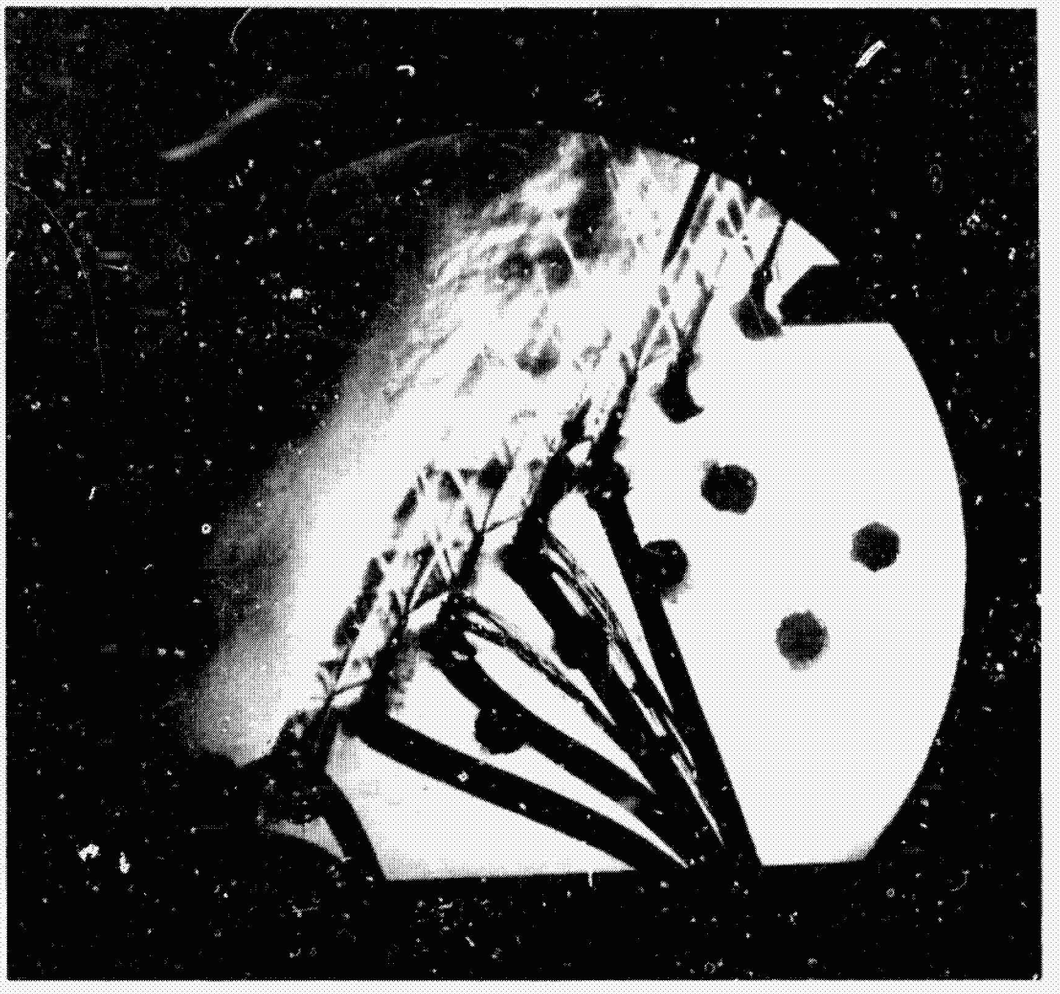

$M_{2_i} = 1.311 \quad \beta_1 = 43.0 \quad W_C/W_M = 0.0$

Figure 136 Schlieren Photograph of Base Blade Mean Section at 1.3 Isentropic Exit Mach Number - $W_C/W_m = 0$

ORIGINAL PAGE
BLACK AND WHITE PHOTOGRAPH

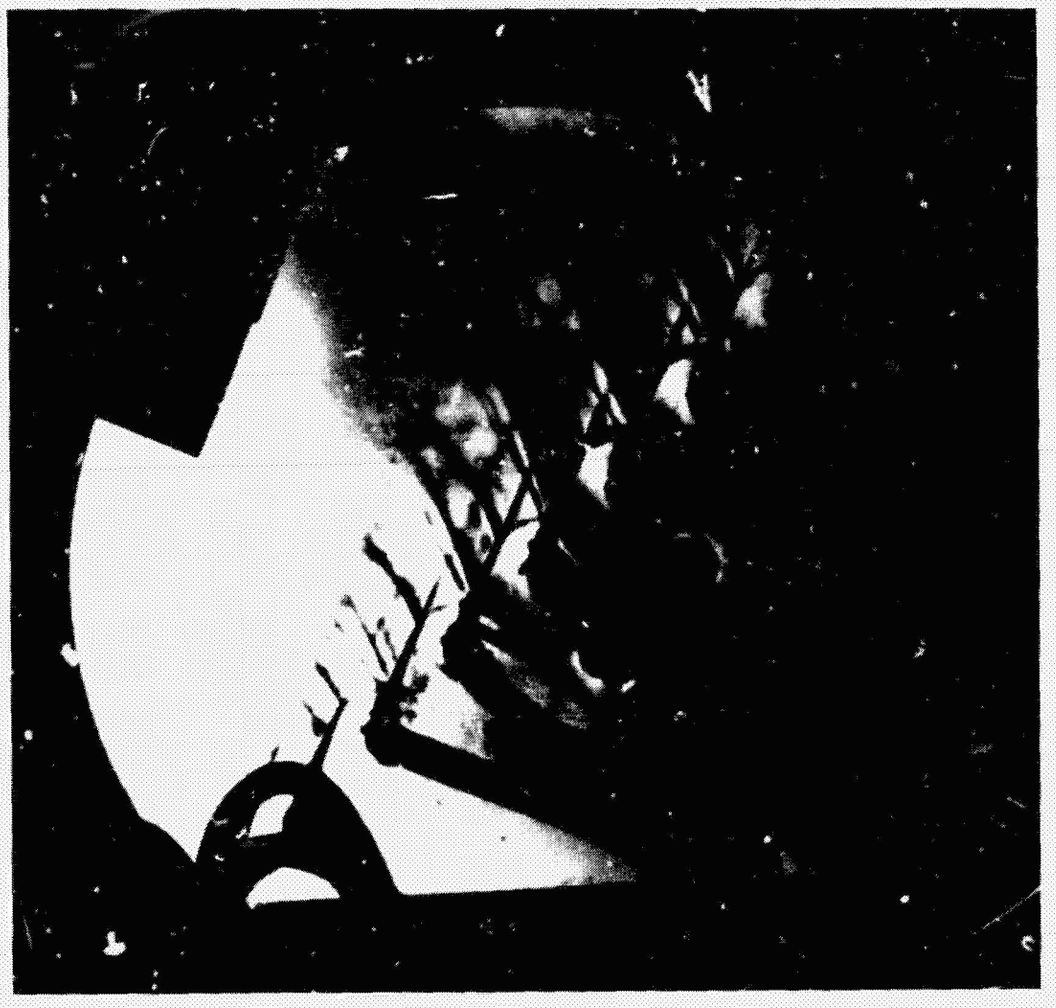

$M_{2_i} = 1.288$ $\beta_1 = 43.0$ $W_C/W_M = 0.0120$

Figure 137 Schlieren Photograph of Base Blade Mean Section at 1.3 Isentropic Exit Mach Number - $W_c/W_m = 0.012$

ORIGINAL PAGE
BLACK AND WHITE PHOTOGRAPH

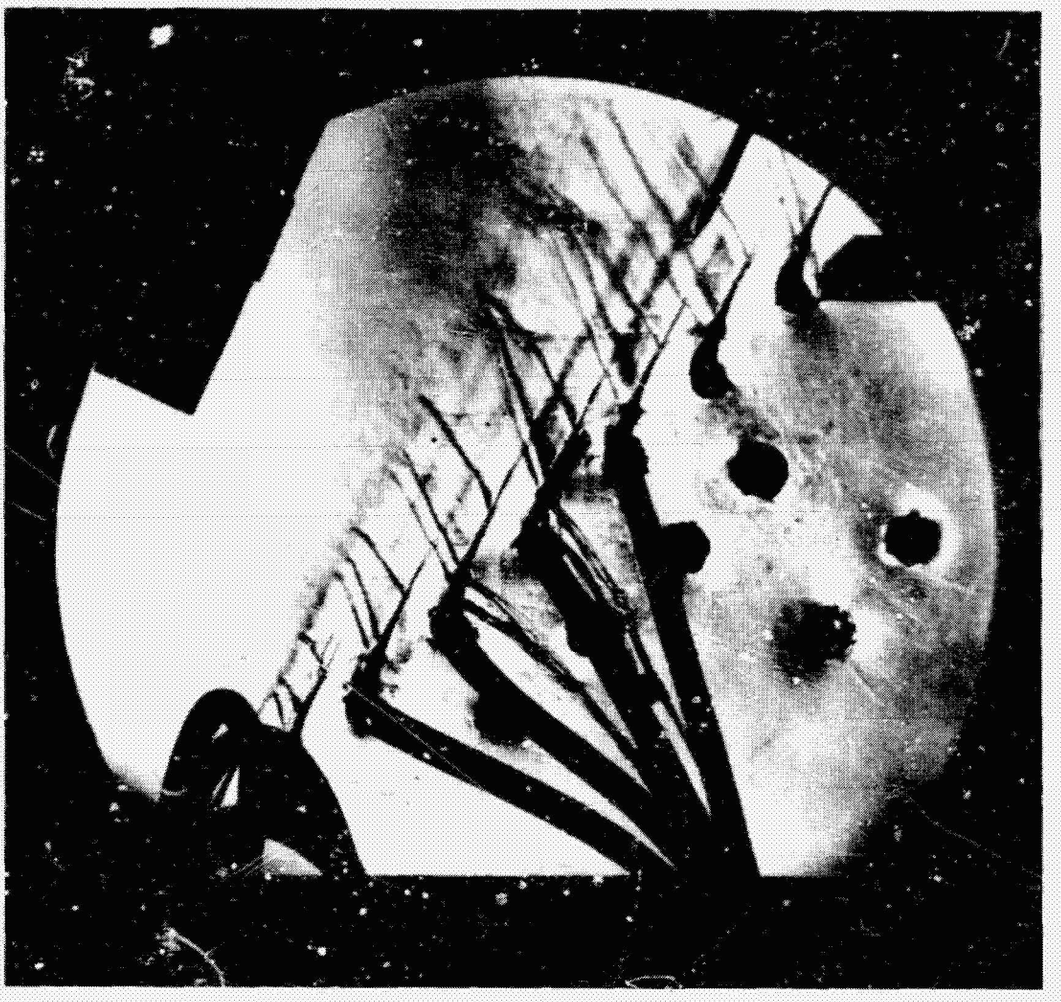

$M_{2_i} = 1.311$ $\beta_1 = 43.0$ $W_C/W_M = 0.0204$

Figure 138 Schlieren Photograph of Base Blade Mean Section at 1.3 Isentropic Exit Mach Number - $W_C/W_m = 0.024$

ORIGINAL PAGE
BLACK AND WHITE PHOTOGRAPH

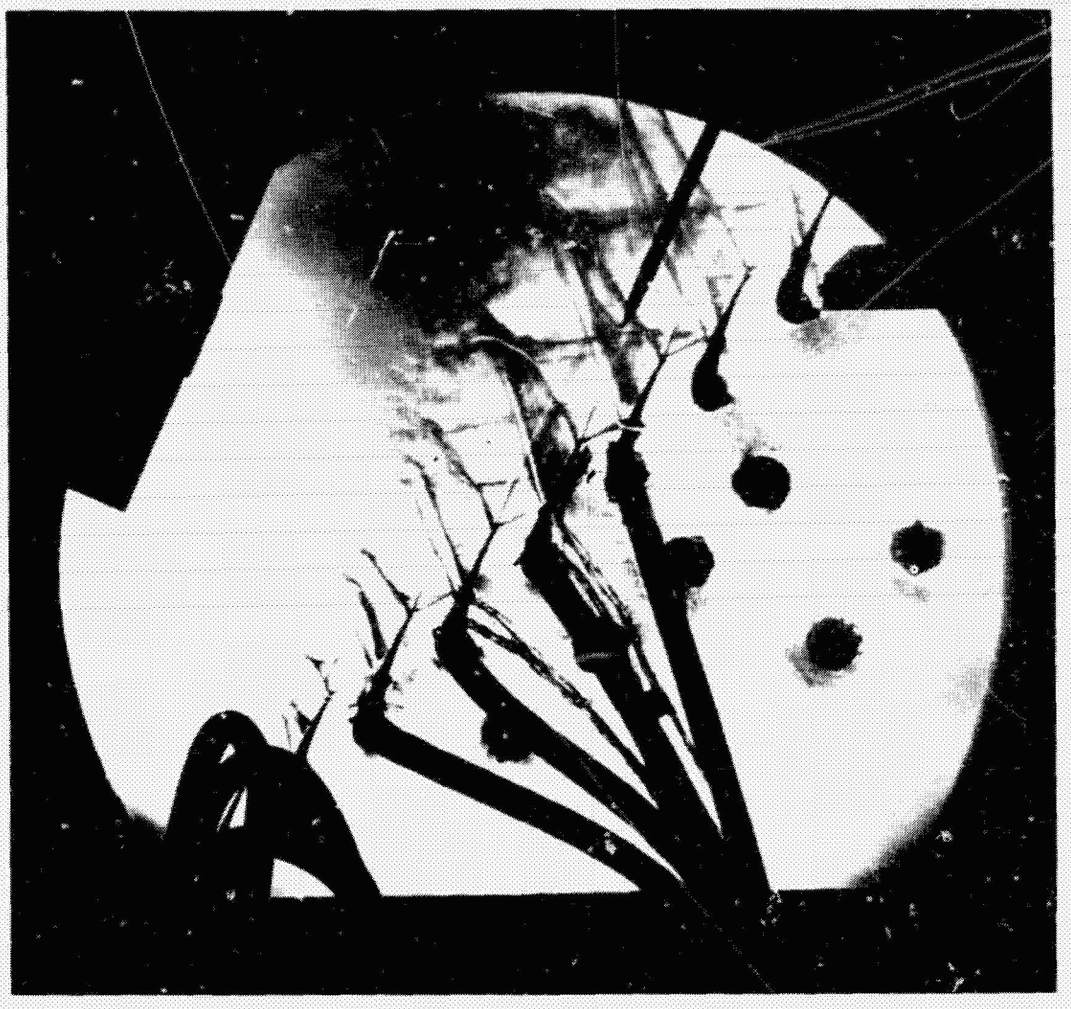

$M_{2_i} = 1.293$ $\beta_1 = 43.0$ $W_C/W_M = 0.272$

Figure 139 Schlieren Photograph of Base Blade Mean Section at 1.3 Isentropic Exit Mach Number - $W_C/W_m = 0.0272$

ORIGINAL PAGE IS
OF POOR QUALITY

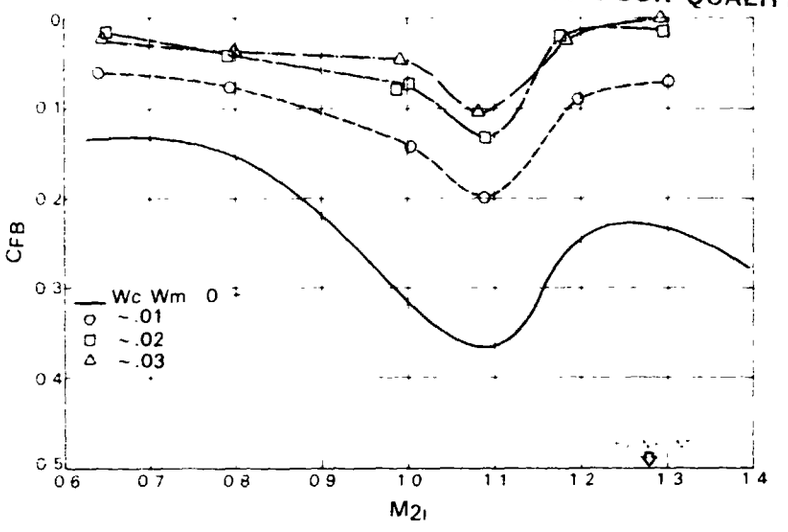

Figure 140 Base Pressure Coefficient vs Plenum Exit Isentropic Mach Number at Various Cooling Flow Rates

4.4.4.4 Total Pressure Loss Assessment

Predictions are compared to measured losses, as a function of cooling flow to mainstream flow ratio (Wc/Wm) and isentropic exit Mach number, in Figures 141-146. Measured base pressure was used in calculating the predicted values.

Figures 141 and 142 indicate that total pressure loss was insensitive to coolant flow ejection rates at subsonic exit Mach numbers, there being only a slight increase in loss at coolant flow rates of 2 and 3 percent. The prediction indicates the same trend but overestimates the losses at the higher flow rates.

Total pressure loss measurements for transonic and supersonic Mach numbers are shown in Figures 143-146. In the transonic range of Mach numbers (1.0 to 1.1), the measured losses are seen to decrease with increasing coolant flow rate. This trend is reasonably well predicted with the loss level being overestimated at the higher coolant flow rates for M_{2i} = 1.0, but well predicted at M_{2i} = 1.1. At higher supersonic exit Mach numbers, the measured loss for coolant flow rates in the 1-3 percent range is essentially constant. The prediction is seen to overestimate the measured losses, in addition to indicating a trend of increasing loss with increasing coolant flow rate. The reason for this apparent discrepancy is discussed in the following section.

ORIGINAL PAGE IS
OF POOR QUALITY

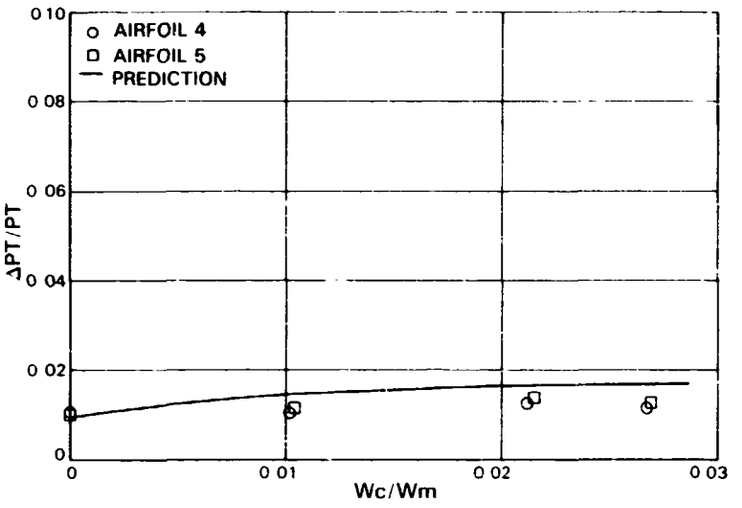

Figure 141 Base Blade Total Pressure Loss vs Cooling Flow Ratio; M_{2i} = 0.65

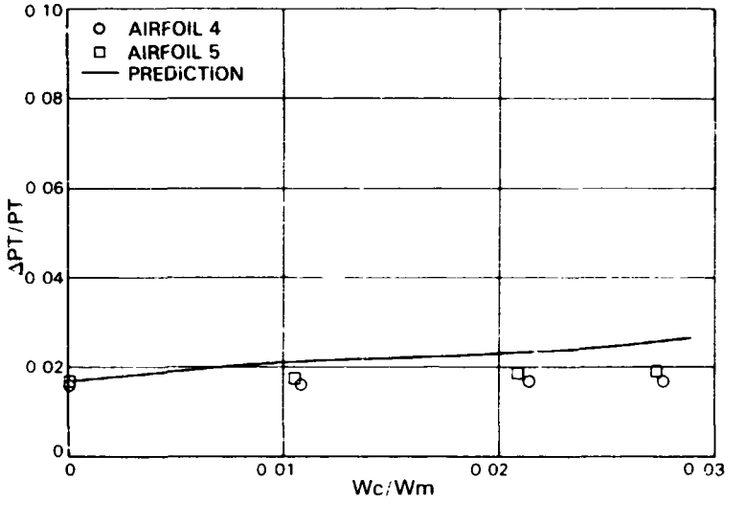

Figure 142 Base Blade Total Pressure Loss vs Cooling Flow Ratio; M_{2i} = 0.79

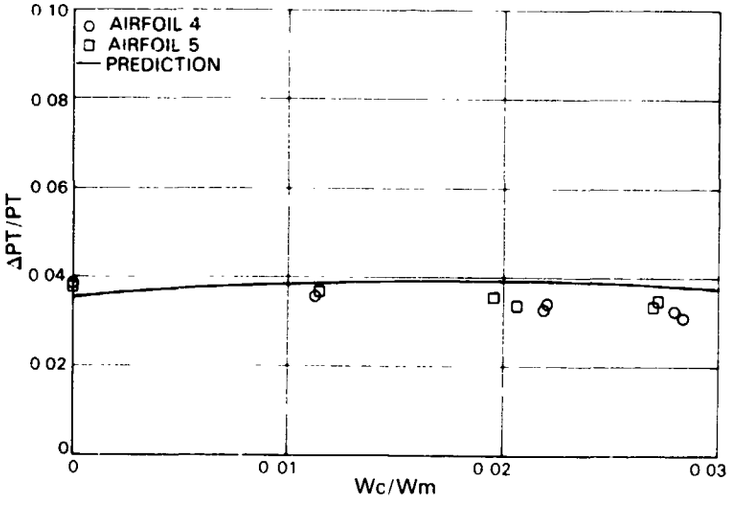

Figure 143 Base Blade Total Pressure Loss vs Cooling Flow Ratio; M_{2i} = 1.00

ORIGINAL PAGE IS
OF POOR QUALITY

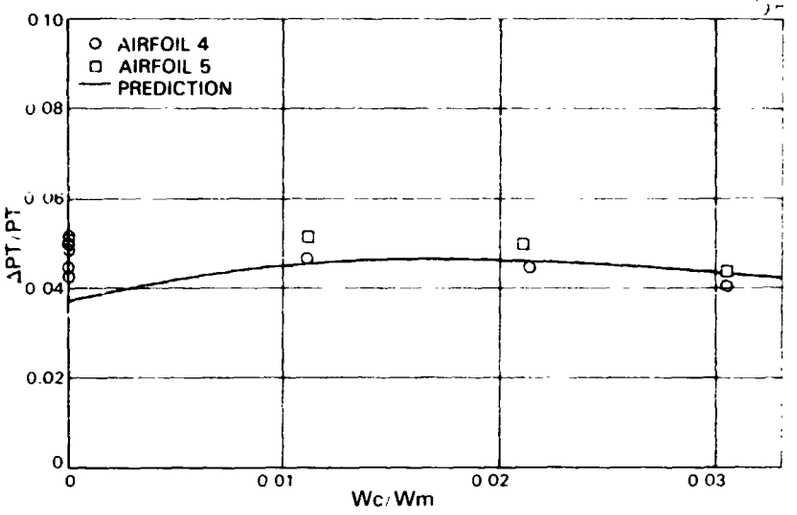

Figure 144 Base Blade Total Pressure Loss vs Cooling Flow Ratio; M_{2i} = 1.1

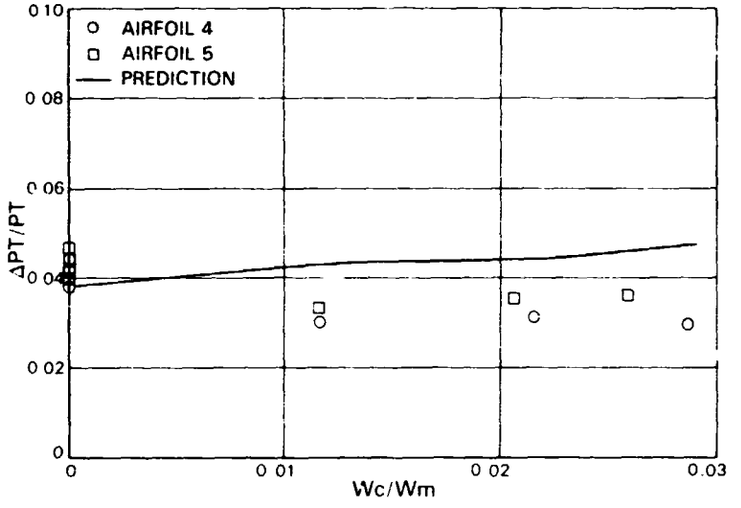

Figure 145 Base Blade Total Pressure Loss vs Cooling Flow Ratio; M_{2i} = 1.2

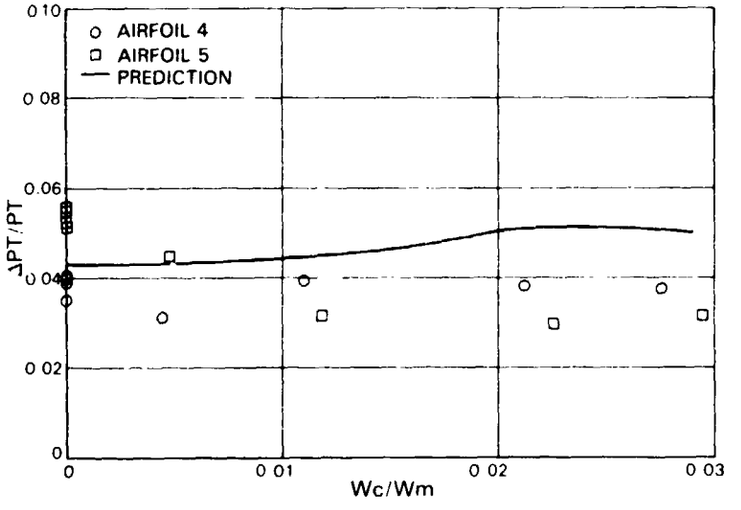

Figure 146 Base Blade Total Pressure Loss vs Cooling Flow Ratio; M_{2i} = 1.3

ORIGINAL PAGE IS
OF POOR QUALITY

4.4.4.5 Shock Losses

In an infinite cascade (truly periodic cascade flow), the distribution of the shock and wake loss contributions to total pressure loss would be as shown schematically in Figure 147. The experimental results discussed in the previous section implied that either, or both of these contributors were affected by coolant flow injection. In order to verify this, measured gapwise distributions of total pressure loss at isentropic exit Mach numbers of approximately 1.0 and 1.3 were examined. These measurements are shown in Figure 148. A comparison of the distributions indicates that shock and wake losses are indeed affected by trailing edge coolant flow. A more detailed assessment of the data was subsequently conducted to better define the distribution of shock and wake losses as impacted by changes in coolant flow ejection rates and isentropic exit Mach number. The results of this assessment are shown in Figure 149, which indicates that trailing edge coolant flow ejection causes an increase in wake loss and a decrease in shock loss; the decrease in shock loss dominating and causing a decrease in total pressure loss. This observation is confirmed by a re-examination of Figure 148. It would appear then, that the coolant flow injected into the trailing edge flow field serves to weaken the trailing edge shocks, thereby reducing the losses associated with the shock structure and, quite possibly, those associated with shock-boundary layer interactions, although the latter cannot be directly shown by the data presented.

As mentioned earlier, the Schlieren visualizations did not indicate a perceptable change in trailing edge shock pattern when coolant flow was injected. This seems to be in direct contrast with the loss results just discussed. However, it is hypothesized that the shocks shown in the Schlieren visualizations formed at the ribs between the trailing edge coolant ejection holes as shown in Figure 150. This would result in an alternating zone of shocks and shock-free (or weak shock) layers along the trailing edge of the blade span. To the Schlieren system, these shock waves would appear identical to those eminating from a solid trailing edge. The presence of these "layered" shocks may have caused some of the "between-wake" total pressure loss indicated at $M_{2i} = 1.3$ in Figure 148. At $M_{2i} = 1.0$, these shocks would be too weak to have a noticable effect on total pressure loss.

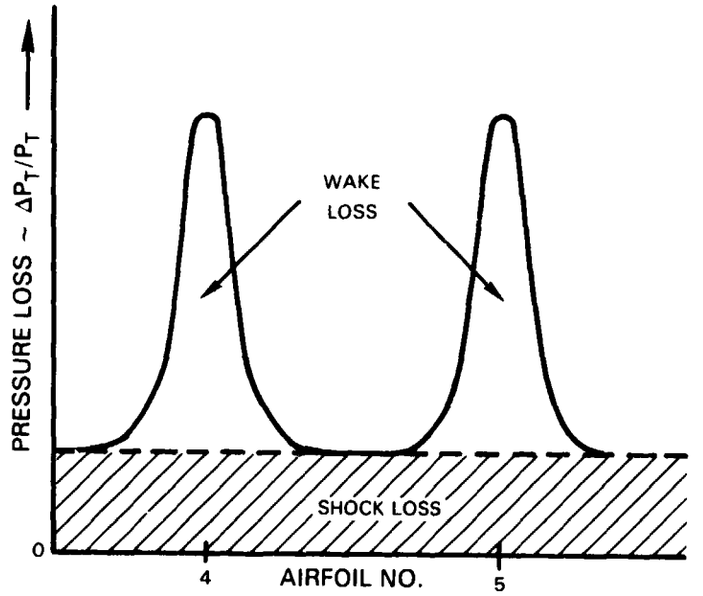

Figure 147 Schematic of Shock and Wake Loss Contributions to Total Pressure Loss

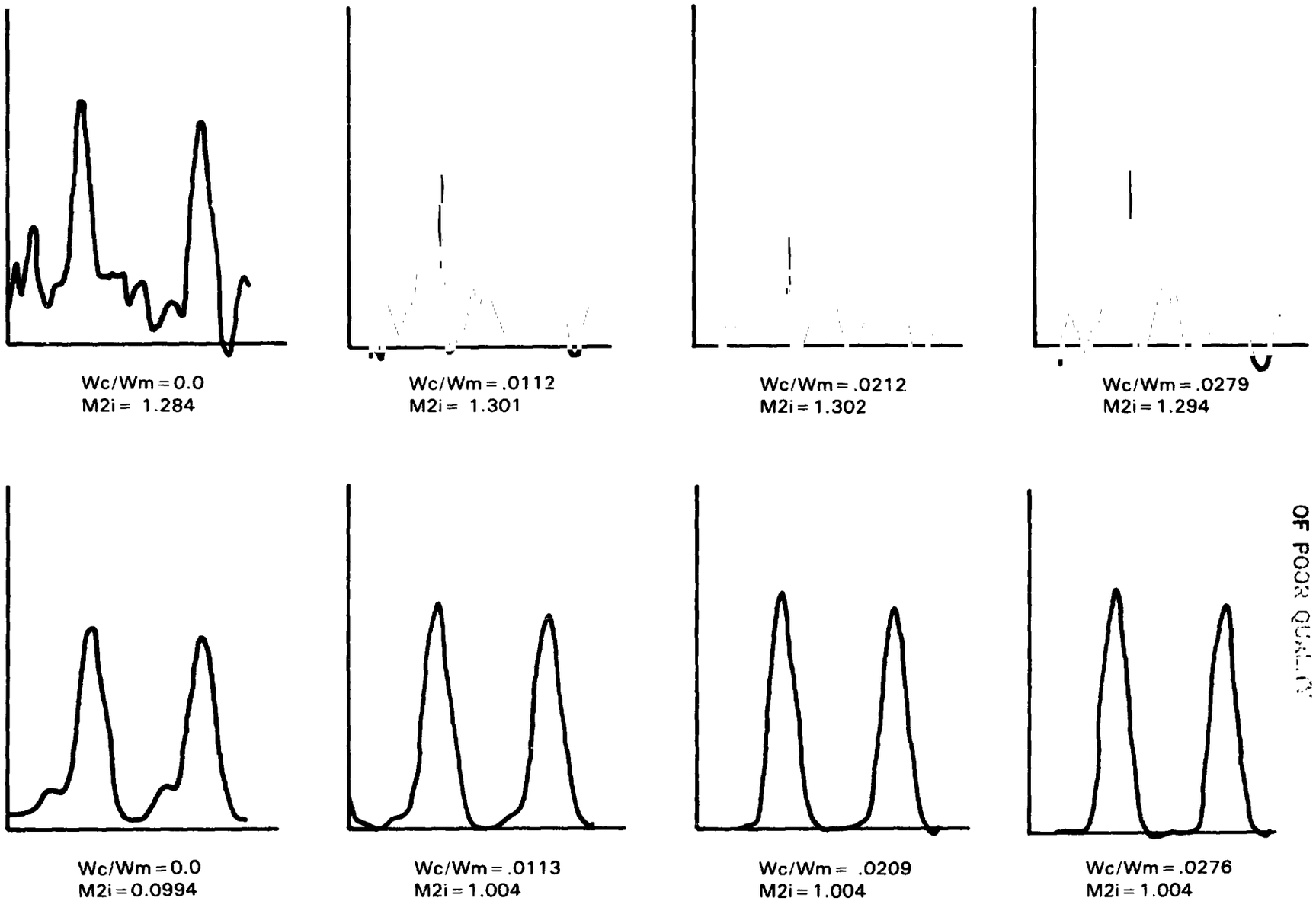

ORIGINAL PAGE IS
OF POOR QUALITY

Figure 148 Gapwise Distributions of Total Pressure Loss For Base Airfoils With Several Cooling Flow Rates And Isentropic Mach Numbers oF 1.0 And 1.3

ORIGINAL PAGE IS
OF POOR QUALITY

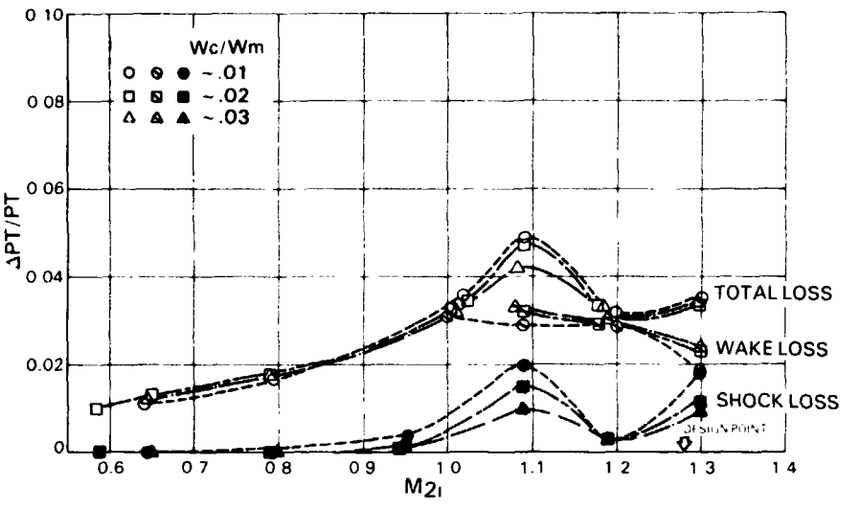

Figure 149 Total Pressure, Shock And Wake Loss vs Exit Isentropic Mach Number at Various Cooling Flow Rates

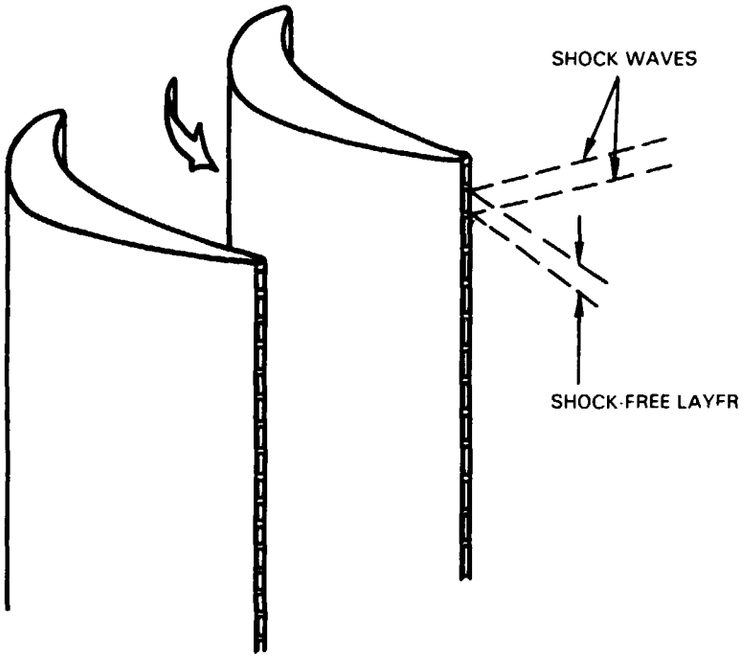

Figure 150 Schematic of Shock Pattern Formed at Ribs Between Trailing Edge Coolant Ejection Holes

4.4.4.6 Exit Gas Angle

The variation of exit air angle with M_{2i} at several coolant flow ejection rates is compared with data obtained with no flow ejection and predicted air angles in Figure 151. Generally, the exit angles obtained for flow ejection rates of 1.0, 2.0 and 3.0 percent were identical and similar to those obtained without flow ejection.

Predictions overestimate measured subsonic and transonic data by approximately 1.5 degrees. The explanation for this difference is the same as that for the discrepancies noted in the base and overcambered airfoil exit gas angle data discussed in Sections 4.4.3.1.5 and 4.4.3.2.5 of this report. If this apparent discrepancy is removed, there is good agreement between measured and predicted values up to $M_{2i} = 1.1$. Beyond that, agreement becomes poor.

4.4.5 Summary of Blade Cascade Results

Results of blade cascade testing are summarized in the following sections. This summary compares the measured total pressure loss, base pressure coefficient, and exit air angles for the base, overcambered, and straightback airfoils. It also presents a comparison of the base airfoil performance with and without trailing edge coolant flow ejection.

4.4.5.1 Comparison of Uncooled Base, Overcambered, and Straightback Airfoils

4.4.5.1.1 Total Pressure Loss

Total pressure losses, $\Delta P_T/P_T$, for the base, overcambered, and straightback airfoils are summarized in Figure 152 as a function of M_{2i}. Also included are base airfoil pressure losses at design point M_{2i} for off-design inlet gas angles of 33 and 58 degrees. The curves shown are faired through averaged data. These data indicate results consistent with the base pressure coefficient results, i.e., the base airfoil provides the lowest total pressure losses for subsonic and low supersonic M_{2i} and the pressure losses for all three airfoils are essentially equal at the design point M_{2i}. Base airfoil pressure loss appears to be relatively insensitive to changes in inlet gas angle over the range shown, indicating that the base blade design has good incidence range capability.

4.4.5.1.2 Base Pressure Coefficient

The variation of base, overcambered and straightback airfoil base pressure coefficients, C_{PB}, with isentropic exit Mach number (M_{2i}) is summarized in Figure 153. Curves have been faired through the averaged data measured from each cascade. As indicated, the base airfoil provides the most favorable overall variation of CP_B with M_{2i}, although at the design point exit Mach number the results for all three airfoils are close. As noted earlier, the straightback airfoil design appears to offer a more favorable CP_B than the base or overcamber designs at M_{2i} greater than 1.3, but this Mach number region is greater than the component design point Mach number.

ORIGINAL PAGE IS
OF POOR QUALITY

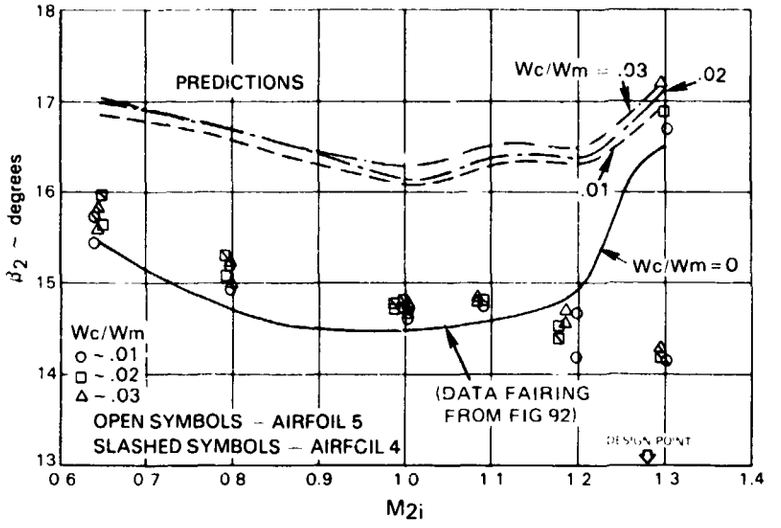

Figure 151 Base Blade Exit Air Angle vs Exit Isentropic Mach Number at Various Cooling Flow Rate

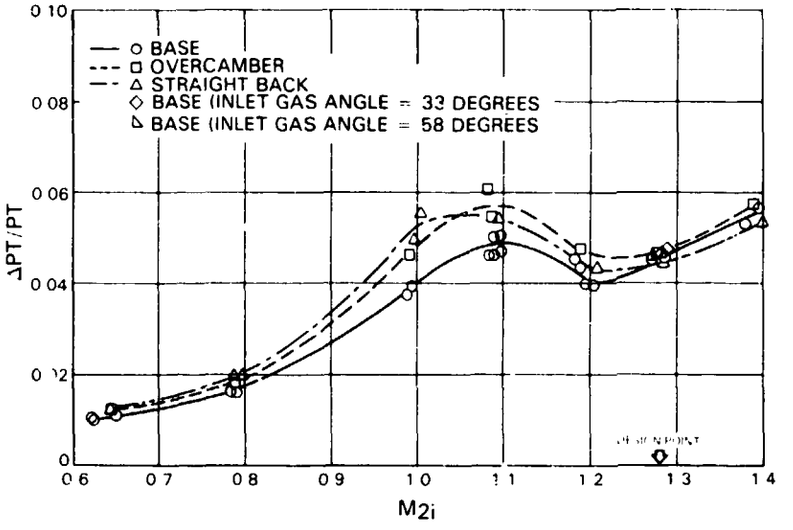

Figure 152 Comparison of Total Pressure Loss vs Exit Isentropic Mach Number

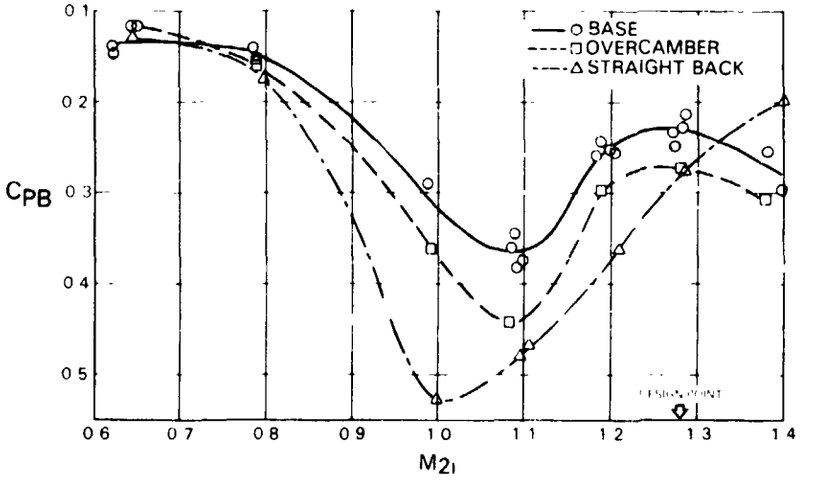

Figure 153 Comparison of Base Pressure vs Exit Isentropic Mach Number

4.4.5.1.3 Exit Air Angle

The variation of exit air angle, β_2, with M_{2i} for the base, overcambered, and straightback airfoils is compared with predicted β_2 in Figure 154. In general, curves faired through the "averaged" data show the same trend, differing only in level. If the base and overcamber airfoil data are adjusted upward by approximately 1.7 and 1.2 degrees respectively, based on continuity checks and airfoil loading calculations, the exit air angles for all three designs become approximately equal and in reasonable agreement with the prediction.

4.4.5.2 Comparison Between Cooled and Uncooled Base Airfoils

4.4.5.2.1 Total Pressure Loss

Total pressure losses obtained for the base airfoil with trailing edge coolant flow ejection rates of approximately 1, 2 and 3 percent are compared with loss obtained with no flow ejection in Figure 155. In general trailing edge flow ejection causes a small increase in total pressure loss at subsonic Mach numbers but reduces total pressure loss at supersonic Mach numbers. The data indicate that flow ejection is most effective in reducing total pressure loss for M_{2i} greater than 1.1. This is attributable to the fact that flow ejection weakens the trailing edge shock strength such that decreases in shock losses predominate over corresponding increases in wake loss caused by the added flow at the trailing edge.

4.4.5.2.2 Base Pressure Coefficient

Trailing edge coolant flow ejection resulted in base pressure coefficients which increased (became more favorable) with increasing trailing edge flow and reflected the decrease in total pressure loss (see Figure 140). The data indicate that 1 percent trailing edge flow ejection increased the base pressure coefficient, C_{pB}, by as much as 0.17 at M_{2i} of 1.3. Increasing the flow to 2 or 3 percent resulted in approximately an additional 0.07 increase in C_{pB} at M_{2i} of 1.3; reducing C_{pB} to approximately zero.

4.4.5.2.3 Exit Air Angle

The variation in exit air angle, β_2, with variations in M_{2i} at several trailing edge coolant flow ejection rates is compared to predictions and data obtained with no flow ejection in Figure 156. The data show that trailing edge flow ejection had little effect on exit air angle. Predictions agreed with the data trends but tended to over-predict β_2 by +1.0 to -2.0 degrees. This discrepancy is unexplained as discussed in previous sections of this report. Continuity and airfoil loading calculations indicated that the data should be adjusted upward by approximately 1.5 degrees to correct the error. This adjustment brings the data and prediction into reasonable agreement with each other.

ORIGINAL PAGE IS
OF POOR QUALITY

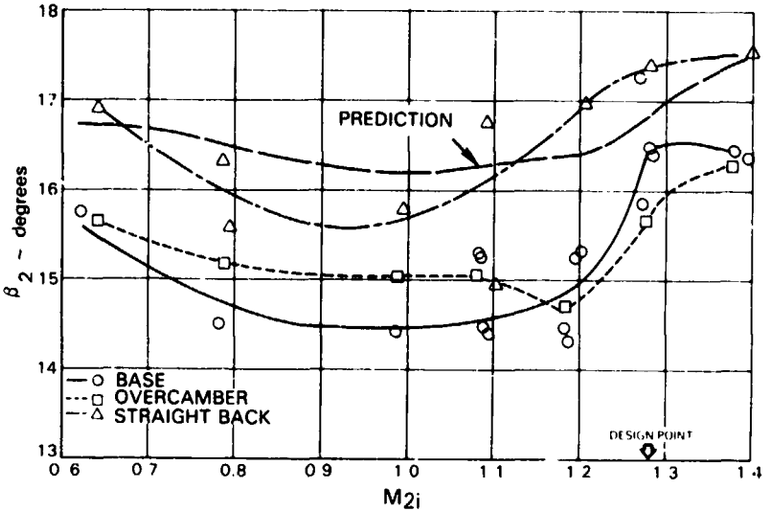

Figure 154 Comparison of Exit Air Angle vs Exit Isentropic Mach Number

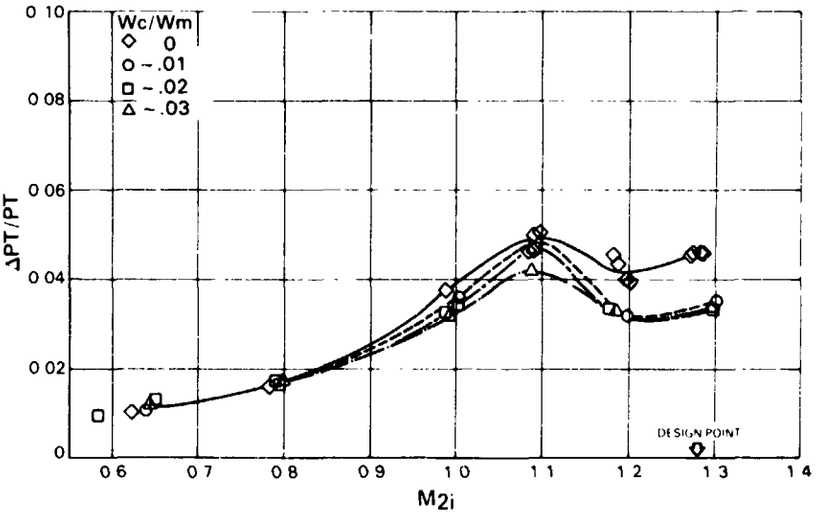

Figure 155 Comparison of Total Pressure Loss vs Exit Isentropic Mach Number

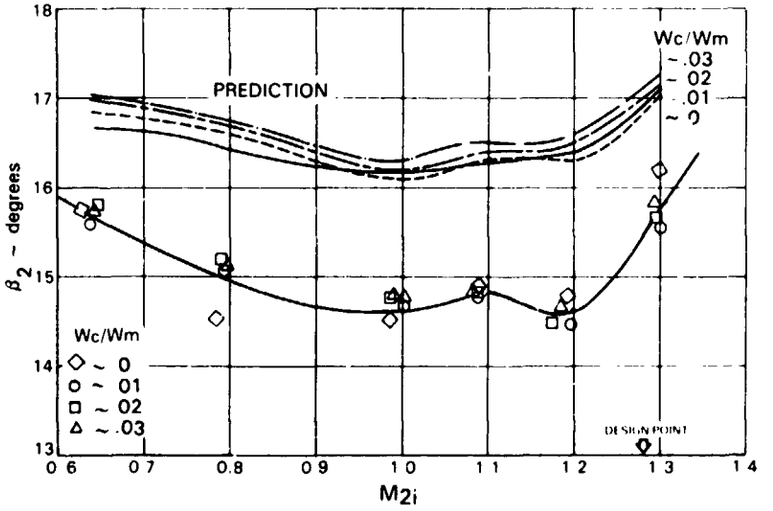

Figure 156 Comparison of Exit Air Angle vs Exit Isentropic Mach Number
(Average of Airfoils 4 and 5)

5.0 CONCLUSIONS

5.1 Vane Cascade

- The performance benefits of the contoured vane endwall design have been confirmed for the high-pressure turbine component. The S-wall cascade has 17 percent less full-passage, mass-averaged pressure loss than the straight wall cascade.

- In the two-dimensional spanwise flow region of the cascade, vane exit air angle is generally insensitive to changes in endwall configuration, variations in exit Mach number, and variation in coolant flow rates.

- Variations in vane exit Mach number, in both the cooled and uncooled straight wall cascades, indicated no abrupt pressure loss increase (transonic drag rise) even at near-sonic conditions. This confirms that the base vane section is acceptable for the component design.

- Mid-span total pressure loss almost doubled when design-point coolant flow was ejected from all film cooling sites. The largest contributor to this increased pressure loss was suction surface coolant flow injection, showing a penalty about 5 times higher than that for pressure surface injection. Trailing edge design point coolant flow injection had little effect on cascade performance.

- Predicted airfoil pressure distributions were in good agreement with measured static pressures for both two- and three-dimensional cascade flow conditions over the range of exit Mach numbers and coolant flow conditions evaluated.

5.2 Blade Cascades

- Testing verified the distribution of curvature selected for the high-pressure turbine component blade airfoil geometry. This geometry (base airfoil) provided the lowest total pressure losses for subsonic and transonic exit Mach numbers, and pressure losses, from an experimental standpoint, equal to the other, airfoils at the design point exit Mach number.

- Base airfoil pressure loss was relatively insensitive to variations in inlet gas angle over a range of 25 degrees, indicating that the component blade design has good incidence range.

- Testing of the base blade cascade with trailing edge coolant flow ejection indicated that this caused a small increase in pressure loss at subsonic Mach numbers, but reduced total pressure loss at supersonic exit Mach numbers relative to the base blade without coolant flow ejection. This behavior is attributable to the fact that flow ejection weakens the trailing edge shock strength such that decreases in shock losses predominate over corresponding increases in wake loss caused by the added flow at the trailing edge.

- Predicted airfoil pressure distributions were in good agreement with measured distributions for both cooled and uncooled cascades at subsonic exit Mach numbers. Agreement between the predicted and measured data for supersonic exit conditions was good except for the suction surface recompression region, where the data were scattered around the prediction. This data scatter is attributed to the nonperiodic nature of the suction surface shock-boundary layer interaction in the cascades.

- For the three uncooled cascades, exit air angle vs Mach number trends were similar and reasonably well predicted. However, experimental difficulties led to unexplained differences between predictions and measured exit air angle data for the base and overcambered uncooled cascades and the base cascade with trailing edge coolant flow ejection. Correcting for these differences through the use of continuity and airfoil loading calculations indicated that the predictions were more nearly correct and that the three uncooled configurations achieve approximately the same exit air angles. The predicted and measured data for all of the cascades were in reasonably good agreement. The addition of trailing edge coolant flow ejection had little effect on exit air angle.

APPENDIX A

The following appendices list the coordinates of the vane and blade airfoils employed in the cascade testing described in this report. Figures A-1 and A-2 define the applicable nomenclature.

ORIGINAL PAGE IS
OF POOR QUALITY

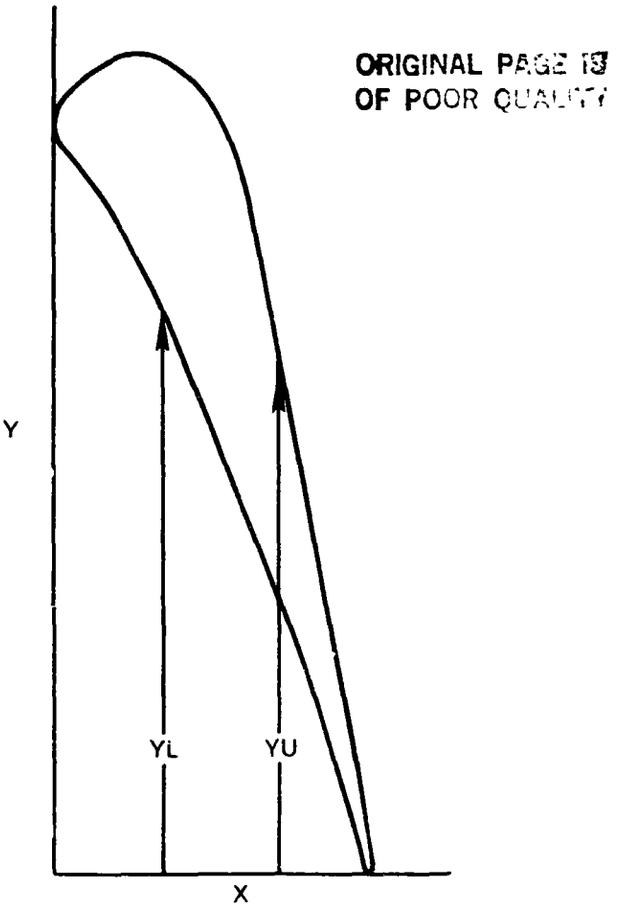

Figure A-1 Nomenclature Used to Define Airfoil Coordinates

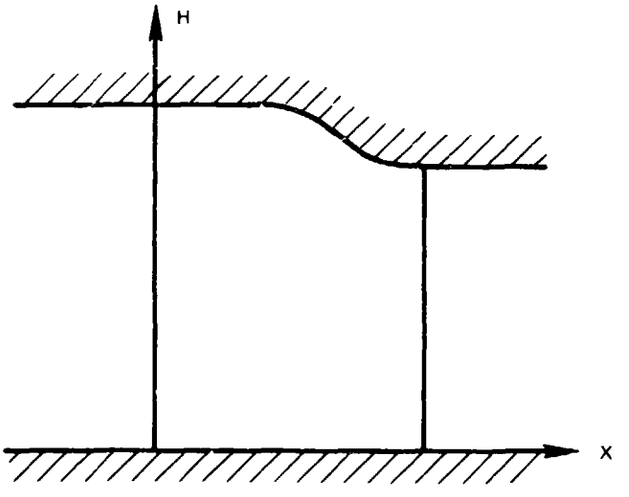

Figure A-2 Nomenclature Used to Define Profiled Wall Coordinates in S-Wall Vane Cascade

TABLE A-1

VANE AIRFOIL COORDINATES FOR S-WALL CASCADE

X/BX	YU/BX	YL/BX	H/BX
0.000	2.442	2.442	1.671
0.010	2.497	2.387	1.671
0.020	2.519	2.366	1.671
0.030	2.534	2.349	1.671
0.040	2.547	2.338	1.671
0.060	2.567	2.316	1.671
0.080	2.585	2.292	1.671
0.120	2.616	2.236	1.671
0.160	2.640	2.172	1.671
0.200	2.658	2.102	1.671
0.240	2.669	2.027	1.671
0.280	2.672	1.948	1.671
0.320	2.668	1.865	1.671
0.360	2.655	1.776	1.671
0.400	2.633	1.689	1.671
0.440	2.599	1.596	1.668
0.480	2.554	1.499	1.663
0.520	2.491	1.401	1.652
0.560	2.407	1.299	1.635
0.600	2.290	1.194	1.611
0.640	2.139	1.085	1.579
0.680	1.958	0.973	1.543
0.720	1.754	0.858	1.507
0.760	1.532	0.738	1.472
0.800	1.295	0.614	1.444
0.840	1.049	0.484	1.421
0.880	0.795	0.347	1.404
0.920	0.535	0.199	1.392
0.960	0.270	0.037	1.386
1.000	0.000	0.000	1.384

Cascade axial chord, B_X = 3.34 cm (1.315 in)

TABLE A-2

VANE AIRFOIL COORDINATES FOR STRAIGHT WALL CASCADE

X/BX	YU/BX	YL/BX
0.0	2.343	2.343
.0/0	2.289	2.397
.020	2.268	2.418
.030	2.252	2.433
.040	2.241	2.445
.060	2.220	2.465
.080	2.196	2.483
.120	2.147	2.514
.160	2.080	2.538
.200	2.019	2.555
.240	1.939	2.564
.280	1.863	2.566
.320	1.783	2.560
.360	1.699	2.544
.400	1.613	7.518
.440	1.523	2.480
.480	1.431	2.429
.520	1.336	2.359
.560	1.238	2.265
.600	1.137	2.138
.640	1.033	1.983
.680	.927	1.805
.720	.816	1.609
.760	.702	1.400
.800	.584	1.181
.840	.460	0.955
.880	.330	.722
.920	.192	.485
.960	.040	.245
1.000	0.0	0.0

Cascade axial chord, B_x = 3.46 cm (1.364 in)

TABLE A-3

BASE BLADE AIRFOIL COORDINATES

X	YL	YU
0.0	1.12072	1.12072
0.00922	1.08834	1.15400
0.01844	1.07681	1.17257
0.02766	1.06937	1.19001
0.03688	1.06437	1.20643
0.04610	1.06118	1.22191
0.05532	1.05954	1.23654
0.06454	1.05930	1.25036
0.07376	1.06046	1.26343
0.08298	1.06310	1.27580
0.09220	1.06744	1.28750
0.11525	1.08131	1.31402
0.13830	1.09022	1.33697
0.16135	1.09455	1.35663
0.18440	1.09487	1.37321
0.20745	1.09160	1.38687
0.23050	1.08510	1.39769
0.25355	1.07563	1.40574
0.27660	1.06341	1.41103
0.29965	1.04863	1.41353
0.32270	1.03143	1.41318
0.34575	1.01192	1.40987
0.36880	0.99023	1.40345
0.39185	0.96642	1.39368
0.41490	0.94057	1.38026
0.43795	0.91273	1.36272
0.46100	0.88296	1.34046
0.48405	0.85127	1.31253
0.50710	0.81770	1.27744
0.53015	0.78227	1.23263
0.55320	0.74498	1.17439
0.57625	0.70583	1.10922
0.59930	0.66481	1.04157
0.62235	0.62191	0.97236
0.64540	0.57709	0.90196
0.66845	0.53033	0.83076
0.69150	0.48157	0.75881
0.71455	0.43075	0.68613
0.73760	0.37781	0.61290
0.76065	0.32266	0.53900
0.78370	0.26518	0.46460
0.80675	0.20527	0.38959
0.82980	0.14275	0.31392
0.83902	0.11698	0.28347
0.84824	0.09075	0.25289
0.85746	0.06404	0.22220
0.86668	0.03685	0.19138
0.87590	0.00914	0.16041
0.88512	-0.01368	0.12931
0.89434	-0.01984	0.09803
0.90356	-0.02076	0.06657
0.91278	-0.01729	0.03491
0.92200	0.00010	0.00010

Cascade axial chord, B_x = 2.34 cm (0.922 in)

TABLE A-4

OVERCAMBERED BLADE AIRFOIL COORDINATES

X	YL	YU
0.0	1.12073	1.12073
0.00922	1.08834	1.15400
0.01844	1.07682	1.17250
0.02766	1.06938	1.18983
0.03688	1.06437	1.20611
0.04610	1.06119	1.22145
0.05532	1.05954	1.23592
0.06454	1.05931	1.24958
0.07376	1.06046	1.26250
0.08298	1.06310	1.27472
0.09220	1.06744	1.28629
0.11525	1.08118	1.31255
0.13830	1.08972	1.33535
0.16135	1.09362	1.35498
0.18440	1.09354	1.37166
0.20745	1.08997	1.38554
0.23050	1.08328	1.39671
0.25355	1.07376	1.40522
0.27660	1.06163	1.41109
0.29965	1.04709	1.41427
0.32270	1.03026	1.41470
0.34575	1.01128	1.41226
0.36880	0.99023	1.40676
0.39185	0.96719	1.39795
0.41490	0.94222	1.38545
0.43795	0.91536	1.36875
0.46100	0.88664	1.34707
0.48405	0.85610	1.31920
0.50710	0.82373	1.28308
0.53015	0.78954	1.23460
0.55320	0.75351	1.16943
0.57625	0.71562	1.10092
0.59930	0.67584	1.03113
0.62235	0.63412	0.96037
0.64540	0.59040	0.88936
0.66845	0.54460	0.81792
0.69150	0.49662	0.74596
0.71455	0.44633	0.67387
0.73760	0.39360	0.60149
0.76065	0.33823	0.52861
0.78370	0.27998	0.45563
0.80675	0.21856	0.38230
0.82980	0.15357	0.30850
0.83902	0.12647	0.27890
0.84824	0.09868	0.24898
0.85746	0.07015	0.21920
0.86668	0.04083	0.18930
0.87590	0.01066	0.15928
0.88512	-0.01279	0.12912
0.89434	-0.01868	0.09874
0.90356	-0.01050	0.06809
0.91278	-0.01596	0.03644
0.92200	0.00154	0.00154

Cascade axial chord, B_x = 2.34 cm (0.922 in)

TABLE A-5

STRAIGHTBACK BLADE AIRFOIL COORDINATES

X	YL	YU
0.0	1.13332	1.13332
0.00922	1.10093	1.16659
0.01844	1.08941	1.18516
0.02766	1.08196	1.20261
0.03688	0.07696	1.21905
0.04610	1.07378	1.23458
0.05532	1.07213	1.24926
0.06454	1.07189	1.26316
0.07376	1.07305	1.27632
0.08298	1.07569	1.28880
0.09220	1.08003	1.30062
0.11525	1.09374	1.32754
0.13830	1.10211	1.35098
0.16135	1.10564	1.37123
0.18440	1.10496	1.38849
0.20745	1.10058	1.40289
0.23050	1.09287	1.41451
0.25355	1.08214	1.42340
0.27660	1.06863	1.42955
0.29965	1.05253	1.43291
0.32270	1.03401	1.43339
0.34575	1.01321	1.43086
0.36880	0.99023	1.42509
0.39185	0.96517	1.41578
0.41490	0.93811	1.40251
0.43795	.90912	1.38467
0.46100	.87823	1.36133
0.48405	.84551	1.33099
0.50710	.81098	1.29102
0.53015	.77467	1.23369
0.55320	.73659	1.16504
0.57625	.69676	1.09322
0.59930	.65517	1.02130
0.62235	.61182	0.94910
0.64540	.56669	0.87769
0.66845	.51977	0.80527
0.69150	.47103	0.73281
0.71455	.42043	0.66028
0.73760	.36792	0.58841
0.76065	.31344	0.51571
0.78370	.25692	0.44300
0.80675	.19828	0.37014
0.82980	.13741	0.29761
0.83902	.11242	0.26875
0.84824	.08703	0.23985
0.85746	.06126	0.21015
0.86668	.03508	0.18122
0.87590	.00848	0.15231
0.88512	-.01206	0.12187
0.89434	-.01766	0.09349
0.90356	-.01835	0.06365
0.91278	-.01472	0.03460
0.92200	0.00292	0.00292

Cascade axial chord, B_X = 2.34 cm (0.922 in)

APPENDIX B

LIST OF SYMBOLS

A	Annulus area
BX	Axial chord
C_{PB}	Base pressure coefficient, $C_{PB} = (P_B - P_2)/Q_2$
C_x	Axial flow velocity
i	Incidence angle
M_{2i}	Isentropic exit Mach number
M_2	Exit Mach number
N	Mechanical speed, rev./min
P_B	Base static pressure (at trailing edge)
P_S	Static pressure
P_T	Total pressure
P	Free stream static pressure
P_{To}	Upstream total pressure
Q_2	Downstream free stream dynamic pressure, $Q = 1/2\ \rho V^2$
Re_{BX}	Reynolds number based on axial chord and exit conditions
T_{oc}	Coolant total temperature
T_{op}	Primary flow total temperature
U	Tangential wheel speed
μ'	Free stream velocity root-mean-square value of velocity fluctuation in the streamwise direction
W_c	Coolant mass flow
W_p, W_m	Cascade primary (mainstream) mass flow
X	Axial direction in turbine
Y	Circumferential direction in turbine

LIST OF SYMBOLS (Cont'd)

α	Vane air angle measured from tangential subscripts
β	Blade air angle measured from tangential subscripts
Δ	Incremental value
Γ	Uncovered turning

subscripts

1	Upstream reference plane
2	Downstream measurement plane
3	Downstream mixed out to homogeneous conditions plane

REFERENCES

1. Deich, M. E., Zaryankin, A. E., Fillipov, G. A., and Zatsepin, M. F., "Method of Increasing the Efficiency of Turbine Stages with Short Blades," Teploenergetika, Vol. 2, February, 1960. pp. 240-254.

2. Ewen, J. S., Huber, F. W., and Mitchell, J. P., "Investigation of the Aerodynamic Performance of Small Axial Turbines," ASME Paper No. 73-GT-3, Washington, D. C., April 1973.

3. Morris, A. W. H. and Hoare, R. G., "Secondary Loss Measurements in a Cascade of Turbine Blades with Meridional Wall Profiling," ASME Paper No. 75-WA/GT-13, Houston, Texas, November 1975.

4. Came, P. M., "Secondary Loss Measurements in a Cascade of Turbine Blades," Institute of Mechanical Engineers Conference Publications No. 3, Heat and Fluid Flow in Steam and Gas Turbine Plant, Warwick, 1973.